MSc thesis

Hydraulic evaluation of longitudinal training dams

B.W. van Linge

HKV CONSULTANTS

TU Delft

Front picture: Longitudinal training dam in the Waal near Wamel (credit: Frank Collas)

Hydraulic evaluation of longitudinal training dams

by

B.W. (Bart) van Linge

to obtain the degree of Master of Science
at Delft University of Technology (TU Delft)
in Hydraulic Engineering (Environmental Fluid Mechanisms)
to be defended on June 22, 2017 at 16:00 in Delft, the Netherlands

Thesis committee:	Prof. dr. ir. W. S. J. Uijttewaal	TU Delft (Chair)
	Dr. ir. E. Mosselman	TU Delft
	Dr. ir. S. van Vuren	TU Delft
	Ir. G. W. F. Rongen	HKV Consultants

An electronic version of this thesis is available at `http://repository.tudelft.nl/`

Preface

The master thesis presented here is part of my Hydraulic Engineering master program in the section of Environmental Fluid Mechanics at Delft University of Technology. I performed this research at HKV Consultants, where I spend the last 9 months (mostly in Delft and once a week in Lelystad).

At first, I would like to thank HKV Consultants and its employees for the past 9 months. I have very much enjoyed the time at HKV, especially the interaction with all colleagues during the daily lunches (inside and outside), Open-space discussions, and many lunch lectures. Particularly I would like to thank Guus Rongen, Saskia van Vuren, Andries Paarlberg and Stefan Jammers for the almost daily conversations and discussions on all subjects. Your support has helped me greatly throughout my research and made it a very fun time at HKV.

In addition, I would like to thank my graduation committee: Wim Uijttewaal, Erik Mosselman, Saskia van Vuren and Guus Rongen for your continuous input. All the discussions and comments during and beyond the committee meetings really helped to structure my research and resulted in many new insights. In particular, the many notes on my draft versions were very helpful.

Also, the many talks and visits with Henk Eerden (Rijkswaterstaat), Adri Wagener (Rijkswaterstaat), Timo de Ruijsscher (WUR) and Frank Collas (RU) were very appreciated. You have helped put all the knowledge on longitudinal training dams in context and I feel that my interest on the subject has largely been the result of your enthusiasm and lively talks. I want to thank you for the many visits to the Waal, Wageningen and Arnhem.

Halfway through my research, I came across several difficulties in using the Delft3D-Flow modelling software. I was lucky to come into contact with several Deltares experts, in particularly Erik de Goede, who showed lots of interest in my research and the related questions. Hereby I would like to thank Erik de Goede for all the help, many conversations, and time spent performing debugging tests.

At last, I would like to thank Jos, Reinier, Martijn, and Amber for the many discussions. Not only was it very helpful to have an ear to listen, but also the detailed discussion that followed always lead to great improvements. Although my explanations were not always very clear, you kept listening and tried to get me on the right track again.

Bart van Linge
Delft, June 2017

Summary

In 2015, the Dutch government initiated the longitudinal training dams pilot project. Its intentions were to reduce the negative effects of ongoing bed erosion and, in combination, improve the rivers flood protection level, navigability, and ecological values. With the help of longitudinal dams, a two-channel system is created in which the river is divided into a main and a side channel. The longitudinal dams are interrupted by several openings. The combination of the inlet and several openings allows water and sediment to be exchanged between the two channels. The inlet and opening crest heights can be altered by adding or removing stones. This is expected to influence the discharge (and sediment) exchange with the side channel. Knowledge about the physical functioning of multiple channel systems in the specific conditions created by longitudinal training dams is limited. Understanding the hydraulic conditions and the impact of the regulatory inlet and opening crest heights is expected to improve the control strategy and future design of river interventions using the concept of longitudinal training dams.

A one-dimensional model is created for this research to schematize the two channel system created by the longitudinal training dams. With the help of a numerical predictor-corrector scheme and the empirical side weir equation by Hager [1987], the backwater curves and weir discharges are calculated. The influence of several mechanisms, factors and dimensional design parameters on the discharge distribution between the two channels is assessed. A second, two-dimensional, model is created with the help of the existing numerical modelling software Delft3D-Flow. With this model, the detailed flow patterns around the inlet and openings are evaluated by schematizing the system of longitudinal training dams within the bed topography. In addition, the use of subgrid weirs in Delft3D-Flow and Waqua is compared to these bed topography model runs.

From the one-dimensional model, it is concluded that the discharge distribution between the two channels is mainly controlled by differences in longitudinal water level slope in both channels. The difference is caused by the combination of too short inlet and opening lengths (to direct enough water towards the side channel) and a difference in bed resistance between the two channels. Both result in different specific discharges. The distribution is not influenced significantly by the placement of the longitudinal training dams in a river bend. With the help of the two-dimensional Delft3D-Flow model, the local velocity magnitudes and flow angles atop the inlet and opening crests are shown to increase in downstream direction. However, for increased crest heights that nearly reach the water level, velocity magnitudes increase and flow conditions change from submerged to free-flowing. In this case, the specific discharge and flow angles atop the crest remain nearly constant in downstream direction. The free-flowing conditions are well described by empirical relationships. For submerged conditions, total discharges are also predicted well but an additional angle submergence coefficient ($C_{s,angle}$) is suggested to parameterize flow angles. The newly determined angle submergence coefficient is best described by a Villemonte-like formulation with a dependence on the submergence factor (S) and dimensionless crest length (L_w/B_{main}).

The schematization of longitudinal training dams within models of (large) river systems has been assessed by comparing schematization using bed topography with subgrid weirs. The available subgrid weirs in Delft3D-Flow show inconsistencies in the parameterization of the energy loss and the resulting calculated discharge towards the side channel. After some modifications, which will be included in the new Delft3D-Flow software release, both schematization types predict similar discharge (≤ 7 % relative difference) with the empirical relationships. If interest is only given to water levels and discharge distributions, the use of subgrid weirs is recommended, which is the case for computations

regarding the level of flood protection. This is motivated from a computation efficiency point of view, as far smaller grid sizes are required when using bed topography schematization. For models assessing other river functions that require information on local flow patterns, such as ecology, navigation, or sediment transport, the use of bed topography schematization is essential. The subgrid weirs do not model the influence of submerged flow conditions on the velocity magnitudes and flow angles resulting in errors for the flow angles as high as 40 degrees. By including the suggested parameterization for flow angles ($C_{s,angle}$) these errors can be reduced significantly showing a statistical R-squared value of 0.97 compared to the Delft3D-Flow bed topography model runs.

The ability to alter the inlet and opening crest heights is specifically included in the design to allow different control strategies in the future. From this research, the adjustable inlet and opening crest heights do not show a large influence on the discharge distribution between the two channels (a $5 - 10\%$ difference between a fully open and almost closed inlet). It mostly impacts the tipping point for submerged to critical flow conditions, after which the side channel discharge quickly decreases. This point is well predicted by the categorization of Bos [1976]. In submerged conditions, the inlet crest height does reduce the specific discharge in the side channel, limits the transverse velocities in the main channel, and greatly influence the flow angles atop the crest (order of 20-40 degrees and thus influence the sediment transport). The side channel width shows a far larger influence on the discharge distribution than the inlet or opening crest heights. A reduction of 10 m reduces the side channel discharge by an order of 10%. The crest length provides good control of the specific discharge in the side channel and flow angles atop the crest. Therefore, the channel width and inlet length should also be included as adjustable parameters in the design or control strategy of new systems of longitudinal training dams.

Contents

List of symbols

General constants		
g	gravitational constant	9.81 m^2/s
κ	Von Karman constant	0.4 -
Coordinates		
s	along-flowline coordinate	m
n	transverse-to-flow coordinate	m
x	x coordinate	m
y	y coordinate	m
z	z coordinate	m
η	relative vertical position ($=\frac{z}{d}$)	-
r	radial coordinate	m
σ	angular coordinate	rad
Fluid mechanisms		
D_t	turbulent diffusivity	m^2/s
F_e	turbulent entrainment flux	m^5/s^2
Fr	Froude number	-
k	inverse length scale	m^{-1}
Re	Reynolds number	-
u	velocity in x direction	m/s
u_*	bed friction velocity	m/s
v	velocity in y direction	m/s
w	velocity in z direction	m/s
α	entrainment coefficient	-
δ	mixing layer thickness	m
η_t	turbulent viscosity	m^2/s
λ	mixing layer parameter	-
ρ	density	kg/m^3
τ	shear stress	N/m^2
River engineering		
A_{con}	conveyance area	m^2
B	channel width	m
b	bed level	m +NAP / m +ref
C	Chezy value	$\sqrt{m}/s$
c_f	bed friction coefficient for turbulent flow	-
c_s	suspended sediment concentration	kg/m^3
d	water depth	m
H	energy head	m +NAP / m +ref
h	water level	m +NAP / m +ref
i_b	bed slope	-
k	permeability	m/s
k_r	Nikuradse roughness height	m
L	river section length	m

L_{inlet}	inlet length	m
L_{LTD}	longitudinal training dam length	m
$L_{opening}$	opening length	m
Q	discharge	m^3/s
Q_{main}	main channel discharge	m^3/s
Q_{side}	side channel discharge	m^3/s
Q_{up}	discharge upstream of the inlet	m^3/s
Q	discharge	m^3/s
q	specific discharge	m^2/s
R	hydraulic radius (R=h*B/(2*h+B))	m
S_r	transverse water level slope	-
S_σ	longitudinal water level slope	-
Z	channel side slope	-

Weir structures

a	coefficient in the Villemonte formula	-
b	coefficient in the Ka-Leung formula	-
B_w	crest width	m
C_d	discharge coefficient	-
$C_{d,0}$	modular discharge coefficient	-
C_s	discharge submergence coefficient	-
$C_{s,angle}$	angle submergence coefficient	-
c	geometry correction factor	-
ΔE_{weir}	energy loss over a weir	m
i_w	crest side slope	-
L_w	crest length	m
$L_{w,effective}$	effective crest length	m
P	channel shape coefficient	-
Q_p	porous discharge	m^3/s
Q_w	weir discharge	m^3/s
q_p	specific porous discharge	m^2/s
q_w	specific weir discharge	m^2/s
S	submergence factor	-
X_c	relative error in discharge coefficient	%
X_s	relative error in submergence coefficient	%
X_b	relative errors in dimensional parameters	%
X_h	relative error in water level	%
y	relative water level above bed ($y = h/H$)	-
w	crest height	m
W	dimensionless crest height above bed ($W = w/H$)	-
θ	width contraction angle	rad
ϕ	lateral outflow angle	rad

Numerical parameters

C	Courant number	-
CFL	CFL condition	-
dM	grid size in M-direction	m
dN	grid size in N-direction	m
dn	space step in n-direction	m
ds	space step in s-direction	m
dt	time step	s

α_r	Reflection parameter	s^2
Δx	space step in x-direction	m
Δy	space step in y-direction	m

Subscripts

0	upstream of the crest
1	atop the crest
2	downstream of the crest
inlet	at the inlet
opening	at the opening(s)
main	in the main channel
side	in the side channel
trans	in transverse (n) direction
long	in longitudinal (s) direction
up	upstream of the inlet
down	downstream of the inlet

Chapter 1: Introduction

1.1 Overview

The Rhine branches are an essential part of the shipping route to and from Germany and the rest of Europe. Next to this river function, they form an important element in the flood protection of the Netherlands. Thirdly, the Rhine branches are interchangeably connected to the development and maintenance of flora and fauna and provide many cultural services. Helping to maintain or improve these river functions is the main task for the Dutch river manager. Over the past centuries, river managers have introduced many projects with the aim to maintain or improve one or more river functions. These projects often have an impact on the water level, bed profile, sediment balance or other aspects in the river reach. Some impacts will positively stimulate specific river functions while at the same time introducing negative consequences for others. For a river manager, it is important to have a good understanding of all impacts resulting from existing and planned river projects. In that way, the present and future functions provided by the rivers can be maintained or even improved. If needed, appropriate measures should be taken to ensure that desired functions are fulfilled on the long term.

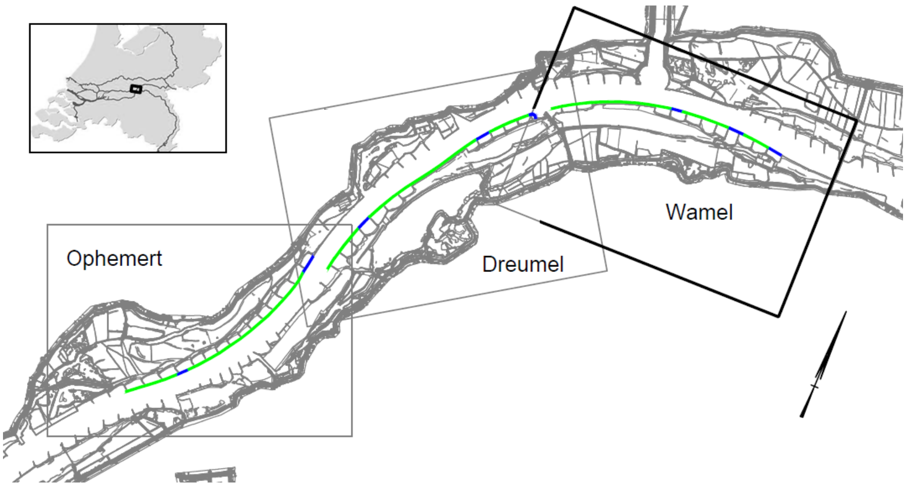

Figure 1.1: Overview of longitudinal training dams pilot project in the river Waal [Herik and Boskalis, 2014]

Over the past centuries, European rivers have been normalized and groyne fields are now dominating the average layout of river banks. Groynes have the function to increase the flood protection level and navigability of a river. With the presence of groynes, a uniform channel width is created, which reduces the risk of ice dam formation and increases the level of flood protection. Simultaneously, a narrow cross-section ensures a larger navigational water depth during low river discharges. The groynes, however, also induce a hydraulic roughness resulting in increased water levels compared to situations without groynes. A lower roughness can be reached by, for instance, lowering the groyne crest heights or, alternatively, replacing the groynes entirely by more streamlined structures. The longitudinal training dams are constructed as part of a pilot project and have the objectives to simultaneously increase the level of flood protection, reduce the negative effects of autonomous bed erosion, improve ecological development, limit the dredging activities in the navigational channel, promote cultural experiences and contribute to several other river functions [Rijkswaterstaat, 2016a; Liefveld et al., 2011]. This pilot has been placed under the Room for the River program as a test case alternative to lowering groynes. Under the research project 'Rivercare', the pilot project will be monitored for multiple years to evaluate the intended impacts on different river functions.

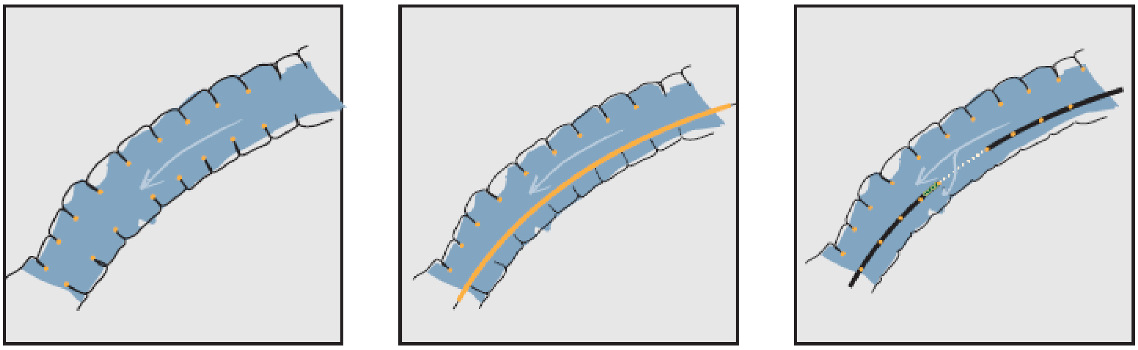

Figure 1.2: Construction steps of the longitudinal training dams near Dreumel [Rijkswaterstaat, 2011]

In the 'longitudinal training dam pilot project', Rijkswaterstaat (part of the Dutch Ministry of Infrastructure and the Environment) constructed several dams that are subdivided into three project areas. Each consists of multiple sand-filled dams that stretch along (part of) an inner bend of the river. Figure 1.1 provides an overview of the three project areas in which the dams are highlighted in green. The longitudinal training dams are placed in a continuous manner with openings in between, highlighted in blue, that are relatively small compared to the dam length. River groynes that were originally present have now been completely removed, as shown in figure 1.2. With help of the longitudinal training dams, a two-channel river system has been created dividing the river into a main and side channel. The side channel has considerably smaller dimensions than the main channel, both in width and depth dimensions. At the beginning and end of each project area, an inlet and outlet region is situated respectively. A schematized form is shown in figure 1.3. The inlet and openings allow water to be divided between the main and side channel and are constructed with the help of a porous rock layer. This means that crest heights of the inlet and openings can be altered by adding or removing stones. The ability to alter the crest height in a later stage has been implemented in the design to possibly influence the amount of water and sediment entering the side channel. When more knowledge is gained on the important mechanisms and factors, altering the crest heights can be used as a means of controlling these processes.

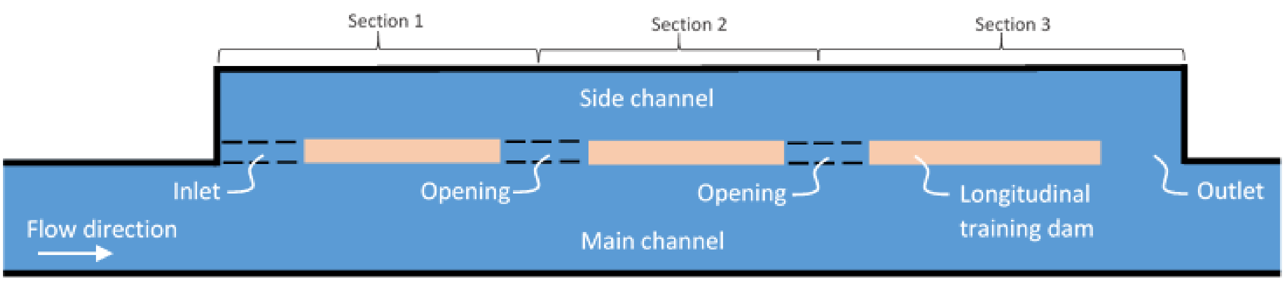

Figure 1.3: Schematization of a longitudinal training dam

1.2 Problem description

All of the river functions intended to be improved by the system of longitudinal training dams are influenced by the fluvial processes in the river. The processes that induce the transportation of water and sediment between the main and side channel are the most important. There is a lack of knowledge on the processes within a multiple channel system created by longitudinal training dams. This is due to lack of previous experience with the concept. Extensive research has been conducted on the processes and schematizing techniques for groyne fields regarding a large variety of processes, physical functioning, and mathematical or numerical modelling. However, because of the used dead-zone assumption (zero net transport between the groyne field and the river channel), this research is not compatible with a two-channel system created by longitudinal training dams. This means that also the processes and impacts on the river functions are different from groynes and uncertain.

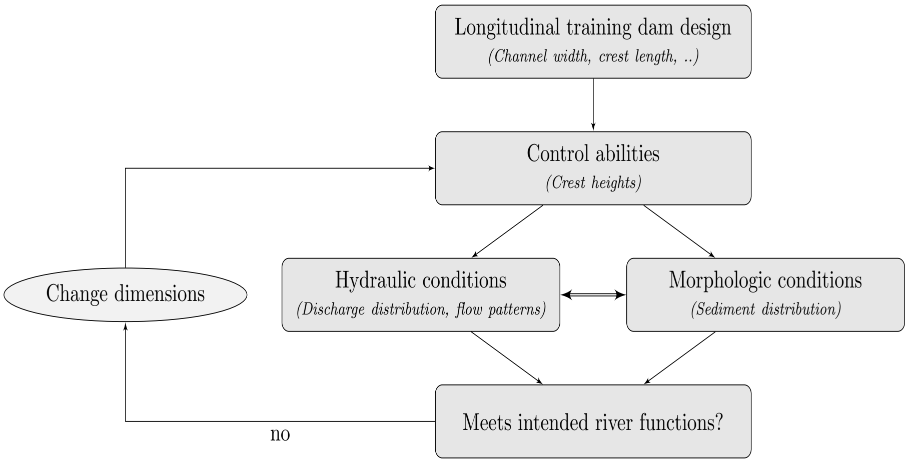

Figure 1.4: Flow diagram of the influence on river functions

In order to assess the impacts of longitudinal training dams on the different river functions, the discharge and sediment distribution between the two channels needs to be understood. Both distributions are governed by a combination of the hydraulic and morphological conditions. This is shown in figure 1.4. The transportation of sediment between the two channels can be evaluated with the input of hydraulic conditions (local flow angles and velocity magnitudes), which is the focus of research by Jammers [2017]. Combining the knowledge of Jammers [2017] with knowledge on the mechanisms and factors inducing velocity magnitudes, flow angles, and discharge distribution will thus result in a better understanding of the impact on river functions. In the design of longitudinal training dams, the inlet and opening crest heights can be altered and used as control abilities to change the discharge and sediment distribution between the channels. Knowledge on how to use these control abilities to most efficiently impact the hydraulic and morphological conditions is expected to improve the control strategy and future design of longitudinal training dams.

If the mechanisms and factors influencing the distribution of water (and sediment) between the two channels are better understood, use can be made of numerical models to simulate and predict the hydraulic conditions. The hydraulic conditions can be predicted on local, as well as larger spatial scale. The two software packages mainly used for these types of calculations in the Netherlands are the two-dimensional modelling software programs Delft3D-Flow and Waqua. Both have the capability of using two methods to schematize the longitudinal training dams. The first is a schematization of the inlet and openings by adjusting the bed topography and the second uses special subgrid elements. Figure 1.5 shows the inlet for both schematizations.

When schematizing the structure as part of the bed topography, the longitudinal training dams are included in the initial bed topography. The conditions required to obtain consistent and correct discharges and flow patterns, in terms of grid sizes or other numerical conditions, have not been studied in detail. When the schematization onto bed topography requires the use of small grid sizes, the modelling time increases considerably, which is not ideal from a computational efficiency point of view. As a solution subgrid elements can be used. For these subgrid elements, instead of adjusting the bed topography, the discharge over or through the structure is parameterized on individual grid cells.

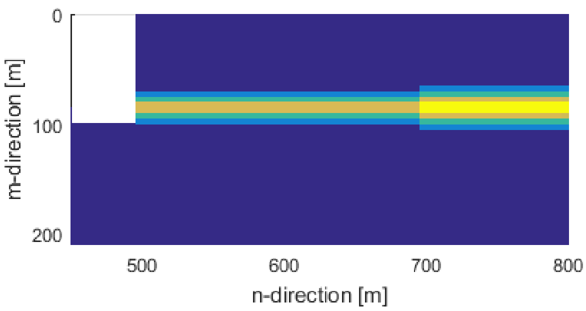

(a) Bed topography

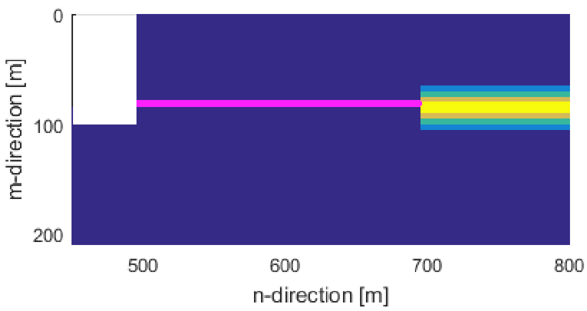

(b) Subgrid weir

Figure 1.5: Schematization of inlet as bed topography and subgrid weir in Delft3D-Flow

Empirical relationships are used for this schematization. One of the available subgrid structures is the subgrid (2D) weir that specifically fits the conditions at the longitudinal training dams. However, problems are found when using subgrid weirs. The modelled discharge, flow angles and sediment transport over the structure [Mosselman, 2001] are found to not be calculated correctly. A new parameterization of sediment transport is suggested in research by Vuik [2010] and Jammers [2017] but an evaluation of the incorrect discharges and flow angles atop side weirs is not found in literature. At this moment it is thus unknown how accurate the use of subgrid weirs is to investigate the impacts of longitudinal training dams on different river functions. The inclusion of correct energy losses in combination with a new parameterization for the flow angles atop subgrid weirs is expected to result in a more accurate modelling of longitudinal training dams.

1.3 Goals and research questions

1.3.1 Research goal

The mean objective of this research is to gain knowledge on the hydraulic conditions around longitudinal training dams. Emphasis is put on the mechanisms and factors influencing the flow patterns and a discharge distribution between the main and the side channel and their relative importance. Better knowledge of the discharge distribution and flow patterns, in combination with knowledge on the sediment transport, will most likely result in more favourable effects on desired river functions, lower costs and a more sustainable river.

1.3.2 Research questions

To reach the presented goal, a combination of four research questions is presented below. Combined, these questions will help to provide a full hydraulic evaluation of the system of longitudinal training dams.

1. What *mechanisms and factors* influence the discharge distribution at longitudinal training dams?

2. What are the local *flow patterns* at the inlet and openings and how can these be parameterized?

3. How can the system of longitudinal training dams best be *modelled* in large river models?

4. How can *control strategies* and the design of longitudinal training dams influence the discharge distribution and flow patterns?

1.4 Methodology

The methodology used to answer the different questions is shortly explained below and will be treated in more detail in chapter 3. Two models have been developed to answer the different research questions. Firstly, a one-dimensional model has been created for this research using the Matlab software program. Secondly, a two-dimensional model has been created using the existing hydrodynamic modelling program Delft3D-Flow. A description of these models and a more extended explanation of the methodology is provided in chapter 3.

Mechanisms and factors

The one-dimensional model is used to analyse the mechanisms and factors that induce a discharge distribution at longitudinal training dams. Compared to a two-dimensional model, mechanisms are more easily parameterized and controlled in such a simplified one-dimensional model without more detailed two-dimensional effects interfering. The one-dimensional model schematizes the system of longitudinal training dams as two parallel channels connected by side-weirs. The water levels and discharge distribution between the main and side channel are calculated according to the equations presented in chapter 2. By enabling and disabling the different equations, the influence of each mechanism and factor is analyzed.

Flow patterns

For a more detailed analysis of the local flow patterns, the one-dimensional model no longer suffices. A numerical two-dimensional depth average Delft3D-Flow model has been built to assess the local flow patterns. Its boundary conditions are created with the help of the one-dimensional model. Two-dimensional flow patterns, including the flow angles and velocity magnitudes around the inlet and openings, are analyzed with help of this model. These flow patterns are relevant in relation to the sediment transport towards the side channel, as discussed in research by Jammers [2017]. The use of empirical relationships in the one-dimensional model is evaluated to determine if they can be used to approximate or parameterize the flow patterns at the inlet. This can then be used to suggest a new parameterization for the impacts of weir-like structures on the flow patterns.

Modelling

An analysis of different schematization techniques is performed for the purpose of increasing knowledge on efficiently modelling longitudinal training dams. A Delft3D-Flow model is used to assess the schematization of longitudinal training dams by including them in the bed topography and by using subgrid weirs. Focus will be laid on correctly modelling the discharge and flow patterns and determining the required numerical aspects for both schematization types. Also, the possible improvement of including a parameterization for the flow patterns in subgrid weirs is evaluated.

Control strategy

The combination of both the one- and two-dimensional models provides the ability to analyse the effects of adjusting the inlet and opening crest heights (control strategy) and crest lengths and side channel width (design dimensions). The impacts on the discharge distribution and flow patterns are analyzed. Several model runs are performed by varying the control and design dimensional parameters.

1.5 Related research

Within the 'Rivercare' research program, several research studies are performed on the sediment transport, hydraulic, cultural and ecological conditions of longitudinal training dams. Large-scale site surveys are performed or planned around the pilot project to gather relevant data on the fluvial processes in the river. The field surveys have not all been performed yet. Despite the lack of relevant field data, the one- and two-dimensional model runs as performed in this research, are expected to already provide relevant insights into the mechanisms, flow patterns and modelling techniques of longitudinal training dams. The insights gained from this thesis directly connect to research performed by Jammers [2017], who concluded that the flow angles and velocity magnitudes around the inlet of longitudinal training dams greatly influence the sediment transport towards the side channel.

1.6 Thesis outline

In chapter 2, background information on the system of longitudinal training dams is gathered. The analysis of different river functions and an overview of useful literature on weir flow and ways of modelling flow at longitudinal training dams is included. This forms the basis of this research. The methodology used to answer the different sub-questions explained in more detail in chapter 3. The results for the various model runs are presented in chapter 4. In chapter 5, the results are discussed. This chapter also provides a reflection on the usefulness of the results and the possible translation to the river functions. Finally, in chapter 6 the conclusions and recommendations are given. Appendix A relates to chapter 1 and provides an overview of the important general fluid mechanisms and (side) weir equations used throughout this research. Appendix B and C describe the one- and two-dimensional models respectively, that are used in more detail. Also, several model outcomes and pictures regarding the validation tests and sensitivity analysis are presented here. The thesis outline is visualized in figure 1.6.

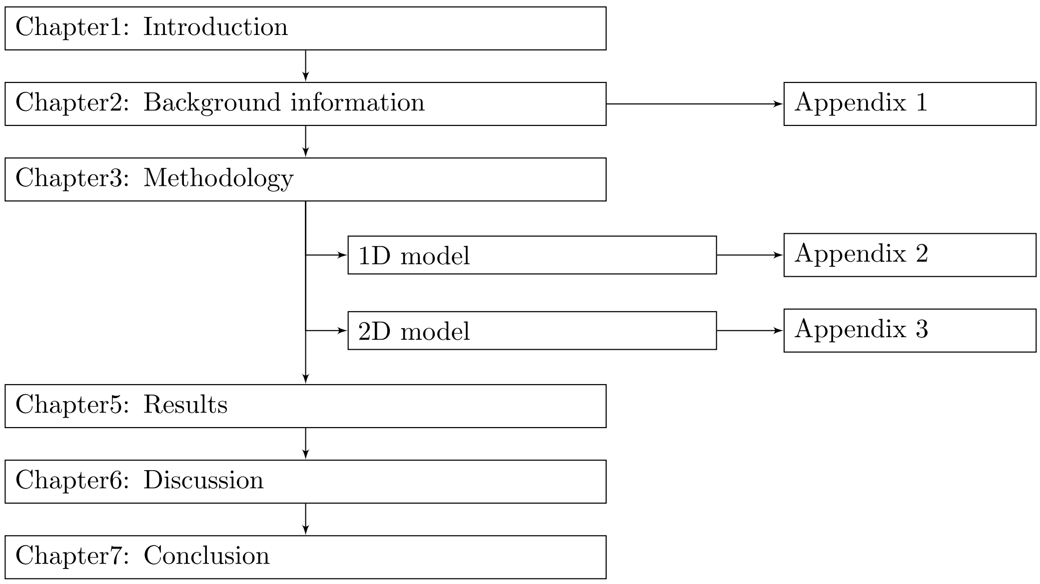

Figure 1.6: Thesis outline

Chapter 2: Background information

2.1 Introduction

This chapter provides an insight into the available information on longitudinal training dams. At first, the river functions that are expected to be influenced by the longitudinal training dams are discussed followed by the available modelling techniques to analyse longitudinal training dams. This includes an overview of the available side-weir formulas as found in literature.

2.2 River functions of longitudinal training dams

The longitudinal training dams that have been constructed in the Waal are an alternative to lowering the groyne fields in this river section. They are designed and constructed with the aim to improve several river functions with respect to the alternative case of lowering the groynes [Rijkswaterstaat, 2016a; Liefveld et al., 2011]. Several of these river functions are discussed below.

1. **Flood protection:**
   When considering flood protection, the river flood conveyance capacity is of great importance. The flood conveyance capacity determines the amount of water that can be transported safely through a specific river section without the river dikes being overtopped. The conveyance capacity of a river is influenced by both the conveyance area and the flow resistance. The removal of groynes and construction of longitudinal training dams is expected to increase the flood conveyance capacity by increasing the conveyance area as well as decreasing the flow resistance in that specific river section. Increasing the flood conveyance area through the construction of longitudinal training dams and the removal of groynes is shown in figure 2.1. The longitudinal training dams are expected to reduce the flow resistance compared to groynes, as the longitudinal training dams are positioned parallel to the flow direction.

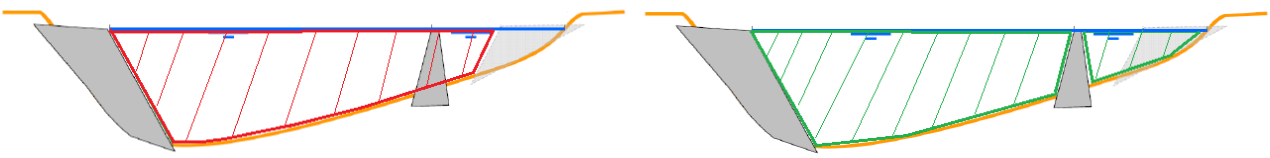

(a) with groyne field **(b)** with longitudinal training dams

Figure 2.1: Cross-sectional view of a river showing the flood conveyance area

   For flood protection, it is important that during high water levels the discharge capacity is large enough (water levels must remain below a maximum level). The discharge capacity is affected by the flow conveyance area which is in turn influenced by the cross-sectional dimensions of the longitudinal training dams and their openings. Considering the flow resistance, mainly the flow patterns between the main and side channel and the flow exchange between the side channel and flood plain are important. To get a better understanding of this, it is important to have a good physical understanding of the flow patterns around longitudinal training dams (as well as summer dikes and groynes) under design flood discharge ('MHW-afvoer' in Dutch). A first step is to gain knowledge on the flow patterns during lower river discharge. This also includes flow under oblique flow angles. The height of the openings can alter the flow patterns and can thus influence the level of flood protection.

The requirements related to flood protection presented by Rijkswaterstaat state that the longitudinal training dams must result in a water level reduction in the channel's center during high river discharge levels that is similar or larger than for lowering the groyne fields. The requirement is a minimal reduction of 9 cm between river kilometres 915.5 and 916.5.

2. **Navigation:**
Safe navigation in the river Rhine requires minimal navigation dimensions. According to CCNR [2016] these are determined at a depth of 2.8 m over a width of 150 m in the main channel in the Waal. Smaller navigation dimensions can result in shipping bottlenecks. Safe navigation is thus largely influenced by the combination of both water and bed levels. With the construction of longitudinal training dams, the navigation depth is determined by both the water and bed levels in the river. These are both influenced by the construction of longitudinal training dams that influence the distribution of water and sediment between the two channels and the flow velocities in the respective channels. The navigation depth during low water discharge is expected to be increased by the longitudinal training dams due to larger water depths in the main channel. The longitudinal training dams slightly narrow the main channel and during small river discharges, the amount of water directed towards the side channel is expected to be minimal due to the inlet and opening crest height. Secondly, with help of the longitudinal training dams, it is expected to have better control over the sediment balance in the river. Sediment can either be transported as suspended or bed load. Suspended sediment can be transported by water through both the inlet and openings. It is not known (in what quantities) bed load transport is transported over the inlet or openings. This will largely depend on the flow patterns and velocity magnitudes at the inlets and openings of longitudinal training dams. By adjusting the inlet or opening crest heights, the flow patterns and thus the navigation depth could be positively influenced.

The design requirements presented by Rijkswaterstaat for navigation purposes are not specifically stated to positively influence navigation but mainly focus on maintaining the required minima [Rijkswaterstaat, 2016a]. In the future, control abilities integrated into the longitudinal training dam design are expected to be a possibility to influence the morphological development and thereby possibly minimize dredging costs and avoid nuisance to shipping. The requirements by Rijkswaterstaat read:

   - No reduction of the navigation channel dimensions may occur during low to medium river discharge.
   - Only limited nuisance to shipping is acceptable as a result of maintenance works (that include dredging).
   - The lateral velocities in the navigation channel, including the effects of the side channel in- or out-take, may not exceed 0.15 m/s to 0.3 m/s.

3. **Improved ecological development:**
The river systems are interchangeably connected to the flora and fauna in the Netherlands. The development of flora and fauna can greatly be increased by improving the amount of nature-friendly bankline protections. Secondly, the created two-channel system is expected to improve the ecological development through the sheltering effect by the longitudinal training dams. Research by Collas [2016] has shown that ecological conditions at longitudinal training dams improve with respect to that of groyne fields. Especially at locations with less variation in depth-averaged velocities and reduced velocity fluctuations. The waves and currents created by ships, as well as noise, are reduced in the side channel, compared to the groyne fields. One method of expressing the sheltering effect is thus through the reduction of velocity fluctuations in the side channel during the passing of a ship. These fluctuations are generated by the combination of the ship propellers as well as the temporarily reduced water levels. Another way is to look for

variation in the depth-averaged velocities around the inlet and openings. The requirements by Rijkswaterstaat read:

- Nature-friendly banklines
- Reduced velocity fluctuations (induced by passing ships)
- Reduced noise nuisance induced by passing ships

4. **Other river functions:**
Several other river functions can be listed. These are not evaluated as extensively as the previous functions, however, this does not mean that the (hydrodynamics of the) longitudinal training dams do not influence these river functions. These river functions include:

- Cultural and social values
- Limited dredging nuisance and associated costs
- Fresh water supply

Design requirements that follow from these other river functions, as presented by Rijkswaterstaat, include [Rijkswaterstaat, 2016a]:

- The discharge distribution at the Pannerdensche Kop and IJsselkop may not change more than 1 m^3/s during low, 20 m^3/s during high and 5 m^3/s during design river discharge ('MHW-afvoer' in Dutch).
- The average bed level may not decrease (no erosion allowed).
- Unwanted transverse displacement of the side channel is not allowed.

2.2.1 Conclusion

From the above sections, it can be concluded that the system of longitudinal training dams influences the river functions on several different spatial scales. Navigation is, for instance, influenced by local transverse velocities that occur on the scale (or dimensions) of a single inlet. The level of flood protection is influenced mainly by the water levels over a much larger length scale than a single inlet or opening. A river function is not solely affected on one length scale, but a rough characterization can be made that is shown in table 2.1. The ecological development is mostly affected by the local flow patterns around a single inlet and average velocities at a length scale of the longitudinal training dams. Navigation is influenced by a combination of navigation channel dimensions, the local transverse velocities, and the nuisance at a scale of the longitudinal training dams. The level of flood protection is influenced mainly by a larger spatial scale extending to lengths stretching an entire river reach. The main conclusion is thus that the different river functions are influenced by a variety of length scales, that are all important to consider in a thorough evaluation of longitudinal training dams.

Table 2.1: Overview of the different river functions

Scale	Hydraulic effects	River functions
Single inlet or opening	Local flow velocities Flow angles	Navigation Ecology
System of LTD	Discharge distribution between channels Water level slope	Flood protection Navigation Culture
River reach	Autonomous bed erosion Discharge distribution at bifurcations	Flood protection

2.3 Mechanisms and factors

The considered potential mechanisms and factors that influence the transportation of water between the main and side channel are listed in figure 2.2 and discussed in more detail below. Both the advective transport, diffusive transport and porous flow will influence the amount of discharge entering the side channel. The diffusive transport by turbulence is considered not to influence the discharge entering the side channel as mass does not "exhibit diffusive transport with itself" [Uijttewaal, 2015] but is expected to be capable of transporting momentum or sediment towards the side channel.

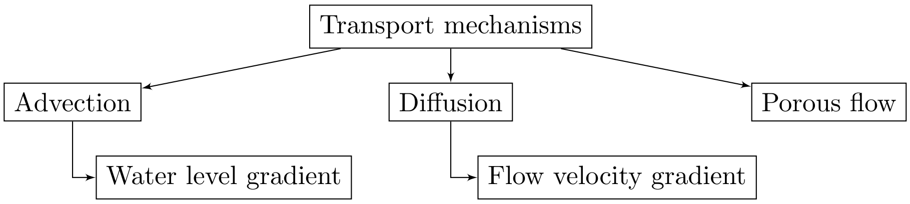

Figure 2.2: Overview of mechanisms affecting the transport between the two channels at a system of longitudinal training dams

2.3.1 Water level gradient

Transport driven by a water level gradient can be described by the pressure term in the y-momentum balance. This is the $(\frac{\partial p}{\partial y})$ term in the y-momentum equation that is treated in more detail in appendix A. In hydrostatic and non-compressible water, a pressure difference is the result of a difference in water level between the two channels. Such a difference can either be the result of different longitudinal or lateral water level gradient in the two channels, as shown in figure 2.3.

A longitudinal water level difference can be caused by differences in flow resistance, bed level gradient or specific discharge in a channel. This can be illustrated by the formulation of equilibrium water depth as shown in equation 2.1.

$$d_e = (\frac{c_f q^2}{i_b g})^{\frac{1}{3}} \tag{2.1}$$

where d_e is the equilibrium water depth, c_f is the friction coefficient, q is the specific discharge, i_b is the bed level gradient and g the gravitational acceleration. The three river parameters influencing the equilibrium water depth (specific discharge, bed resistance, and bed level gradient) are interconnected, however, can also be looked at separately. A difference in specific discharge can be the result of the inlet or opening dimensions that direct too much or too little water towards the side channel for equal specific discharges. A difference in flow resistance results in a blocking effect in one of the channels. A difference in bed level gradient can be created due to the presence in a river bend. This effect is interconnected with the induced secondary motion that is discussed under the flow velocity difference in section 2.3.2. The difference in bed level gradient can be expressed by the different channel length with the help of equation 2.2, where r is the bend radius and L is the (main or side) channel length.

$$\frac{L_{side}}{L_{main}} = \frac{r_{side}}{r_{main}} \tag{2.2}$$

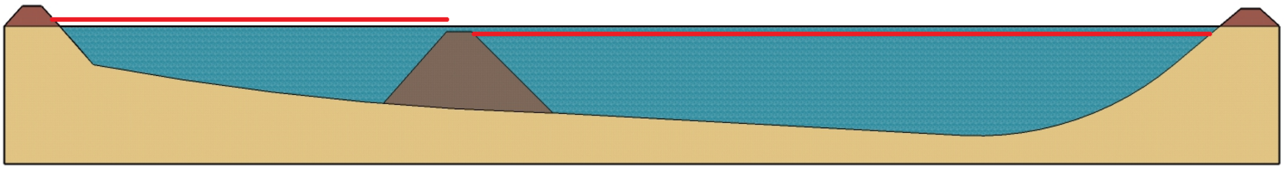

(a) Longitudinal water level gradient

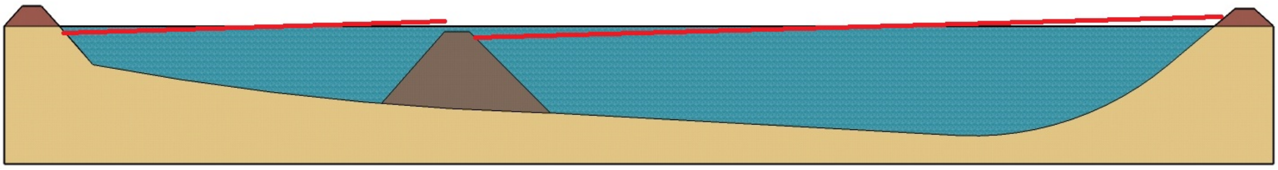

(b) Transverse water level gradient

Figure 2.3: Cross-section of the inlet showing the water level gradients

In river bends a transverse water level gradient, or gradient in transverse direction (i_{trans}), is created as a result of the centrifugal force in the bend. The transverse water level gradient can be approximated with a simple formula from which the water levels at the inner- and outer bend can be calculated, as shown below [Njanga, 2012].

$$i_{trans} = \frac{u^2}{gr} \tag{2.3}$$
$$h_{innerbend} = h_{center} - i_{trans}\frac{B}{2}$$
$$h_{outerbend} = h_{center} + i_{trans}\frac{B}{2}$$

where u is the depth average longitudinal velocity in the channel, r is the bend radius and h the water level (in the channel centre, inner or outer bend). Due to a higher water level in the outer main-channel bend and a lower water level in the inner side-channel bend (see figure 2.3b), the transverse water level gradient effects the water level difference between the two channels. This can, in turn, influence the transport of water between the two channels.

2.3.2 Flow velocity gradient

A velocity difference between the two channels can occur in both longitudinal and transverse direction. Transport between the channel that is driven by a velocity difference in longitudinal direction results in a turbulent mixing layer at the inlet or openings. This can take the form of a shear layer or wake, as discussed in appendix A.5. This is not included here as it is considered a turbulent transport and discussed in the next section. A velocity difference in lateral direction can be caused by the secondary flow that is present in a river bend, as shown in figure 2.4.

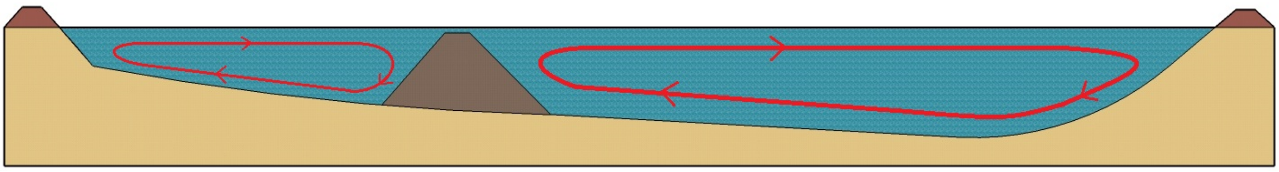

Figure 2.4: Cross-section of the inlet showing the secondary flow

The lateral (or radial) velocity component (v) can be obtained with the help of Rozovskii's equation as shown in equation 2.4 [Rozovskii, 1957].

$$v = \frac{ud}{r}\frac{1}{\kappa}[F_1(\eta) + \frac{\sqrt{g}}{\kappa^2 C}F_2(\eta)][1 - exp(-\frac{2\kappa C}{\sqrt{g}}\frac{x}{d})] \tag{2.4}$$

where d is the water depth, C is the Chzy coefficient, κ is the Von Karman constant ($\kappa = 0.4$) and F_1 and F_2 are empirical coefficients. The first part on the right hand side of equation 2.4 represents the general relationship for lateral velocity that is corrected by F_1 and F_2 for the relative vertical position ($\eta = \frac{z}{d}$). The last part of the right-hand side represents the growth with longitudinal distance. Both F_1 and F_2 can be estimated with the help of figure B.8 taken from Tanguy [2009]. It should be noted that Rozovskii's equation tends to "overestimate the lateral velocity" [Baek and Seo, 2009] but can be used to estimate an order of magnitude for the strength of the secondary flow velocity as shown in equation 2.5.

$$\begin{aligned} O(v) &= \frac{O(d)O(u)}{O(r)}\frac{1}{\kappa}[O(F_1(\eta)) + \frac{\sqrt{g}}{\kappa^2 O(C)}O(F_2(\eta))] \\ &= \frac{O(10^1)O(10^0)}{O(10^3)}\frac{1}{0.4}[O(10^{-1}) + \frac{10^1}{10^{-1} * O(10^1)}O(10^{-1})] \\ &= O(10^{-2}) \end{aligned} \tag{2.5}$$

2.3.3 Porous flow

The inlet and openings between the longitudinal training dams are constructed by rocks with a single mass-grading of 40 - 200 kg. The porous rock layer results in flow through the openings between the main and side channel, even during water levels below the crest of the inlet or openings. Flow through porous soils and rocks can be approximated with the general Darcy formula for flow through porous media, given by equation 2.6.

$$v_{porous} = kI \tag{2.6}$$

where v_{porous} is the fluid velocity through the porous medium, k is the permeability and I is the hydraulic pressure gradient. The hydraulic pressure gradient can easily be calculated by the water levels on opposite sides of the openings in the main and side channel and the transverse width (B_w) of the openings. The permeability can be approximated with the help of literature and is estimated at 0.4 (see appendix B).

2.3.4 Conclusion

Concluding from the analysis above, a set of mechanisms and factors is considered to possibly influence the discharge distribution between the two channels at a system of longitudinal training dams. These mechanisms and factors will be investigated in this research and include a longitudinal water level gradient difference due to different channel lengths or bed roughness heights, transverse water level gradient, transverse velocities, and porous flow.

2.4 Modelling

To investigate the impacts of river interventions on different spatial scales, a large variety of models is available. When studying the impacts on the scale of a single inlet of the longitudinal training dams, different modelling methods can be used that include field observations, empirical relationships, physical scale tests and numerical models. When the need for a better functional understanding arises, empirical relationships found from scale tests or analytical models are often used. With the help of such methods, river interventions are schematized to only include their basic essence. The advantage is that this provides good insights in the relevant fluvial processes without including too much complexity. When the need for more detailed and complex analysis is required, several numerical hydro-morphodynamic modelling programs are available. Two of the widely used programs (in the Netherlands) include Delft3D-Flow and Waqua that are designed to assess the impacts of a large range of river interventions on hydraulic, morphological or several other criteria within often complicated environments. These models can provide more detailed insights into two-dimensional processes that play a role, although a difficult aspect lies in correctly and efficiently representing (and analysing) the effects caused by specific river interventions.

When analysing the impacts of longitudinal training dams on a larger scale, the effects of many different hydraulic structures and conditions has to be included in the modelling. These are also often spread over a long spatial distance. This means that only using empirical relationships is not applicable anymore. Large river models that analyse impacts on a reach scale have therefore been developed. These models, such as the DVR ('Duurzame Vaardiepte Rijndelta') models, make use of the previously mentioned Delft3D-Flow or Waqua programs. The DVR models have grid-size that are too coarse to efficiently analyse all detailed processes of single river interventions and therefore require parameterization or grid refinement techniques.

2.4.1 Modelling with empirical relationships

The system of longitudinal training dams with an inflow and openings shares many similarities with the well studied side weir. In literature, side weirs are considered a special case of general (plain) weirs and similar basic formulations are used. Literature on weirs can roughly be divided into the following categories, as figure 2.5 shows.

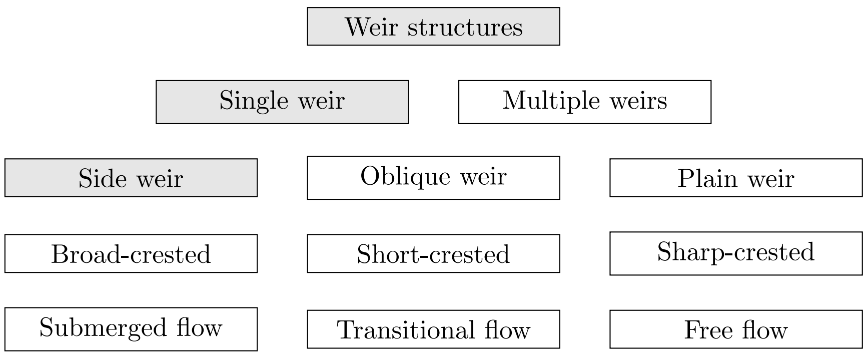

Figure 2.5: Overview of weir categorizations

The first categorization made is between considering all weirs as single independent weirs that do not influence one another or a system of multiple weirs that also impact neighbouring weirs. When weirs are positioned close enough with respect to one another, the locally induced water level and velocity variations influence the neighbouring weirs and this effect should be taken into account. The second distinction, as shown in figure 2.5, is made between side, oblique, and plain weirs. This is made on the basis of the weir crest obliqueness relative to the flow lines. Flow lines running perpendicular to the crest (90-degree angle) are referred to as plain, while an angle deviating from 90 degrees is referred to as oblique. When flow lines are running parallel to the weir crest, this is known as side weirs. The weir type classification of broad-, short- and sharp-crested weirs relates to the flow lines atop the weir crest. For a broad-weir, flow lines eventually run parallel atop the weir and a hydrostatic pressure distribution can be assumed whereas for sharp-crested weirs the flow lines will separate from the crest edge without reattaching or running parallel. The ratio of energy level above the weir crest $(H-w)$ to the crest width B_w seems to determine the weir type [Bos, 1976]. See appendix B for a more extensive explanation. Table 2.2 shows the values for the different classifications as proposed by Bos [1976]. Lastly, the distinction between several flow conditions atop the weir crest can be made. These are categorized in submerged, transitional and free-flow conditions.

In this research, the inlet and openings in the system of longitudinal training dams are considered as separate (single) side weirs. The influence of one weir on neighbouring weirs is thus not taken

Table 2.2: Categorization of weir types based on the energy level above the weir crest $(H - w)$ over the crest width (B_w) [Bos, 1976]

Weir type	Categorization
Sharp-crested	$(H - w)/B_w > 15$
Short-crested	$15 > (H - w)/B_w > 1/3$
Broad-crested	$(H - w)/B_w < 1/3$

into account. This is indicated by the grey shaded blocks in figure 2.5. The weirs are considered in a transitional or submerged regime and are, due to the given crest width in the pilot project, categorized as short- to broad-crested [Bos, 1976]. An overview of general literature and formulas on plain and oblique weirs is discussed in appendix A. In the sections below, an overview of side weir literature is given.

2.4.2 Side weirs

The flow over side weir structures is well studied and finds practical uses in many areas including urban drainage systems, irrigation channels, intake channels, side channel bifurcations, side channel confluences, storage basins, and flood control. The research on flow over side weirs, due to the nature of the application areas, considers what is called spatially varied river flow that can either be increasing (e.g. outflow of storage basin) or decreasing (inflow of storage basin). This means that the river discharge is non-uniform in longitudinal direction due to the presence of weir-like structures. A top and side view of a side weir is shown in figure 2.6.

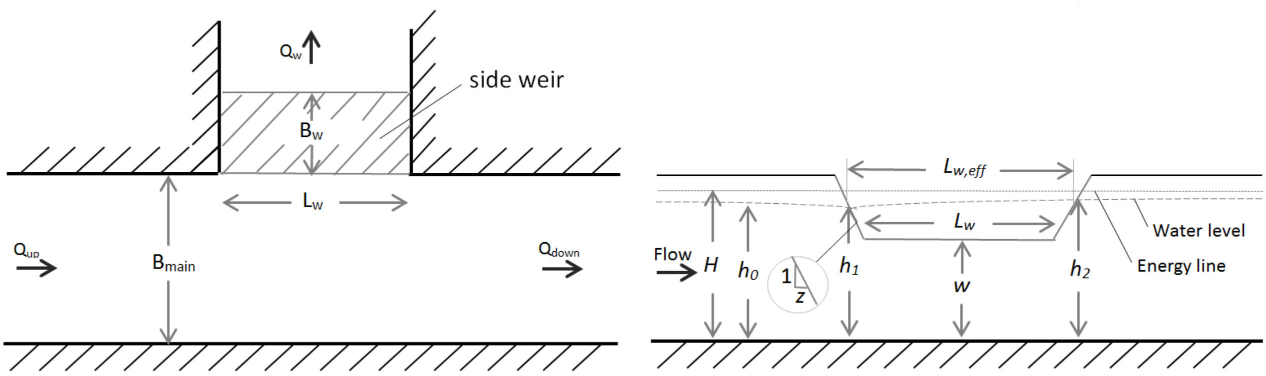

(a) Top view (b) Side view

Figure 2.6: Schematization of a side weir

In literature, the general weir formula, as given by equation 2.7, forms the basis of all side-weir equations.

$$q_w = C_s C_d \frac{2}{3} \sqrt{2g} (H_0 - w)^{3/2} \tag{2.7}$$

where H_0 is the energy level upstream in the main channel, w the weir crest height above bed level, C_d the discharge coefficient and C_s the submergence coefficient. The largest part of this equation $(C_s C_d \frac{2}{3}\sqrt{2g})$ consists of constants that are mostly dependent on the weir type and flow condition as shown previously in figure 2.5. The fact that $H - w$ is raised to a power 3/2 shows that increasing the energy level above the weir crest increases the specific discharge by the power 2/3. This equation is treated in more detail in appendix A. Most of the side weir research focuses on accurately determining the discharge coefficient C_d for specific weir types and flow conditions in order to obtain the correct weir discharge. The submergence coefficient is introduced to allow for the use of the same equation in free-flowing, transitional, and submerged conditions.

Discharge coefficients

De Marchi [1926] tried to solve the discharge coefficient analytically by assuming that the energy head along the side weir can be considered constant and by ignoring friction. The De Marchi method is discussed in more detail in appendix A. Dimensional analysis shows that C_d is theoretically dependent on many different parameters of which most are shown in figure 2.6. These parameters can be converted into several dimensionless variables ([Haddadi, 2012; Rosier, 2007]) as given below.

$$C_d = f(u, H_0, g, w, B_{opening}, B_{main}, z_{opening}) \tag{2.8}$$

$$C_d = f(Fr_1, \frac{w}{H_0}, \frac{B_w}{B_{main}}, \frac{L_w}{B_{main}}, \frac{H_0}{L_w}\frac{dz}{dx}) \tag{2.9}$$

It has been concluded that a "complete analytical solution" of equation 2.9 is not yet possible and "only approximate methods have been suggested" [Honar and Javan, 2007]. There are two approaches to approximate the discharge coefficient:

1. The discharge coefficient of a similar plain weir can be reduced by a correction factor representing the lateral flow conditions, as used by Hager [1987].

2. The discharge coefficient can be obtained from (experimental) data on specific channel shapes and weir types ([Ali, 2013; Subramanya and Awasthy, 1972; Raju et al., 1979; Cheong, 1991; Singh et al., 1994; Swamee et al., 1994; Borghei, 2003]).

Considering the second method, a large number of studies has been performed that all aim at correctly representing the discharge coefficient for specific weir types. An overview of the most important studies is provided in appendix section A.4 and summarized in table A.2. The different experiments still present a limited experimental range, especially limited for increasing weir lengths and water depth to crest height ratio. The result is that most of the formulations also do not (completely) resemble the dimensions given by the longitudinal training dams in the Waal. For instance, the crest height to length ratio in Singh et al. [1994] and Keshavarzi [2014] is much larger than is the case at the longitudinal training dams. Also, the crest height is often not directly included in the formulas and in most older literature only the dependence on the upstream Froude number is considered. This also does not include the local variations of the Froude number over the weir as discussed by [Hager, 1987]. Therefore, the first method of plain weir correction factors, as given by Hager, will be used in this research and is treated in more detail below.

Plain weir coefficient

The weir coefficient for plain weir has been well studied and is treated in many articles and books, including Bos [1976], Ackers et al. [1978], and Tracy [1957]. In accordance with many experiments, the plain weir coefficient shows to vary according to a number of dimensionless parameters describing the geometry and flow conditions at the considered weir. The influence of a large number of dimensionless parameters on the plain weir coefficient has been studied. A first distinction that is often made relates to the type of weir that is characterized by the ratio of energy level above the inlet over the crest width ($\frac{H-w}{B_w}$). With help of this ratio, weirs can be categorized into broad-, short-, or sharp-crested weirs. According to the categorization by Bos [1976], the inlet and openings at the longitudinal training dams are in the transitional region between short-crested for low weir heights and broad-crested for crest heights reaching the water level (W>0.9). The proposed formulation of the discharge coefficient by Raju et al. [1979] for weirs becoming broad-crested is:

$$C_d = 0.8(1 + \frac{H_0 - w}{8 * B_w})C_{d,0} = c * C_{d,0} \tag{2.10}$$

where C_d is the general discharge coefficient, $C_{d,0}$ the modular plain weir coefficient for sharp-crested weirs, B_w the crest width, and c is the geometry correction factor. Figure 2.7 shows the theoretical evolution of C_d for different values of B_w. A constant value for $C_{d,0}$ of 0.61 is used that was found by Subramanya and Awasthy [1972] and is in good agreement with Ackers et al. [1978] and Borghei [2003]. It must be noted, however, that C_d is found to also depend on other geometric dimensions and head correction factors. This is not considered significant in relation to the geometry correction factor and not treated in more detail (reference is made to literature, such as Ackers et al. [1978], for more details).

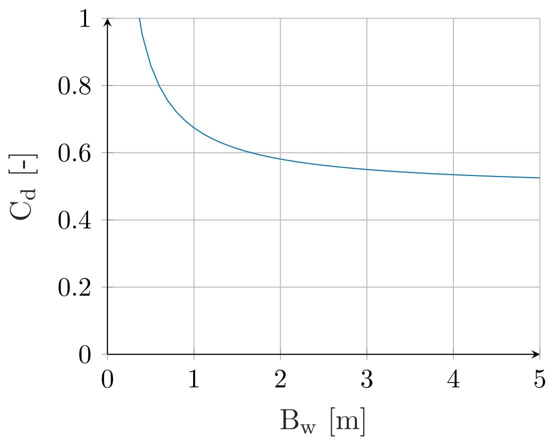

Figure 2.7: Theoretical discharge coefficient (C_d) for different crest widths (B_w) for $H_0 = 6.5$ and $w = 3$ m

Reduction of plain weir coefficients

In the analysis of lateral flow over side weirs, Subramanya and Awasthy [1972] were among the first to consider side weir flow by including a deflection coefficient in the formulation for plain weirs that takes into account the lateral outflow angle (ϕ) over a side weir. A definition of the lateral outflow angle is shown in figure 2.8. This concept is somewhat similar to the streamline angles over oblique weir as discussed by Ali [2013] and treated in appendix A. Subramanya and Awasthy argued that the lateral outflow angle for side weirs can be approximated by:

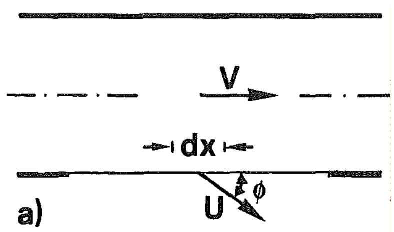

Figure 2.8: Lateral outflow angle [Hager, 1987]

$$sin(\theta) = sqrt(1 - \frac{v_i}{v_j}^2) \tag{2.11}$$

By noting that $Fr = U^2/(g * h)$, Subramanya and Awasthy [1972] proposed a side weir equation on the basis of the upstream Froude number as shown by equation 2.12 and figure 2.9.

$$sin(\theta) = \sqrt{1 - \frac{3Fr_0^2}{2 + Fr_0^2}} \tag{2.12}$$

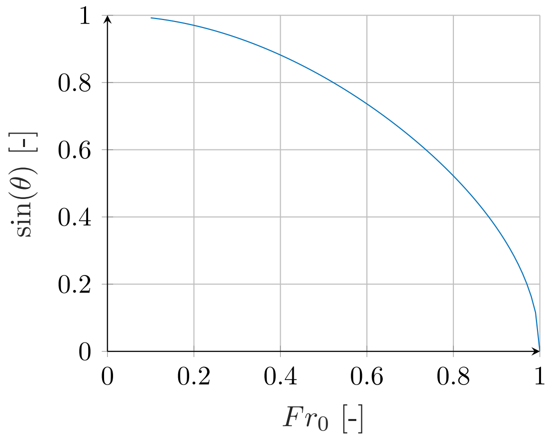

Figure 2.9: Relation between the deflection coefficient for side weirs ($\sin(\theta)$) and the upstream Froude number (Fr_0) [Subramanya and Awasthy, 1972]

In their paper, Subramanya and Awasthy [1972] verified the lateral outflow coefficient in experimental conditions with upstream numbers ranging according to table 2.3 and for zero crest height. They noted that for Froude numbers reaching critical flow and larger, the discharge coefficient is expected to be independent of the upstream Froude number as the "zone of influence will be confined to the flow region in the immediate neighbourhood of the weir". For Froude numbers above the value of 2, they concluded the following relationship:

$$C_d = 0.36 - 0.08 * Fr_1 \tag{2.13}$$

It can be seen that the water level to crest length ratio is considerably smaller for the longitudinal training dams in the Waal than in the experimental conditions.

Table 2.3: Overview of investigated parameters by Subramanya and Awasthy [1972] in relation to the conditions at the longitudinal training dams in the Waal (LTD Waal)

Parameter	**Symbols**	**Experimental range**	**LTD Waal**
Froude number	Fr_0	0.02 - 4.3	0.1 -1.2
Crest length / channel width	L_w/B_w	0.2 - 1.0	0.56
Crest height / water level	w/h	0.2 - 0.96	0.0 - 1.0
Water level / crest length	h/L_w	0.1 - 2.4	0.01

Hager [1987] extended the concept of adjusting the standard weir equation with a lateral coefficient for side weirs. Hager adjusted equation 2.12 to account for variable crest height and "local variations of the Froude" number, instead of using the Fr_1 and thus assuming "no significant change of Fr along the lateral outflow length" Hager [1987]. This resulted in equation 2.14 for the average cross-sectional lateral outflow angle.

$$sin(\phi) = [\frac{y - W}{3 - 2y - W}]^{\frac{1}{2}} \tag{2.14}$$

where y is the relative water level measured above the bed ($y = h/H$), W is the dimensionless crest height ($W = w/H$) and H is the energy head. From figure 2.10a it can be seen that for larger weir heights, the lateral outflow coefficient ($sin(\phi)$) decreases. This can be explained by a lower water depth above the weir crest that draws less water in (q $(h-w)$). A larger y value, in turn, results in an increasing angle. This can be explained by the fact that a large y value refers to a lower lateral velocity head and the flow thus having a smaller tendency to continue in longitudinal direction and being deflected more easily. When y approaches 0, a plain weir situation is simulated and $sin(\phi)$ and ϕ converge to 1 and 90 degrees respectively, as shown in figures 2.10a and 2.10b.

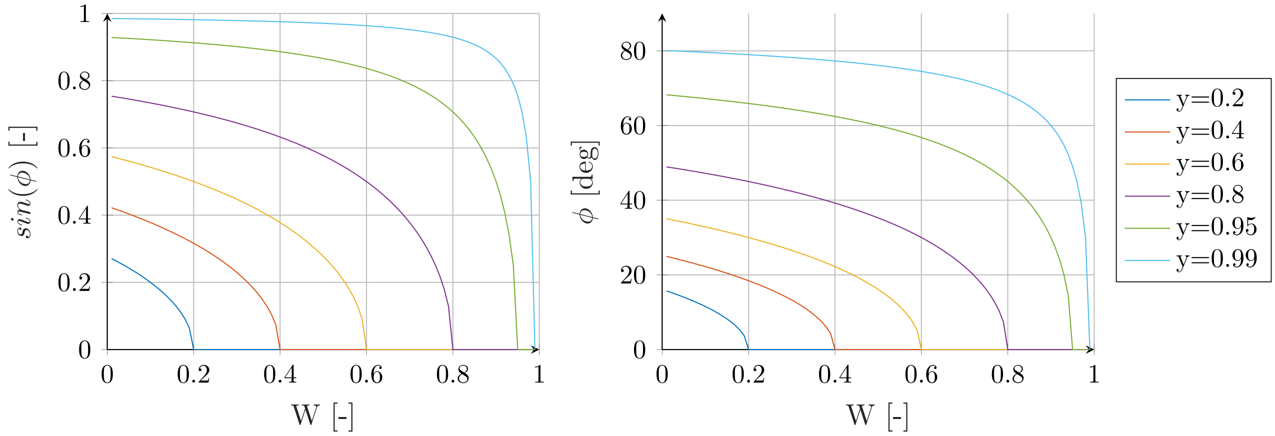

(a) Deflection coefficient

(b) Lateral outflow angle

Figure 2.10: Theoretical outflow angle (ϕ) and deflection coefficient ($sin(\phi)$) as function of the dimensionless crest height ($W = w/H$) and dimensionless water level measured above the bed ($y = h/H$) for free-flow conditions

Hager also included coefficients for the impacts of flow depth ($q(H) \rightarrow q(h)$), approach velocity (ω_U), and contraction angle (ω_Θ). These coefficients are then multiplied with a geometry and modular weir coefficient for plain weirs ($cC_{d,0}$) to achieve a side-weir discharge coefficient. The resulting equation is given by equation 2.15, which is the result of applying all correcting factors to equation A.16. The complete derivation of the different coefficients is described in more detail in appendix A.4.

$$\begin{aligned} q_{w,side} =& \omega_U \omega_\phi \omega_\Theta c C_{d,0} \sqrt{2g}(H_0 - w)^{3/2} \\ \text{where } \omega_U =& [\frac{1-W}{y-W}]^{1/2} \\ \omega_\phi =& sin(\phi) = [\frac{y-W}{3-2y-W}]^{\frac{1}{2}} \\ \omega_\Theta =& (1-(\theta+i_b)[\frac{3(1-y)}{y-W}]^{\frac{1}{2}}) \end{aligned} \tag{2.15}$$

where h is the water level, y is the relative water level ($y = h/H$), W is the relative weir height ($W = w/H$), H is the energy head, θ is the tangent of the width contraction angle, i_b is the bed level gradient, c is a geometry correction factor and $C_{d,0}$ is a plain weir coefficient. Figure 2.11 shows the influence of dimensionless weir height ($W = w/H$) on the lateral flow coefficients for different relative water levels ($y = h/H$).

When combining all lateral flow coefficients, a combined ω is formed as shown by equation 2.16. The combined effect of the dimensionless crest height on ω is shown in figure 2.11d.

$$\omega = [\frac{1-W}{3-2y-W}]^{\frac{1}{2}}(1-(\theta+i_b)[\frac{3(1-y)}{y-W}]^{\frac{1}{2}}) \tag{2.16}$$

When combining ω with the general weir formula, the new side-weir equation is created as given by equation 2.17.

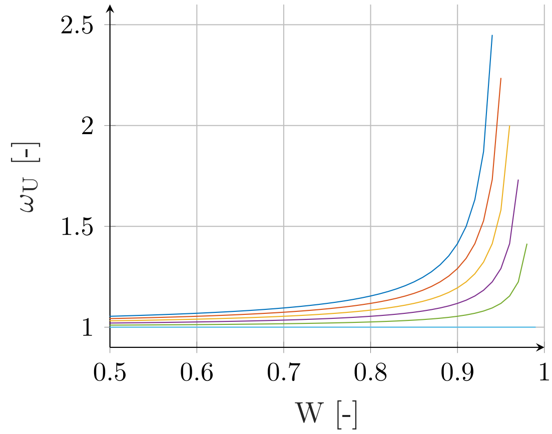

(a) ω_U

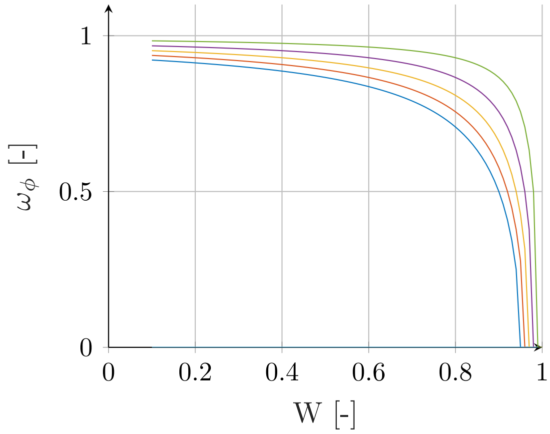

(b) ω_ϕ

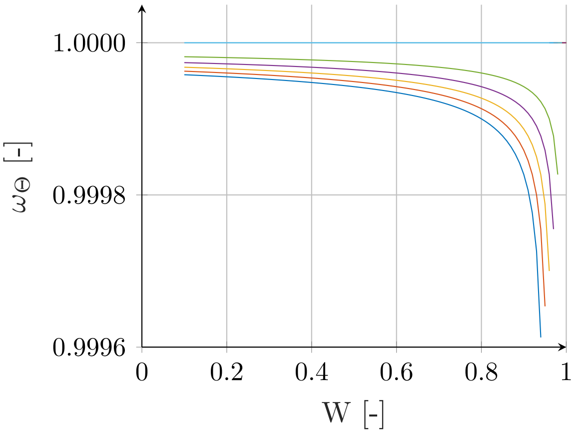

(c) ω_Θ

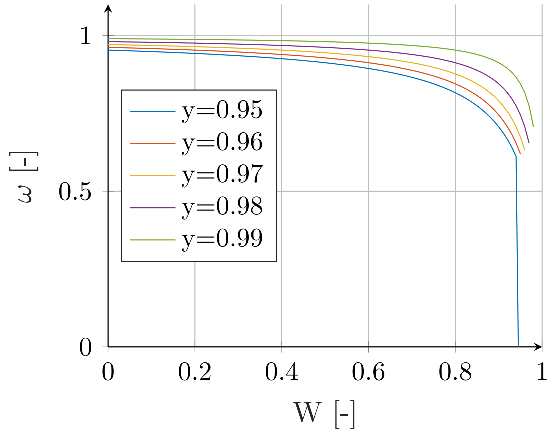

(d) Comined ω factors

Figure 2.11: Influence of the dimensionless crest height ($W = w/H$) and dimensionless water level ($y = h/H$) on the side weir correction factors (ω)

$$q_w = [\frac{1-W}{3-2y-W}]^{\frac{1}{2}}(1-(\theta+i_b)[\frac{3(1-y)}{y-W}]^{\frac{1}{2}})cC_{d,0}\sqrt{2g}(h-w)^{3/2} \tag{2.17}$$

Hager validated the above equation with the help of experiments with a large range of Froude numbers (0.3 - 2) and weir dimensions as shown in the table below. As shown in figure 2.11, the influence of the contraction angle and bed level gradient are negligible with regard to the other coefficients [Hager, 1987] and will therefore be neglected in future calculations.

Table 2.4: Overview of investigated parameters by Hager [1987]

Parameter	**Symbols**	**Experimental conditions**	**Waal conditions**
Crest length / channel width	L_w / B_{main}	0.33	0.56 - 0.75
Crest height / water level	w / h	O(0-0.5)	0.0 - 1.0

Submergence coefficients

As discussed before, the submergence coefficient (C_s) is a coefficient that allows for weir discharges to also be determined in transitional and submerged conditions (see figure A.11). A general formula to determine C_s for flow over plain weirs was introduced by Villemonte [1947]. In the generalized form, the submergence coefficient is influenced by the channel geometry and the level of submergence according to equation 2.18.

$$C_s = \sqrt{1 - S^P} \tag{2.18}$$

$$\text{where } S = \frac{H_2 - w}{H_0 - w}$$

where P is an exponent depending on the weir geometry and S is the submergence factor. The submergence coefficient for oblique weirs is evaluated by Borghei [2003] and discussed in appendix A.4.2. The submergence coefficient for side weirs has been investigated with the help of thirty-five tests for submerged flow over a side weir at the Center for Research in Water Resources in Austin (CRWR). These projects are discussed by Tynes [1989] and Ka-Leung Lee [2002]. The determined side weir submergence coefficient, as given by equation 2.19, deviate slightly from the general submergence formula (equation 2.4.2). The presented formulas for plain (Villemonte), oblique (Borghei) and side (Ka-Leung) weirs are shown in figure 2.12, in which the general plain weir equation is plotted for several arbitrarily chosen P exponents. It can be seen that the C_s value for the side weir formula stays very close to 1 for submergence values up to 0.7. Thereafter it drops to 0 much quicker than is the case for the general submergence coefficient formula by Villemonte.

$$\begin{aligned} C_s &= 1 && \text{for } 0.0 < S < 0.5 \\ C_s &= 1 - 28.84(S - 0.5)^{4.85} && \text{for } 0.5 < S < 1.0 \end{aligned} \tag{2.19}$$

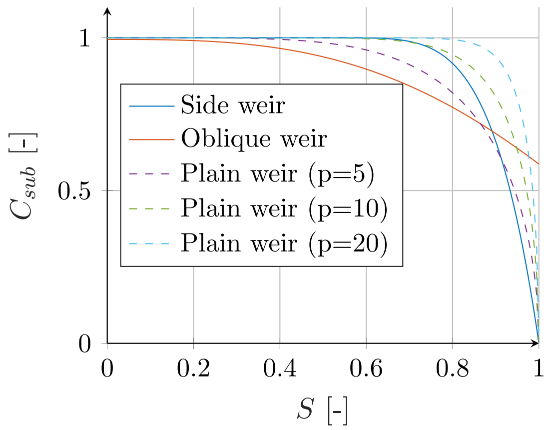

Figure 2.12: Submergence coefficients (C_s) from literature for plain, oblique, and side weirs as function of the submergence factor (S)

The lateral outflow angle, as previously presented in figure 2.10b, does not hold anymore for transitional and submerged flow conditions. The submergence coefficient that transforms the calculated discharge for free-flow conditions to submerged conditions can be seen as a type of adjustment to the lateral outflow angle and weir velocities. It must be noted that combining equations 2.14 and 2.19, as shown in figure 2.13a, will thus not directly result in an adapted lateral outflow angle as adjustments for the velocities at the weir crest are also included in the submergence coefficient.

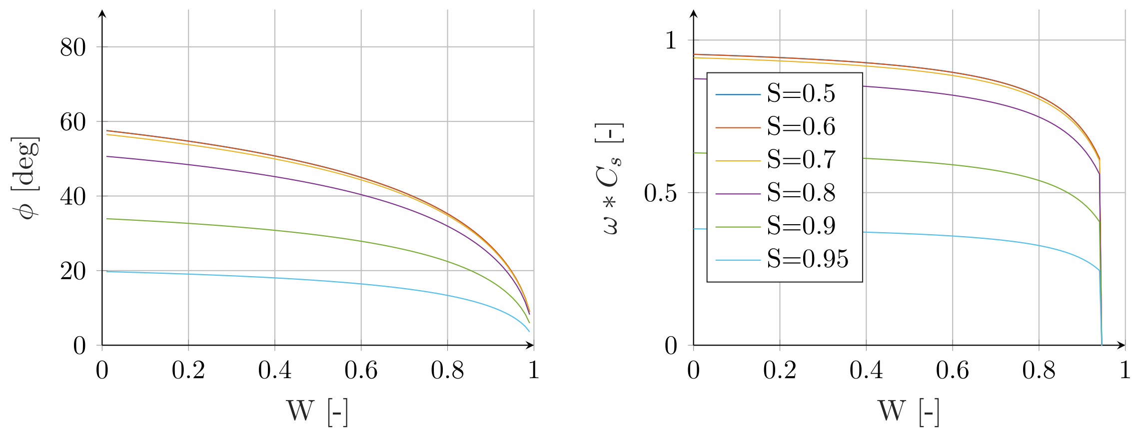

(a) Lateral outflow angle

(b) $\omega * C_s$

Figure 2.13: Lateral outflow angle (ϕ) and side weir coefficients ($\omega * C_s$) as function of the dimensionless crest height ($W = w/H$) and the submergence factor (S)

Combining the different lateral flow coefficients (ω) and the submergence coefficient C_{sub} presents the total effects on the discharge over the weir for the transformation of free-flowing plain weirs to submerged side weirs. Figure 2.13b presents the influence of the dimensionless crest height, given different submergence factors and $y = 0.95$. It can be seen that an increasing S, as well as an increased crest height W, result in a smaller combined submerged discharge coefficient ($\omega * C_s$). However, it can also be seen that if W decreases, the combined discharge coefficient ωC_s can still increase in combination with an increasing S. Because the level of submergence is also affected when adjusting the crest height ($S = (H_{main} - w)/(H_{side} - w)$), the lateral weir discharge will in physical situations probably not be decreasing precisely along one of the lines as shown in the figure.

2.4.3 Schematization in model of river systems

To analyse the impacts of longitudinal training dams on a full river scale, use can be made of larger models of river systems such as the DVR models. Problems arise when incorporating small-scale features, because "scientific and engineering computation has become so complex that traditional numerical computation on uniform meshes is generally not possible or too expensive" [Bern et al., 1999]. To solve this problem, two methods have been developed over the years. These include special techniques that locally decrease the grid size and the parameterization of hydraulic structures as subgrid features. Decreasing the grid size allows for calculations with the use of a defined bed topography on grid size level where subgrid structures allow for manually assigned reduction coefficients to specific grid cells.

1. **Calculation on bed topography:** when calculations are performed on grid level, the local bed topography is used to schematize structures and bed features. This means that a river intervention (or hydraulic structure) is schematized by locally adjusting the bed topography. Widely used modelling software allow grid cells to be locally refined such that small structures or features can be imposed onto the bed topography. In order to do so, parts of a grid structure are replaced by a grid mesh of finer grid size. This allows for advanced techniques to decrease grid sizes, compared to other software programs. As an alternative to refining or replacing parts of a grid mesh, the latest version of the Delft3D software package (D-Flow Flexible Mesh) allows the use of a flexible grid. In this case, the grid mesh can be altered in any way or location needed, provided that the grid meets some criteria that include those of smoothness of grid cells and limited deformation. This will not be treated in this research.

Care must be taken with applying grid refinement in models. Firstly, because refinement can result in unwanted numerical errors (truncation or inherited errors). At places where grid refinement is applied, numerical errors will be generated due to the rough transition in grid size. These errors are acceptable for small refinements but increase with increasing level of refinement. Secondly, refining a grid results in the rapid increase of required computational power. In larger river models, grid refinement can only be applied until a certain level after which calculations become too computationally expensive. A grid should thus only be refined when the use of a larger grid would result in insufficient detail or incorrect representation of the flow characteristics. Several validation tests have been carried out on the level of detail required for the modelling of plain obstacles in a river [Deltares, 2008]. However, these validation tests have not been found for laterally orientated obstacles, as is the case in longitudinal training dams.

2. **Subgrid structures:** subgrid structures parameterize the effects of hydraulic structures within the dimensions of a grid cell. These subgrid structures use the flow conditions and geometrical dimensions to empirically calculated the values of the parameterization. The flow conditions are calculated similarly to a regular Delft3D-Flow computation using bed topography. Figure 2.14 shows the subgrid structures by the thick lines that can either be defined in v- or u-velocity direction (shown in the left and right figure respectively). The location of water level points (+), depth points (•), and velocity points (| and ˘) are also shown. The geometrical dimensions for the weir are provided in the form of a crest height. For such a weir, the Delft3D-Flow modelling software calculates the discharge over a weir structure by parameterizing an additional energy loss term in the momentum equation.

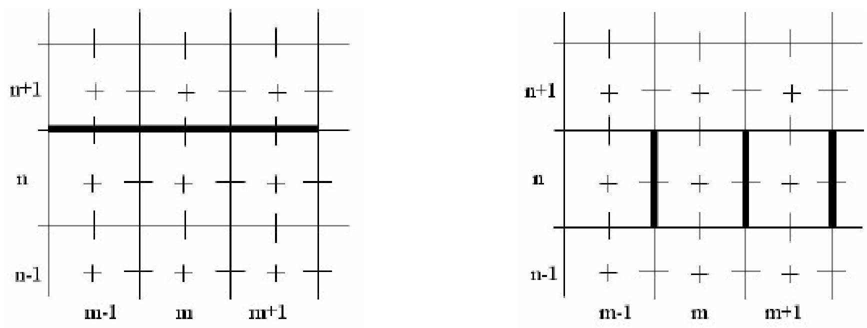

(a) v-direction **(b)** u-direction

Figure 2.14: Staggered grid with subgrid structures in Delft3D-Flow [Deltares, 2014]

However, at the start of this research, it was found that the discharge over a weir structure is not calculated correctly. The calculated energy loss seems to not be influenced by the assigned weir crest heights. Additionally, problems arise as this method does not model the impacts on the flow patterns (flow angles over the crest) nor the transport of sediment correctly. The incorrect modelling of sediment transport has been mentioned by Mosselman [2001] and investigated for side channels by Vuik [2010]. Vuik recommended the inclusion of an additional parameter that relates the discharge distribution between the main and side channel to the sediment distribution. Vuik suggested to numerically change the weir crest height in the model to influence the discharge distribution and thereby the sediment distribution. When adjusting the weir crest height numerically, however, problems arise when hydraulic conditions are also of importance as mentioned in section 2.2. The lack of parameterization for flow angles atop the weir crest means that the flow angles and velocity magnitudes atop subgrid weirs in the Delft3D-Flow model runs are not influenced by the user defined dimensions. These are important aspects to determine the sediment transport towards the side channel and the associated morphological development of the system of longitudinal training dams correctly.

A limitation of applying calculations on grid level is the large computational time and the difficulty of quickly analysing different dimensional designs of hydraulic structures. Especially for calculations on a larger or complicated grid mesh, adjusting design dimensions becomes very time-consuming. Also, when using the above-mentioned two-dimensional software programs Waqua and Delft3D-Flow, it can proof to be difficult to distinguish the relative influence of different mechanisms and factors from other physical or numerical effects. When only considering hydraulics, the use of subgrid weirs provides useful insights. In Delft3D-Flow software, however, the hydraulic nor morphologic conditions over subgrid weirs are modelled correctly. Also, there is no capability to assign specific side weir coefficients to subgrid weirs.

2.5 Conclusions

Considering the different intended improvements of river functions by longitudinal training dams, the mechanisms and factors influencing the transportation of water and the resulting discharge distribution and flow patterns between the main and side channel play an important role. Better insight into the mechanisms and factors is crucial to understanding the discharge distribution and influence of regulation strategies. Additionally, both the impacts on the scale of a single inlet or opening, as well as on the reach scale are important to analyse the influence on the different river functions.

The inlet and openings of longitudinal training dams are found to be well schematized by side weirs. The flow patterns of these structures are well studied and can provide useful insight of a two-channel system connected by inlets or openings. Studies on side weir flow in submerged conditions have been conducted in fewer quantities but can still be found. However, not all physical aspects of submerged weir flow are fully understood yet and calculations still require empirical discharge coefficients. Detailed flow patterns around side-weirs can thus not be computed with the help of these weir formulations, but they do provide useful insights and are suitable to analyse mechanisms, factors and control strategies influencing discharge distributions for a system of longitudinal training dams.

Studying large-scale impacts of river interventions is mostly performed with the help of numerical modelling programs Delft3D-Flow and Waqua. They provide the ability to schematize the system of longitudinal training dams either as part of the bed topography (with grid alteration techniques) or as subgrid weirs. Both present difficulties and uncertainties that will be studied in more detail in this research.

Chapter 3: Methodology

3.1 Introduction

To help answer the research questions, use is made of two different models. The first is a one-dimensional model that is specifically created for this research. This model is built from scratch using the Matlab software programming tools and uses the empirical relationships for side-weirs as described in chapter 2. The second model is a two-dimensional hydrodynamic model in the existing Delft3D-Flow hydro-morphodynamic modelling software. The two models are first explained shortly, after which the methodologies used to answer the different questions are presented in this chapter.

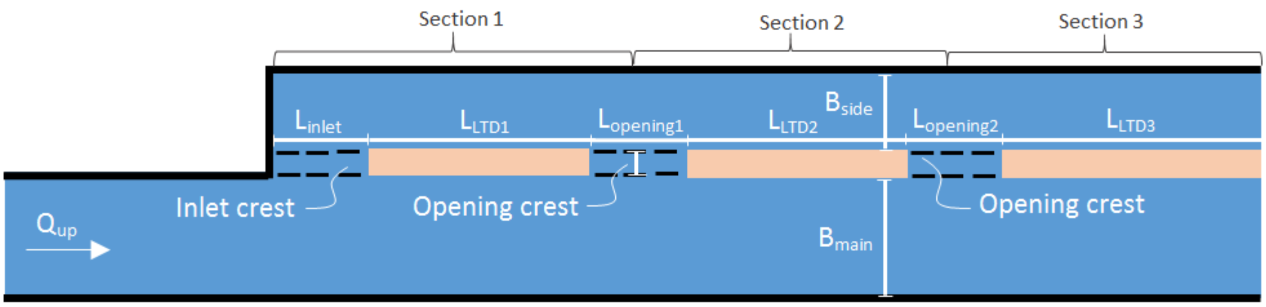

Figure 3.1: Overview of longitudinal training dam schematization

It is important to note that in this research, only dimensions similar to the specific conditions in the pilot project near Wamel are used (see figure 3.1). The parameters are provided in table 3.1. Some parameters are presented in the dimension m +NAP, which refers to metres above 'Normaal Amsterdams Peil'. This is a vertical datum as used in the Netherlands.

Table 3.1: Overview of the input parameters for the pilot project in the Wamel

Parameter	**Symbol**	**Value**	**Dimension**
Number of openings	-	2	-
Main channel width	B_{main}	230	m
Side channel width	B_{side}	90	m
Dam lengths	$L_{LTD1,2,3}$	350, 670, 1530	m
Inlet and opening length	$L_{inlet,opening}$ (L_w)	200	m
Inlet crest height:	w_{inlet}	0.6	m +NAP
Opening crest heights	$w_{opening}$	4.6 and +3.5	m +NAP
Bed elevation side channel	$elevation_{side}$	0.0	m
Upstream discharge	Q_{up}	2000	m^3/s
Side channel length	L_{side}	3100	m

3.2 Models

The one-dimensional model is used to provide insights into the relevant mechanisms and factors influencing the discharge distribution between the channels. Also, the effects of different the control strategies are considered. The Delft3D-Flow modelling software is used for a more detailed analysis of the flow patterns around the inlet and openings, that includes the most relevant processes as found by the one-dimensional model. With help of the Delft3D-Flow model, also the modelling of longitudinal training dams in large-scale models is investigated. The main differences between the two models are summarized in table 3.2. The two model set-ups are shortly discussed below and for a more elaborate description, reference is made to appendices B and C.

Table 3.2: Model approach comparison

Category	**1D model**	**Delft3D-Flow model**
Water levels	1D backwater curve	2D mass and momentum balance
Inlet schematization	Empirical relationship	Bed topography / Subgrid weirs
Weir discharge	1D weir equation	2D mass and momentum balance
Porous transport	Constant permeability	Not included

3.2.1 One-dimensional model

The one-dimensional model is specifically created for this research and built from the ground up. In this model, the system of longitudinal training dams is approximated with help of a network of branches and nodes as shown in figure 3.2. The model makes use of the empirical relationships for side weirs, as found in literature and discussed in chapter 2, to calculate the discharges between the two channels. The one-dimensional model is iteratively run until it converges towards a steady-state solution for a given upstream discharge and several dimensional parameters. The one-dimensional numerical model is created with the help of Matlab as this mathematical program provides useful tools to efficiently integrate the large number of (numerical) calculations required. This section will shortly discuss the model set-up. A more extensive description of the one-dimensional model, including an elaborate model set up and overview of consistency tests and the sensitivity analysis, can be found in appendix B.

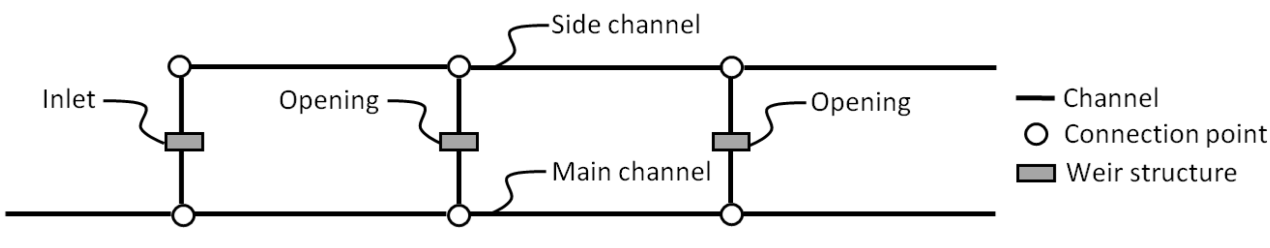

Figure 3.2: Overview of the one dimensional model schematization including inlet

Calculations

The river channels in the model are uniform and depth- and width-averaged. As input for the empirical weir formulations, the one-dimensional model uses backwater curve equations to provide the required flow conditions at the inlet and openings, as shown by the model outline in figure 3.3. The backwater curves are calculated with the help of a numerical implicit predictor-corrector scheme as shown in equation 3.1.

$$d_{s+1} = d_s - 0.5 * (\frac{\mathrm{d}d}{\mathrm{d}s}_{pred} + \frac{\mathrm{d}d}{\mathrm{d}s}_{corr}) * \mathrm{d}s \tag{3.1}$$

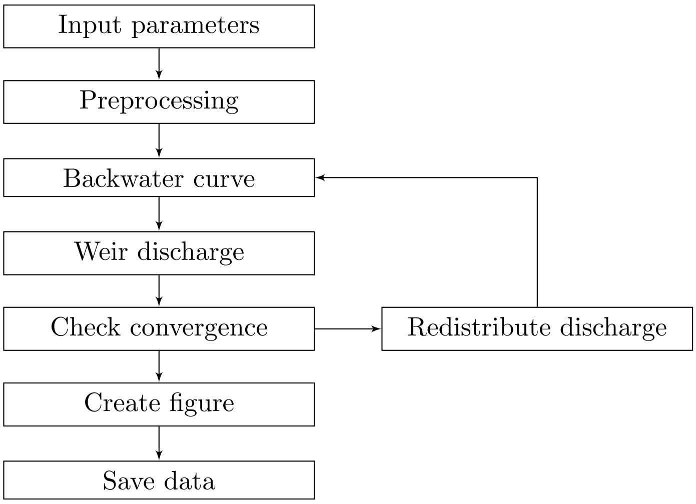

Figure 3.3: One-dimensional model outline

$$\text{where } \frac{\mathrm{d}d}{\mathrm{d}x}_{pred} = \frac{i_b - \frac{q^2}{C^2 d_x^3}}{1 - \frac{q^2}{9.81 h_x^3}}$$

$$d_{pred} = d - \frac{\mathrm{d}d}{\mathrm{d}x}_{pred}\mathrm{d}x$$

$$\frac{\mathrm{d}d}{\mathrm{d}x}_{corr} = \frac{i_b - \frac{q^2}{C^2 h_{pred}^3}}{1 - \frac{q^2}{9.81 h_{pred}^3}}$$

where d_s and d_{s+1} are the water depth in the channel centre at location s and $s+1$, $\mathrm{d}h/\mathrm{d}s$ is the water level slope and $\mathrm{d}s$ is the space step in a curvilinear orthogonal $s,n-$coordinate system. This coordinate system uses the channel centre line to define the $s-$coordinate with the $n-$coordinate transverse to this [Merwade et al., 2005]. This allows easy representation of curved channels in a one-dimensional model. The actual weir discharge is thereafter calculated with the side weir equation as previously discussed in 2. When combining the general side weir formula with the plain weir coefficients and the lateral correction coefficients, equation 3.2 is found.

$$Q_w = L_w[\frac{1-W}{3-2y-W}]^{\frac{1}{2}}[0.8*(1+\frac{H_0-w}{8*B_w})]C_{d,0}C_s\sqrt{2g}(h_0-w)^{3/2} \tag{3.2}$$

where L_w is the crest length in longitudinal direction, w is the crest height, H_0 is the energy level upstream, h_0 is the water level upstream, y is the relative water level ($y = h_0/H_0$), W is the relative crest height ($W = w/H$), $C_{d,0}$ is the modular plain weir coefficient, c is the geometry correction factor and C_s is the submergence coefficient. The submergence coefficient transforms the weir equation from free to transitional flow conditions (see section 2.4.1). Figure 2.6 shows the definitions for the above-mentioned parameters. The model is run with several iteration loops in which the discharges in the two branches are adjusted for the next iteration step.

River bend

The above equations are valid for a straight channel without any curvature. To include a bend radius and the resulting differences in length between the main and side channel, the space step $\mathrm{d}s$ can be adjusted for the side channel. This method is applied to ensure that the inlet and opening locations in both channels still align. The side-channel bend radius is corrected with help of the following equation:

$$r_{side} = r_{main} - 0.5(B_{main} + B_{side}) \tag{3.3}$$

where r_{main} and r_{side} the main and side-channel bend radius and B_{main} and B_{side} the respective channel widths. The bend radius is kept constant in downstream direction, meaning that an equal bend radius is considered for the entire river section. The space step ds for the side channel is converted using the following formula:

$$\mathrm{d}s_{side} = \mathrm{d}s_{main}\frac{r_{side}}{r_{main}} \tag{3.4}$$

where ds_{main} is the space step in the main channel and ds_{side} the space step in the side channel. This is illustrated in figure 3.4.

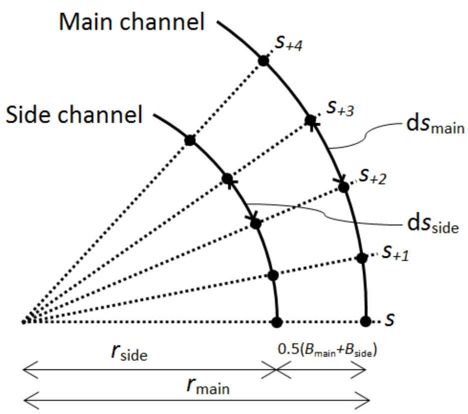

Figure 3.4: Schematization of the coordinate system used in the one-dimensional model

Model configurations

Several parameters can be defined in the model. These parameters are described by one value for an entire branch. The bed level in the channels is not, by definition, equal in both channels. Therefore, a value can be defined that uniformly elevates the bed level in one river branch. In addition, the number and dimensions of the different openings need to be defined. For the discharge calculations, different weir coefficient formulations and permeabilities can be defined. Also, several parameters can be adjusted that influence the numerical, iteration and convergence calculations. At last, the initial conditions need to be defined and the different mechanisms and factors can be included or excluded in the calculations. Figure B.4 shows the graphical user interface created for the one-dimensional model, in which the most important parameters as discussed above can be defined.

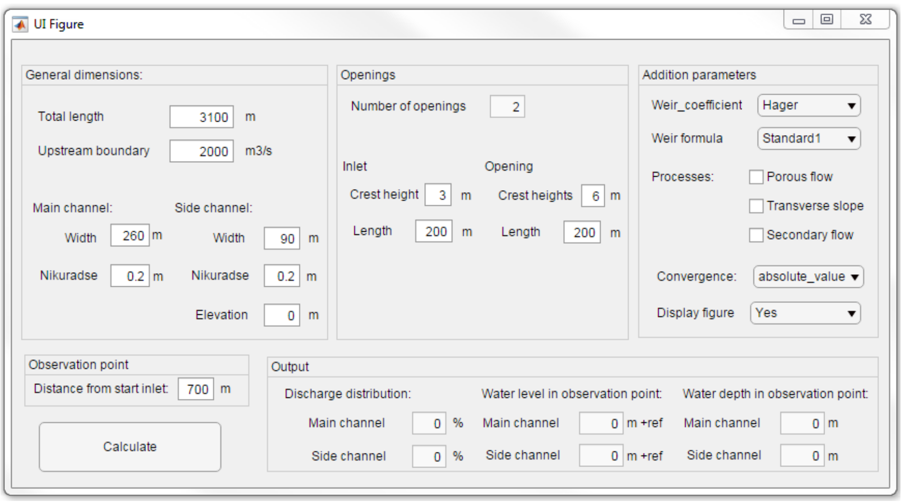

Figure 3.5: One-dimensional model GUI outline

Figure 3.6 is a visual representation of the model outcome from the one-dimensional model that is created after each model run. In the top left subfigure, the calculated backwater curves (continuous lines), bed levels (striped lines) and equilibrium water levels (dotted lines) are plotted. The main channel is represented by the blue lines and the side channel by the red lines. The subfigure below presents the difference in calculated water levels and the overview subfigure on the right side provides a top view of the project area and shows the calculated discharge distribution between the two channels.

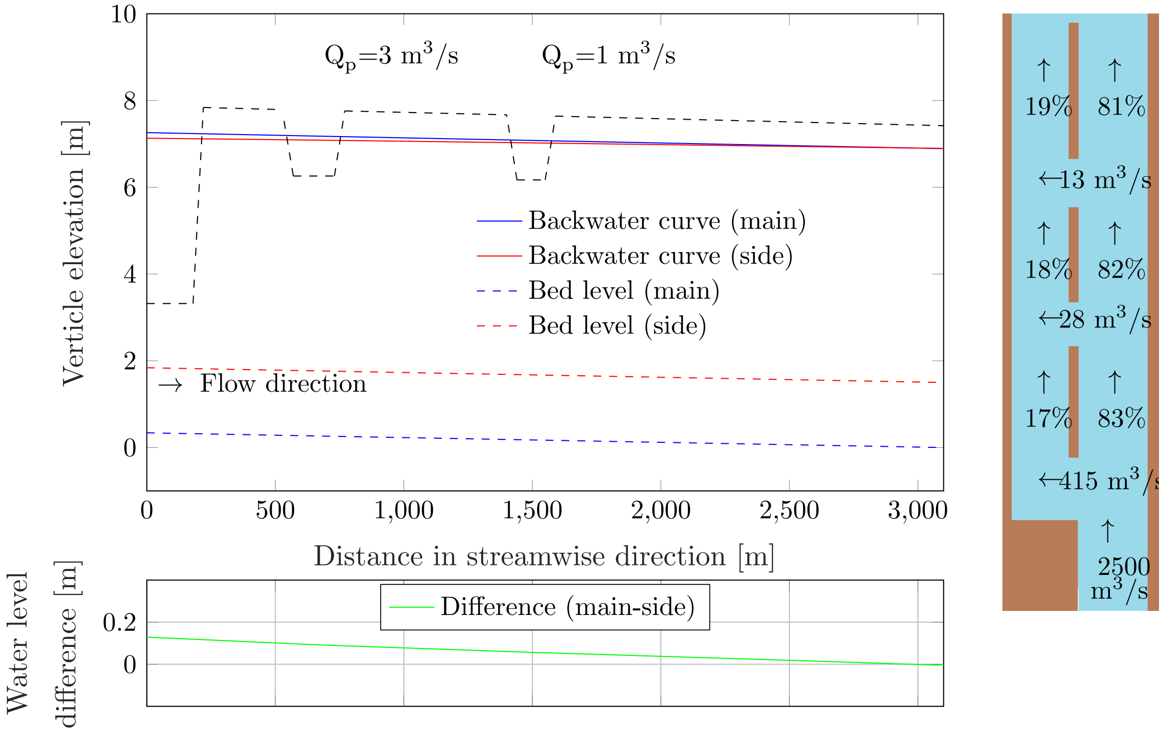

Figure 3.6: Preview of output figure created by the one-dimensional model

3.2.2 Two-dimensional model

The two-dimensional model is made with the help of the Delft3D-Flow modelling software. This is a numerical hydrodynamic modelling program that uses the Navier-Stokes equations to calculate flow conditions on a rectangular or curvilinear grid. The newer version of Delft3D-Flow also considers unstructured grids, which will not be treated in this research. Further explanation of Delft3D-Flow is given in appendix A and in the associated user's and technical reference manuals [Deltares, 2008].

Two models are created in Delft3D-Flow. The first is a representation of only the first inlet opening. This including 400 m before and 500 m after the inlet to ensure a uniform flow from upstream direction and enough length to evaluate the effect downstream of the inlet, as shown in figure C.1. In horizontal direction, a rectangular grid of 105 by 330 cells is used with grid sizes of dM=3.33 m by dN=3.33 m. In vertical direction, only a single layer has been defined (resulting in a 2DH model). In a later stage, a second model is created by extending the first model in downstream longitudinal direction by an additional 2000 m (total of 3500 m) to a grid size of 105 by 1050 grid cells. Two openings are included in downstream direction, that are similar to the inlet. Thereby an entire section of longitudinal training dams is schematized that will be used to further investigate the system of longitudinal training dams.

Model set-up

A bed topography is schematized over the grid mesh in which the longitudinal training dams are included as raised bed levels until a crest heights of 7 m above the initial local bed. Side slopes are

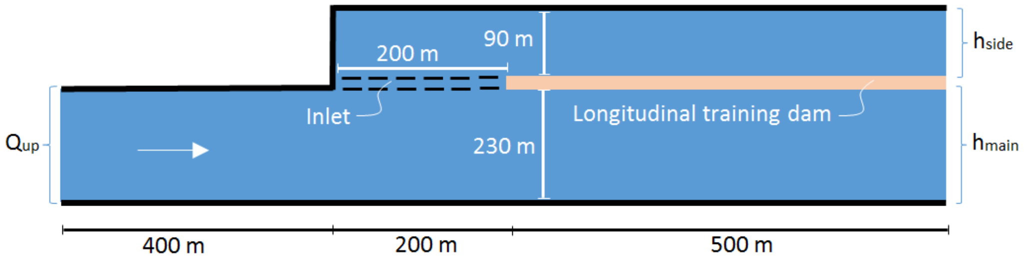

Figure 3.7: Short two-dimensional Delft3D-Flow model schemetization (top view)

imposed with a 1:2.5 slope (see figure C.3). A longitudinal bed slope of $i_b = 10^{-4}$ is also included in the bed topography. As boundary conditions, a total discharge is assigned to the upstream boundary, a water level boundary at the downstream side of both the main and side channel. The combination of these downstream water level boundaries provides the ability to set the submergence factor in the 'small' model as explained in equation 2.4.2 and equal downstream water levels in the 'large' model. A uniform initial condition of 6.5 m has been applied that closely matches the boundary conditions to minimize the model's spin-up time. In later model runs, a restart file is used, as created by previous runs, to minimize the required spin-up time. A grid size of 3.3 by 3.3 m is used in order to ensure a reasonably detailed representation of the longitudinal training dams. The time step has been chosen such that a CFL criterion conditions relating to a Courant number of 1 is satisfied. The CFL condition is given by equation C.1.

$$C = \frac{\Delta t u}{\Delta x} < 1 \tag{3.5}$$

where C is the Courant number, Δt is the time step, Δx the grid size and u the maximum velocity in the simulation. Considering the chosen grid sizes and maximum velocities around 2 m/s, a time step of 0.02 min is used. As will be discussed in the following chapters, for a flood scheme and large crest heights a smaller time step of 0.005 min is required. Water level boundaries of $h_{side} = 6.39$ and $h_{side} = 6.47$ m +bed level are used. These values are obtained from the one-dimensional model at a distance of 500 m from the downstream end of the inlet for a crest height of 3 m + bed level. These boundary conditions are kept constant to compare the different model results. A constant upstream discharge boundary of $Q_{up} = 2000$ m^3/s is used.

Inlet and opening schematization

As mentioned before in chapter 2, there are two ways of including the inlet and openings in a two-dimensional model: either by schematization within the bed topography or as a subgrid weir. Both methods are evaluated and briefly discussed below.

Bed topography

The inlet and openings can be schematized by elevating grid cells within the initial bed topography. For this purpose, the bed has been elevated to the required crest height. Side slopes of 1 : 2.5 on both sides are also included, as shown in figure C.3. The crest is defined with a minimum of 2 data points to prevent strange numerical phenomena (such as unreasonable water levels and velocity magnitudes) at the crest.

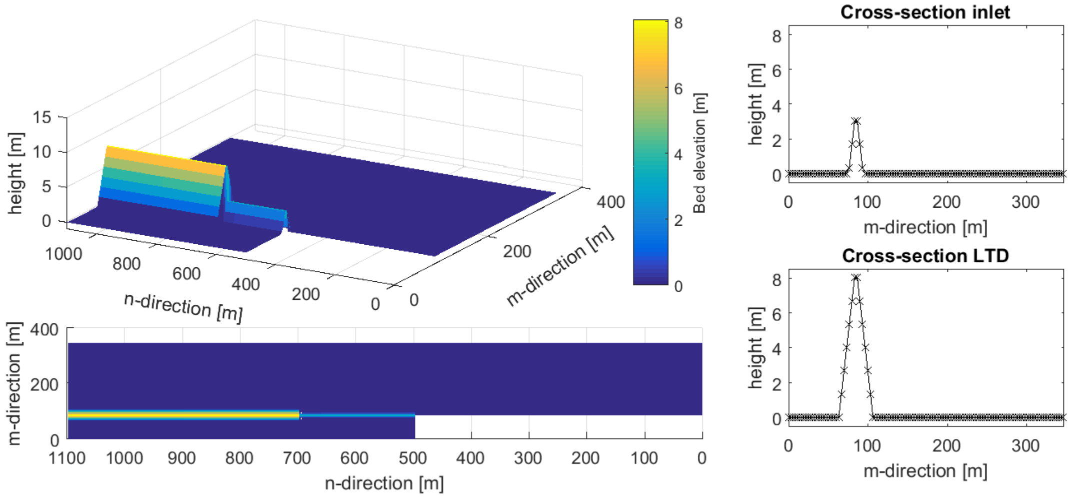

Figure 3.8: Two-dimensional model schematization of inlet crest in bed topography

Subgrid weirs

To evaluate the parameterization of the inlet and openings, a 2D weir is specified upon grid cells with the help of an additional weir file (.2dw file). Figure C.5 shows the weir as schematized in Delft3D-Flow. The pink line depicts the 2D weir. With help of a defined crest height, a parameterized energy loss is calculated and added to the momentum equation. The energy loss over the weir is either based on experimental data as given by Vermaas [1987] or on the submergence relationship found by Villemonte [1947] (an extended version of equation 2.18). Thereby, only the flow component perpendicular to the crest (only the u or v velocity component depending on the user defined weir type) is taken into account in the calculation of flow over the weir. This means that no difference is made in calculations for plain, oblique or side weirs and thus no lateral outflow coefficient (ω_ϕ) is applied. This also results in no alteration of the flow angle over the weir crest. This is treated in more detail in chapters 4 and 5 and in appendix B.

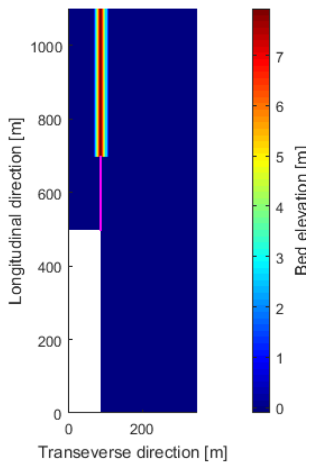

Figure 3.9: Two-dimensional model schematization of inlet crest using weir structure

Due to the inconsistent results found in the use of subgrid weirs in Delft3D-Flow, a second modelling program has been used to evaluate the use of subgrid weirs. The model schematization of Delft3D-Flow, as proposed above, has been converted to a Waqua model (also known as a Simona model). The conversion has been performed with the help of Matlab tools that automatically convert the model files. New weirs have been defined in the exact same location as in the Delft3D-Flow models. The resulting model input and inlet schematization are identical to that of the above-described Delft3D-Flow model (see figure C.5). Also, the calculation core of Waqua is identical to the Delft3D-Flow Waqua advection scheme.

3.2.3 Model comparison

In order to ensure model consistency, the empirical relationship formulation used in the one-dimensional model is compared to runs modelled with the two-dimensional Delft3D-Flow model. This is done using several model runs with a variety of inlet crest heights. Variations of this parameter are specifically considered as this is the most interesting parameter. Different from, for instance, the crest width or channel width, the crest height is designed to be adjustable in time and seen as part of the control strategy. Using the results found in the two-dimensional model runs, several input parameters (energy head, water levels, and submergence factors) are gathered as input for the empirical relationships used in the one-dimensional weir discharge and backwater curve calculations. The calculated discharges and water levels in both models are compared. The results are presented in chapter 4.

3.3 Mechanisms and factors

This section treats the methodology used for studying the mechanisms and factors that potentially influence the discharge distribution between the main and side channel, as discussed in section 2.3. The one-dimensional model is used to study these mechanisms and factors, as it provides a simplified and not-too-complex environment in which the different they can be controlled. Both are implemented in the one-dimensional model and can be enabled or disabled in the calculations for the discharge distribution between the channels. The mechanisms include secondary flow and porous flow. The effects of secondary flow are divided in the influence of a water level and velocity difference in lateral direction. Other factors considered are the bed roughness and different channel lengths resulting from adjusting the bend radius (both are causing a water level difference in longitudinal direction). Several runs are performed with help of the one-dimensional model, that are shown in table 3.3. Atop these model runs, the influence of different bend radius on the discharge distribution is also evaluated. Several model runs a performed for a varying bend radius with all mechanisms and factors enabling.

Table 3.3: One-dimensional model runs for different mechanisms and factors

Model run	**Longitudinal slope** Reduced length L_{side}[m]	Reduced roughness kr_{side} [m]	**Lateral slope** [-]	**Lateral velocity** [-]	**Porous flow** [-]
A0	2891	0.2	Enabled	Enabled	Enabled
A1	3100	0.2	Enabled	Enabled	Enabled
A2	2891	0.4	Enabled	Enabled	Enabled
A3	2891	0.2	Disabled	Enabled	Enabled
A4	2891	0.2	Enabled	Disabled	Enabled
A5	2891	0.2	Enabled	Enabled	Disabled

3.3.1 Longitudinal water level gradient

The effects of a longitudinal water level gradient through channel length or bed roughness are included in the one-dimensional model through the calculation of backwater curves, given by equation 3.1. The calculated backwater curves converge towards an equilibrium water level depending on the bed slope, specific discharge, and bed roughness coefficient. With help of the polar coordinate system, a different bend radius can be assigned for each channel. Thereby, a difference in channel length is created between the main and side channel. A difference in bed roughness is considered by adjusting the Nikuradse roughness height in the side channel. Either this is set equal to the roughness in the main channel ($k_r = 0.2$ m) or increased by a factor 2 ($k_r = 0.4$ m).

3.3.2 Lateral water level gradient:

The effects of a decreased water level in the outer main-channel bend and an increased water level in the inner side-channel bend (see figure 2.3b), are added to the calculated backwater curves. The water levels are thus adjusted for the schematized influence of lateral water level gradient in river bends according to equation 3.6.

$$h_{outerbend} = h_{center} + i_{trans}\frac{B}{2} = h_{center} + \frac{u^2 B}{2gr} \tag{3.6}$$

$$q_{weir} = \omega c C_{d,0} C_s \sqrt{2g}(H_0 - w \pm \frac{u^2 B}{2gr})^{3/2} \tag{3.7}$$

3.3.3 Increased lateral velocity:

The lateral velocity, occurring in a river bend, results in an increased velocity head in lateral direction at the inlet and opening locations. The lateral velocity can be approximated with Rozovskii's equation as shown in chapter 2. An additional velocity head in lateral direction ($v^2/2g$) is added to the regular side weir equation, as shown by equation 3.8.

$$q_{weir} = c C_{d,0} C_s \sqrt{2g}(\omega(H_0 - w)^{3/2} + v^2/2g) \tag{3.8}$$

where $H_0 - w$ is the energy head above the weir crest and $v^2/2g$ the additional lateral velocity head. For these lateral velocities, the inlet and openings can be considered as plain weirs and therefore the lateral velocity heads are not multiplied with a lateral reduction factor (ω). It must be noted that the lateral velocity component at the inner main-channel bend will be smaller than in the channel centre. The combination of estimating the velocity component in the channel centre and the use of Rozovskii's equation will thus result in an overestimation of the influence of secondary flow.

3.3.4 Porous flow

The inlet and openings between the longitudinal training dams are constructed by rocks with a single mass grading of 40 - 200 kg. The porous rock layer results in a flow through the inlet and openings between the main and side channel, even during water levels below the crest of the inlet or openings. Flow through porous soils and rocks is approximated with the general Darcy formula for flow through porous media, given by equation B.9.

$$v_{porous} = kI \tag{3.9}$$

$$q_{porous} = v_{porous} w = kIw \tag{3.10}$$

where v_{porous} is the fluid velocity through the porous medium, k is the permeability and I is the hydraulic pressure gradient. The hydraulic pressure gradient can easily be calculated by the water levels on opposite sides of the crest and the average width. The permeability can be approximated with the help of literature and is estimated at 0.4 (see appendix B)

3.4 Flow patterns

In this section, the methodology of investigating the flow patterns at the inlet and openings is described in more detail. It is very relevant to gain a better understanding of the way discharge is distributed at the inlet and openings and study the associated velocity magnitudes and flow angles. The angles and velocity magnitudes greatly determine if sediment will be transported into the side channel. Sediment transport is not considered in this research, although this research can be used as input for future morphological analysis. At first the flow regimes above the weir crest, as discussed in chapter 2, will be evaluated. This will determine the need for a submergence coefficient when analyzing the suitable empirical relationships. The one-dimensional model is expected to no longer suffice as all lateral components are neglected or strongly schematized and, as mentioned in section 2.4.2, the empirical discharge coefficients only determine cross-sectional averaged lateral outflow angles for a free-flowing weir. The evolution of velocity magnitudes and flow angles under submerged conditions are expected to not be calculated correctly. Therefore the two-dimensional Delft3D-Flow model is used that schematizes a single inlet within the bed topography as shown in figure C.3. This short model allows similar water levels at the downstream end of the channels. The empirical relationships used in the one-dimensional model will thereafter be used to assess if, with possible alterations, reasonable cross-sectional averaged flow angles and velocity magnitudes can be predicted. Table 3.4 presents the model runs for various inlet crest heights that are performed. The values -1.60 m NAP and +5.60 m NAP correspond to the average bed level to which is excavated in the side channel and the dam height at the location of the inlet near Wamel respectively [Herik and Boskalis, 2014].

Table 3.4: Two-dimensional model runs for different crest heights with h_{side} =6.39 m, h_{side} = 6.47 m+bed level, and Q_{up} =2000 m^3/s

Model run	**Crest height**			
	w [m +NAP]	w [m +OLR]	w [m +bed]	W [-]
B-0	-2.40	-5.20	0	0.0
B-1	-1.40	-4.20	1	0.15
B-2	-0.40	-3.20	2	0.30
B-3	0.60	-2.20	3	0.46
B-4	1.60	-1.20	4	0.62
B-5	2.60	-0.20	5	0.77
B-6	3.60	0.80	6	0.92
B-7	4.60	1.80	7	>1.0

- **Flow regimes:** The Froude number atop the inlet and the submergence factor will be evaluated to determine the flow regime at the inlet and openings. Different longitudinal water level profiles along the inlet can indicate the flow regime alongside the inlet or opening in the main channel, as further explained in appendix A and figure A.11. A water level increasing in downstream direction corresponds to a sub-critical regime, whereas a decreasing water level or hydraulic jump indicates super-critical flow in the main channel.

- **Weir type:** Considering whether the flow lines are running parallel and a critical water depth is reached above the crest, Bos [1976] introduced a categorization of weir types according to the energy level above the crest ($H - w$) to crest width (B_w). Bos showed that values below 0.3 correspond to broad-crest weirs where flow line are running completely parallel over the crest. Values above 15 correspond to short-crested where flow lines separate completely from the crest and values between 0.3 and 15 correspond to short-crested weirs (see section 2.4.1 and table 2.2).

- **Longitudinal discharge variation:** The relative distribution of specific discharge in longitudinal direction over the inlet is evaluated. The transverse velocity magnitude in each grid cell is used to compute the specific discharge and compare the relative discharge variation and assign a weight to each longitudinal distance, as shown in schematized form in figure 3.10.

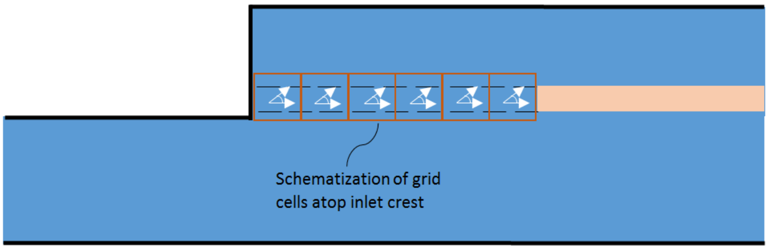

Figure 3.10: Schematization of modelled velocity magnitudes and flow angles atop the inlet

- **Flow angles:** Flow angles atop the inlet and openings are evaluated using the two-dimensional models. Specifically, the flow angles atop the inlet are considered as the maximum angles that are reached at this point and thereby provide a good comparison for the different runs. From a sediment transport point of view, the flow angles (in combination with slope angle) on the slope of the main channel to the weir crest mainly determine the sediment transport conditions [Jammers, 2017]. Because the flow angles atop the slope converge towards the flow angles atop the crest, using the flow angles atop the crest is expected to also predict the maximum value atop the slope reasonably well. A slight over-estimation will thus result from using the flow angles atop the weir crest for sediment transport calculations. The flow angles atop the crest are expected not to be varying greatly in transverse direction as the crest width (B_w) is relatively small (2 m) and thus considered constant. The one-dimensional model is used to predict possible alterations to the submergence coefficient as presented in chapter 2. The submergence coefficient as found in literature is designed to predict discharges correctly but not the average cross-sectional flow angles. Length averaged flow angles as calculated by the two-dimensional model will be used to determine a new submergence coefficient for the flow angle atop a weir crest.
- **Flow velocities:** The flow velocity variation in longitudinal direction directly atop the weir crest are extracted from the Delft3D-Flow runs and evaluated.
- **Circulation cell:** As a result of the sharp 90 degree angles at the upstream end of the inlet, it is expected that a circulation zone is formed in the side channel. The location and size of this circulation cell are evaluated.

3.4.1 Influence of crest length

In addition to the model runs presented in table 3.4, the influence of the inlet crest length on the flow patterns is also investigated. This is done by adjusting the crest length in the Delft3D-Flow model to include lengths of 100, 150, 200, 250, 300, 350, and 400 m. These runs are performed for all crest heights as shown in table 3.5.

Table 3.5: Two-dimensional model runs for different crest lengths ($L_{w,inlet}$) with various crest heights

Model run	**Crest length** $L_{w,inlet}$ [m]
C100-0:7	100
C150-0:7	150
C200-0:7	200
C250-0:7	250
C300-0:7	300
C350-0:7	350
C400-0:7	400

3.4.2 Submergence coefficient for flow angles

As discussed before in chapter 2, the submergence coefficient used in the empirical formulations allows for a conversion of the discharge over a free-flowing weir to a submerged weir. The submergence coefficient, however, is only a correction factor for the discharge. This means that the submergence coefficient not only corrects for flow angles but, for instance, also for different velocity magnitudes over a submerged weir. A different submergence coefficient is, therefore, investigated to specifically convert the flow angle from free to submergence flow conditions. Such an adjusted flow angle submergence coefficient is also expected to be a function of the submergence factor $S = (H_{main} - w)/(H_{side} - w)$. As presented in chapter 2, there are two submergence coefficient formulations that are relatively similar and both depend on S. They are presented again below in equations 3.11 and 3.12. It is not known beforehand which formulation type best suits a submergence factor for the flow angle. Therefore, the submergence factor (S) and the flow angles from the model runs presented in table 3.5 will be used to determine the coefficients a and b according to both formulas. Using a least root-mean-square error method and comparing the R-squared values, the two new submergence formulas can be compared to determine the most suitable one as a new angle submergence coefficient $C_{s,angle}$.

$$Cs_{angle,1} = \sqrt{1 - S^a} \tag{3.11}$$

$$Cs_{angle,2} = 1 - \frac{1}{0.5^b}(S - 0.5)^b \tag{3.12}$$

3.5 Modelling

In order to evaluate the modelling of the system of longitudinal training dams in larger river models, use is made of the Delft3D-Flow model and a comparable Waqua model. The schematization by bed topography and by subgrid weirs are evaluated and the resulting discharge distribution and flow patterns are compared to evaluate if either method proves suitable for use in larger river models.

3.5.1 Bed topography

In order to evaluate the schematization within the bed topography, use if made of the two-dimensional Delft3D-Flow model. The simulation of flow over rapidly increasing bed levels with calculations on grid level is expected to possibly be influenced by the used grid size and advection scheme. Both are discussed below.

Grid size

Too small grid sizes might not represent the structure well enough and thus also not represent the correct flow patterns or discharge over the inlet or opening. Several different grid sizes are considered to determine the minimally require grid size that provides a converged discharge distribution between the two channels. Table 3.8c presents an overview of the considered model runs.

Table 3.6: Two-dimensional model runs for different grid sizes

Model run	**Refinement**	**Number of grid cells**		**Grid size**	
	[-]	M [#]	N [#]	dM [m]	dN [m]
E-1	1	35	110	10	10
E-2	2	70	220	5	5
E-3	3	105	330	3.3	3.3
E-4	4	140	440	2.5	2.5
E-5	5	175	550	2	2

Advection schemes

Three numerical schemes are available in the Delft3D-Flow modelling program to calculate the normal and cross advection of water. From these advection schemes, the 'Waqua' and 'Cyclic' scheme make use of the central differences and ADI/BDF schemes respectively, to reduce the amplitude and the phase error Stelling [1983]. These two schemes are most commonly used in large river models due to their computational efficiency. The third option is the flood scheme, which is very suitable for rapidly varying depth-averaged flows as flow contraction and flow expansion are modelled according to the conservation of energy and momentum respectively. For each of the advection schemes, a set of 8 model runs is performed with the short Delft3D-Flow model as described at the beginning of this chapter. The 8 model runs relate to different crest heights, similar to those as presented in table 3.4.

Table 3.7: Two-dimensional model runs for different advection schemes

Model run	Advection scheme
F-0:7	Waqua
G-0:7	Cyclic
H-0:7	Flood

3.5.2 Subgrid weirs

To investigate the use of subgrid weirs, several model runs are performed. Various crest heights are used, similar to the crest heights used in the model runs presented in table 3.4. The different crest heights are modelled using both Delft3D-Flow and Waqua, as presented below in table 3.8. Also, the use of different grid sizes is investigated for Delft3D-Flow model runs with a relative crest height of $W = 0.46$.

Table 3.8: Delft3D-Flow and Waqua subgrid weir model runs

(a) Delft3D-Flow: different crest heights

Model	Crest height w [m]	W[-]
W1-0	0	0.0
W1-1	1	0.15
W1-2	2	0.30
W1-3	3	0.46
W1-4	4	0.62
W1-5	5	0.77
W1-6	6	0.92
W1-7	7	>1

(b) Waqua: different crest heights

Model	Crest height w [m]	W[-]
W2-0	0	0.0
W2-1	1	0.15
W2-2	2	0.30
W2-3	3	0.46
W2-4	4	0.62
W2-5	5	0.77
W2-6	6	0.92
W2-7	7	>1

(c) Delft3D-Flow: different grid sizes

Model run	dM [m]	dN [m]
W3-1	10	10
W3-2	5	5
W3-3	3	3
W3-4	2	2
W3-5	1	1

3.6 Control strategy

In the design process of the longitudinal training dams, several control abilities were included of which the effects on the discharge distribution and flow patterns are presented below. The control dimensions include the inlet and opening crest heights. Other design choices that are considered include the side channel width and crest length. The channel width can vary over time due to the natural morphological development that influences the bed elevation and bank erosion in the side channel.

The crest length in the pilot project is chosen as 200 m but could be varied in future longitudinal training dam designs. Other design choices, including permanent dimensions, such as the crest width and positions of inlet and openings, are not treated here.

Table 3.9 presents the ranges considered for design choice. The chosen ranges are based on values that could potentially be realized. This means that the inlet crest height can vary between bed and crest level of the longitudinal training dams itself. Similarly, the opening crest heights can potentially vary between the bed level and the crest level of the longitudinal training dams. The channel width ratio can roughly vary between an equal channel width and the main channel being several times wider than the side channel. A side channel that is wider than the main channel is not considered as this will undermine the idea of a side channel. An inlet crest length of 100 to 400 m is considered for practical reasons as a longer crest lengths are not assumed feasible in a river inner bend. Some parameters are presented in the dimension m +bed level, which refers height above the main channel bed level at that location. The influence on the discharge distribution is evaluated with the help of the one-dimensional model that provides easily changeable parameters. The influence on flow patterns is evaluated with the help of the two-dimensional model.

Table 3.9: Overview of parameters in sensitivity analysis

Model runs	Parameters	Symbol	Min	Max	Dimension
I-1:7	Inlet height	$w_{opening}$	0	7	m+ bed level
J-1:7	Opening heights	$w_{opening}$	0	7	m+ bed level
K-1:7	Channel width ratio	B_{main}/B_{side}	1	4	-
L-1:7	Inlet crest length	L_w	100	400	m

Chapter 4: Results

4.1 Introduction

Several model runs have been performed with the help of the one-dimensional model that has been developed for this research. Additionally, several model runs have been performed with the two-dimensional models created using the existing Delft3D-Flow modelling software. These models and the different model runs have been described in chapter 3. In this chapter, the two models are first compared to one another on their calculated discharge towards the side channel to determine their consistency. Thereafter, for each of the research questions presented in chapter 1, a set of model runs is performed that is also found in the various tables in the previous chapter. In this chapter, the results for these models runs are summarized and presented in the order of the research questions.

4.2 Model comparison

The discharge distribution to the side channel, as calculated by the short two-dimensional model, is compared to the weir discharges calculated by the empirical discharge formulations. These are discussed in chapter 2.4.1 and used in the one-dimensional model. The water levels and submergence factor are imported from the two-dimensional model and used as input in the empirical equations. The method of calculation is very different for the two models but should provide reasonably similar results. Figure 4.1a shows the calculated discharge distribution towards the side channel for different crest heights in both models, compared to several different empirical relationships found in literature. The empirical relationships make use of weir coefficients (C_dC_s, see chapter 2) that are compared to these coefficients obtained from the two-dimensional Delft3D-Flow model runs and shown in figure 4.1b.

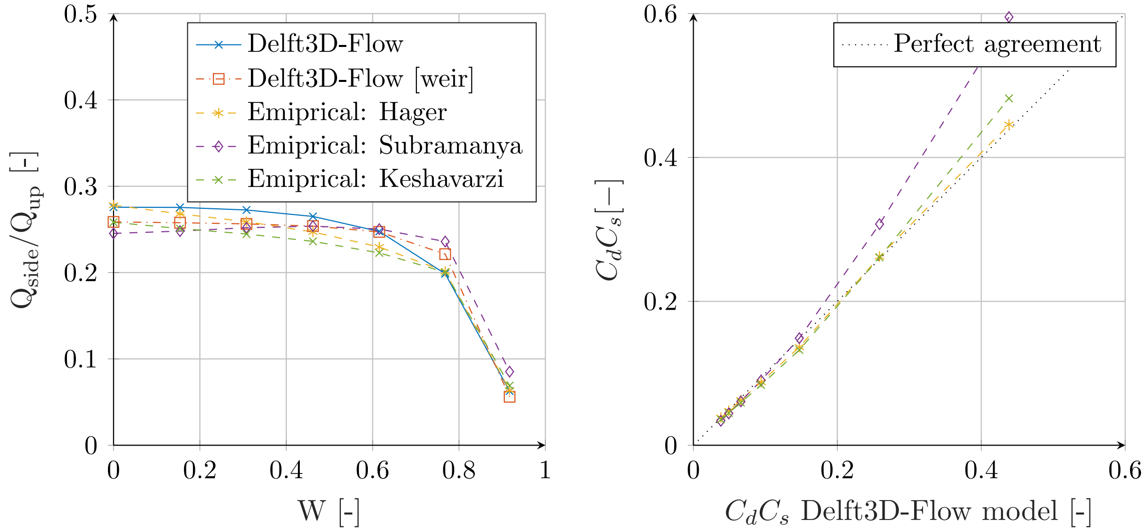

(a) Comparison of discharge distribution　**(b)** Comparison of C_dC_s

Figure 4.1: Comparison of the calculated discharge distribution (Q_{side}/Q_{up}) and weir coefficients (C_dC_s) using the empirical relationship and the Delft3D-Flow model results for different dimensionless crest heights ($W = w/H$)

The two-dimensional models (bed topography and subgrid weirs) and the one-dimensional model show similar results for discharges over a single inlet or opening with a relative difference in the order of

5 − 10%. Figure 4.1b shows that the relationship by Hager compares best with the two-dimensional model results (relative difference of 1 − 3%). Several other empirical relationships are compared but show less agreement (see appendix A.4 for an overview of the other relationships). The models compare best in case the submergence coefficient by Ka-Leung Lee [2002] is used in the one-dimensional model and the flood advection scheme and a small enough grid size are used in the two-dimensional model. Both models will be treated in more detail later on. The relative difference with the empirical relationship in calculated discharge distribution is 5 - 7 % for both the bed topography and subgrid weir model runs.

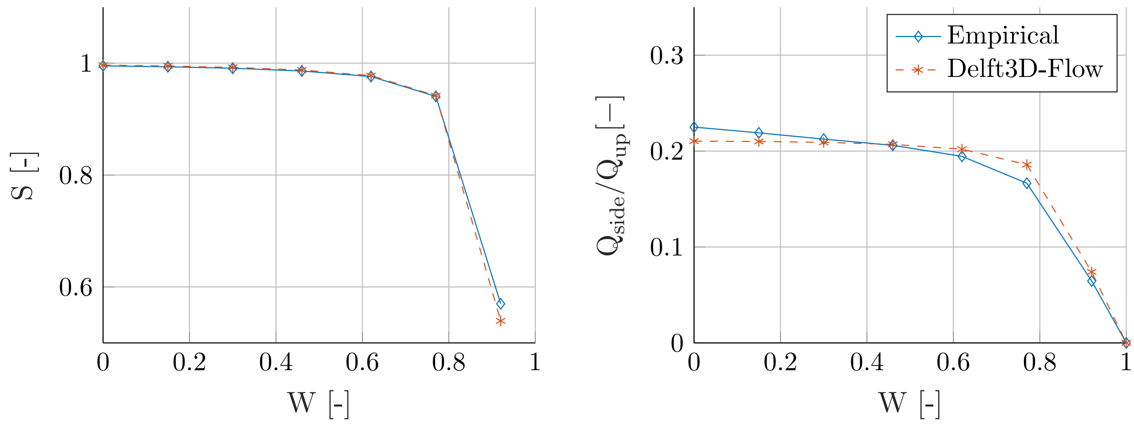

(a) Comparison of submergence factor

(b) Comparison of discharge distributions

Figure 4.2: Comparison of the empirical relationship with the Delft3D-Flow model results for the submergence factor (S) and discharge distribution of system with two openings and different dimensionless inlet crest heights ($W = w/H$)

When considering the large system of several longitudinal training dams including two openings, the backwater curve calculations in the one-dimensional model also become important. When looking at figure 4.2a, the level of submergence (S) in both models are only differs by a maximum of 3 %. The calculated water levels at the upstream side of the inlet thus compare very well. The calculated discharge over the inlet, for a 3100 m long system with closed openings, is also relatively similar. The empirical relationship and two-dimensional model show a maximum relative difference in the order of 8 % for various dimensionless crest heights. This is seen in figure 4.2b. This indicates that both models provide comparable predictions for discharge over weir-like structures and are expected to provide good estimations for the discharge distribution in a two-channel system.

4.3 Mechanisms and factors

The influence of different mechanisms and factors on the discharge distribution is included in the one-dimensional model and can be enabled or disabled. By comparing the discharge distributions from enabled and disabled model runs, the influence of the mechanisms and different factors can be distinguished from other influencing parameters. Table 4.1 shows the order of magnitude of the difference in discharge over the inlet when enabling or disabling the different mechanisms and factors. In the last column, the influence of each mechanism is scaled to the maximum influence (value of 1.0). The largest influence is created by the bed roughness in the side channel. The effects of channel length, transverse slope, and porous flow are each in the same order of magnitude but two orders smaller than that of the side channel bed roughness. The secondary flow does not show any significant influence. The results, including those for the model runs with different bend radius values, are further discussed in chapter 5.

Table 4.1: Results of model run A0-A5 showing the influence of the different mechanisms and factors

Model run	Mechanism or factors disabled	Discharge $\frac{Q_{main}}{Q_{up}}$	rel. to A0	Difference rel. to A2
A0	None (test case)	79.63%	-	
A1	Reduced channel length	79, 66%	$O(10^{-4})$	0.02
A2	Reduced bed roughness	81.10%	$O(10^{-2})$	1.0
A3	Transverse slope	79.59%	$O(10^{-4})$	-0.03
A4	Transverse velocity	79.63%	$< O(10^{-5})$	0.0
A5	Porous flow	79.66%	$O(10^{-4})$	0.02

4.4 Flow patterns

4.4.1 Flow regime

As discussed in chapter 2, looking at the transverse and longitudinal water level profile over and along the inlet and openings, the flow regime categories can be determined. Because the one-dimensional model does not include transverse variations, the two-dimensional model is used. Considering the submergence factor S, the flow can be free or submerged. A value of roughly $S > 0.5$ indicates that submergence influences the discharge distribution, see section 2.4.2. Figure 4.3 shows that for nearly all crest heights, flow atop the crest is under submerged conditions. Only for crest heights that nearly reach the water level, the submergence factor does drop considerably and reaches free-flowing conditions.

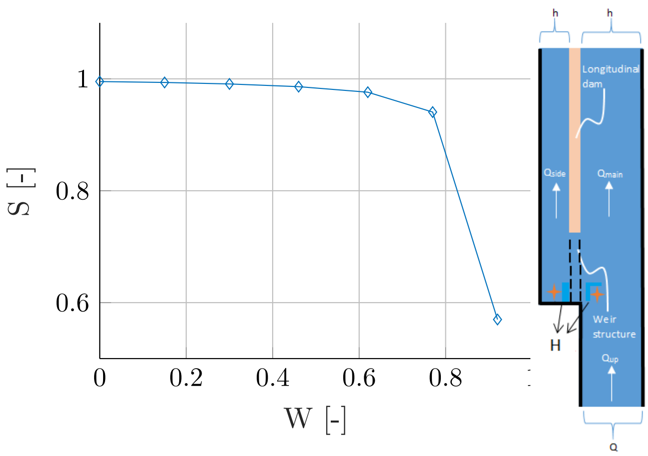

Figure 4.3: Submergence factor (S) for two-dimensional model runs with different dimensionless crest heights ($W = w/H$)

Figure 4.4 shows that the flow along the inlet in the main channel follows the water level patterns corresponding to sub-critical flow for both low and height crest heights. However, looking at the flow atop the crest, a difference is noticed for increasing weir crest heights. Plotting the Froude number above the crest (see figure 4.5) shows that for larger crest heights the Froude number eventually exceeds 1. This means that in that case flow atop the crest becomes super-critical and is thus also not influenced by conditions in the side channel. The point at which this occurs shows to be very well predicted by the categorization of broad- to short-crested weirs by Bos [1976], as shown in figure 4.5 as well.

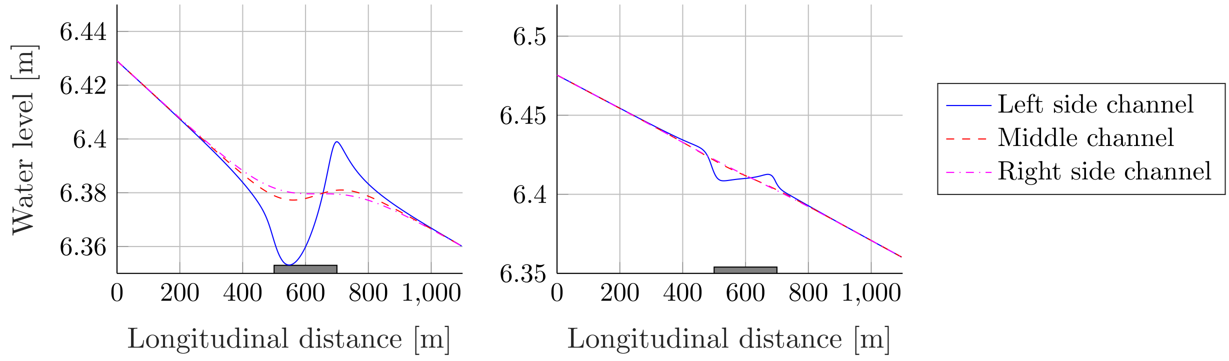

(a) Inlet crest height = 3 m

(b) Inlet crest height = 6 m

Figure 4.4: Longitudinal water levels in main channel along inlet for Delft3D-Flow model runs

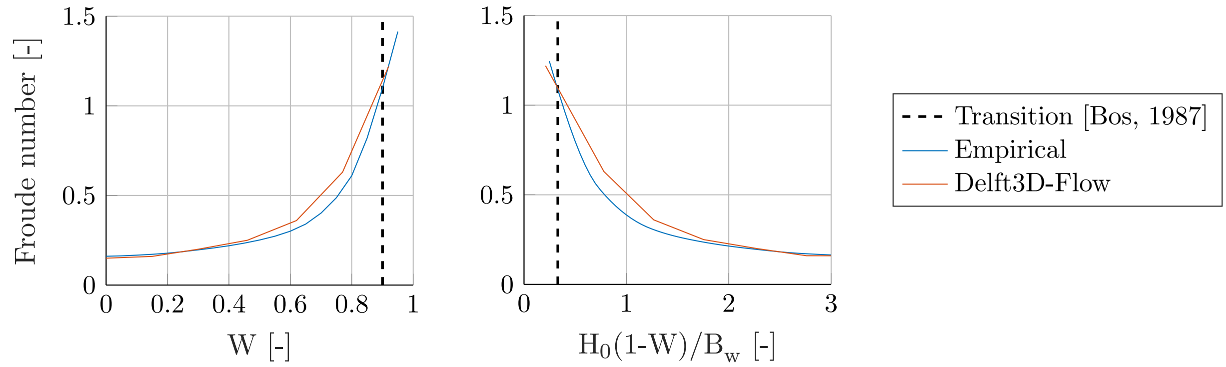

(a) Dimensionless crest height

(b) Energy head above crest to crest length ratio

Figure 4.5: Weir type classification according to Bos [1976] for different dimensionless crest heights ($W = w/H$) in the Delft3D-Flow model runs

4.4.2 Flow angles and velocity magnitudes

Using the two-dimensional Delft3D-Flow model of the system of longitudinal training dams including two openings, a more detailed analysis is made of the actual flow patterns at the inlet and openings. The model represents a situation with an inlet and opening crest of 3 and 6 m above bed level respectively (similar to the current situation in the Waal). Figure 4.6 depicts the modelled depth-averaged velocity magnitude in colour and the flow direction in vectors.

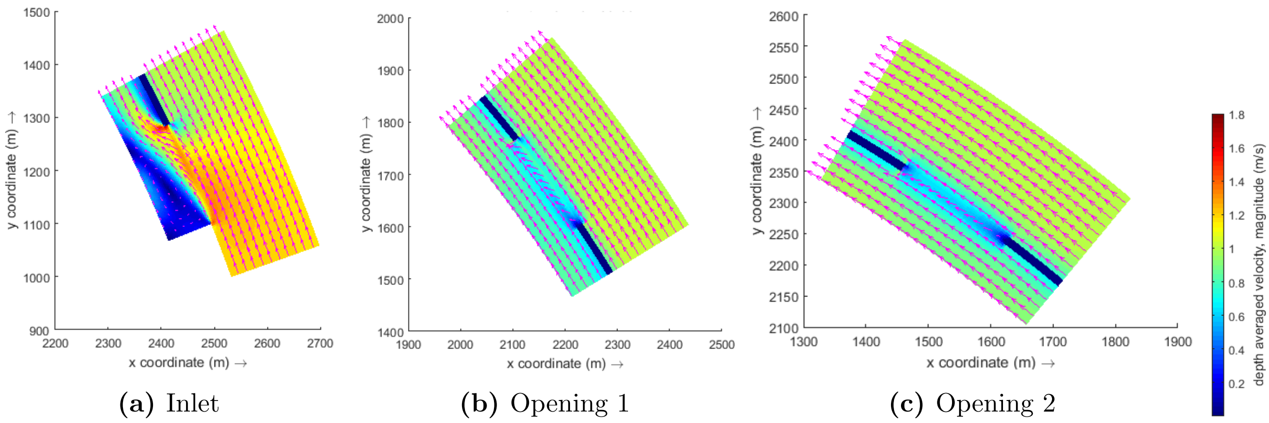

(a) Inlet

(b) Opening 1

(c) Opening 2

Figure 4.6: Velocity magnitudes and flow angles from the Delft3D-Flow model runs with $W_{inlet} = 0.46$ and $W_{opening} = 0.92$

It is noted that a secondary circulation cell is formed in the side channel at the location of the inlet. This circulation cell roughly extends the entire inlet length creating a reverse flow at the bank in the side channel. The reverse flow shows a maximum flow velocity in the order of 0.5 m/s. Just downstream of the inlet, directly against the longitudinal training dam, a stagnant zone is noticed. This zone with velocities quickly dropping to nearly zero at the longitudinal training dam extends in downstream direction with a length scale in the order of half the inlet length. The secondary circulation cell and stagnant zone are not seen at the two openings due to the presence of already conveying side channels.

Longitudinal discharge variation

The total discharge over the inlet - into the side channel - (Q_{side}) is computed in the two-dimensional model and transformed to a cross-sectional averaged specific discharge by dividing by the total inlet length. This is shown in equation 4.1.

$$q_{w,averaged} = Q_w/L_w \tag{4.1}$$

Comparing the variation of specific discharge in longitudinal direction to the cross-sectional averaged discharge shows at which location most discharge enters the side channel. Figure 4.7 presents the results for several two-dimensional model runs with different dimensionless crest heights. For small crest heights, the specific discharge increases considerably in downstream direction. For crest heights corresponding to critical flow above the crest ($W > 0.9$), the discharge remains nearly constant.

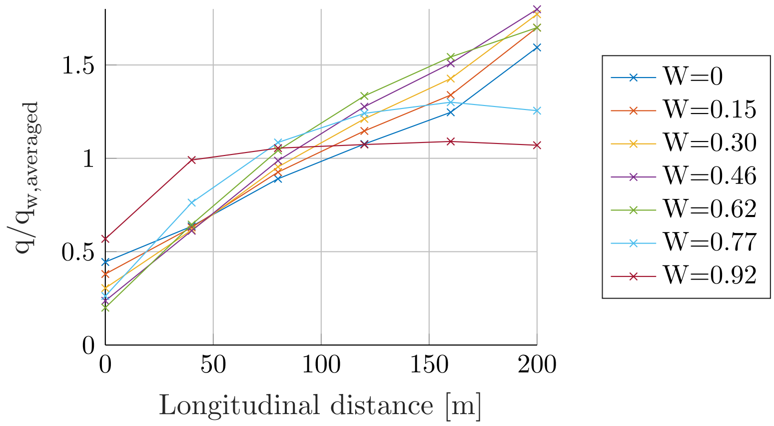

Figure 4.7: Longitudinal variation of specific discharge over the inlet for various dimensionless crest heights ($W = w/H$)

Lateral outflow angle

The flow angles for different crest height, as calculated by the two-dimensional (bed topography) model, are summarized in figure 4.8. The flow angle increases in downstream direction from 0 to roughly 30 to 50 degrees depending on the crest height. At the downstream end, the flow angle increases sharply to 90 degrees at the contact point between the inlet and longitudinal training dam. At this point, the flow is blocked by the longitudinal training dam tip and is forced to flow in lateral direction, which explains the 90-degree flow angle. Comparing the flow angles to the angles found in the one-dimensional model is difficult as the one-dimensional calculation does not include a spatial variation atop the crest. Therefore, the two-dimensional length and discharge averaged flow angles are compared with the one-dimension model. To calculate the discharge averaged flow angles, the longitudinal discharge variation shown in figure 4.7 is used. The discharge averaged flow angles show to be larger than the length averaged due to larger specific discharge and flow angles in downstream direction. The maximum difference is in the order of 10 degrees. The averaged flow angles atop the crests increase for increasing crest height. For crest heights corresponding to critical flow conditions (W>0.9, see figure 4.5), the lateral outflow angles becomes relatively constant in longitudinal direction. The flow angle under free-flow conditions is, with an underestimation of 1-2 degree relative to the length and discharge averaged Delft3D-Flow model, predicted relatively well by the empirical relationship (equation 2.14). For submerged conditions, the empirical relationship models a much larger angle. The reason for this lower angle is that the submergence is not taken into account.

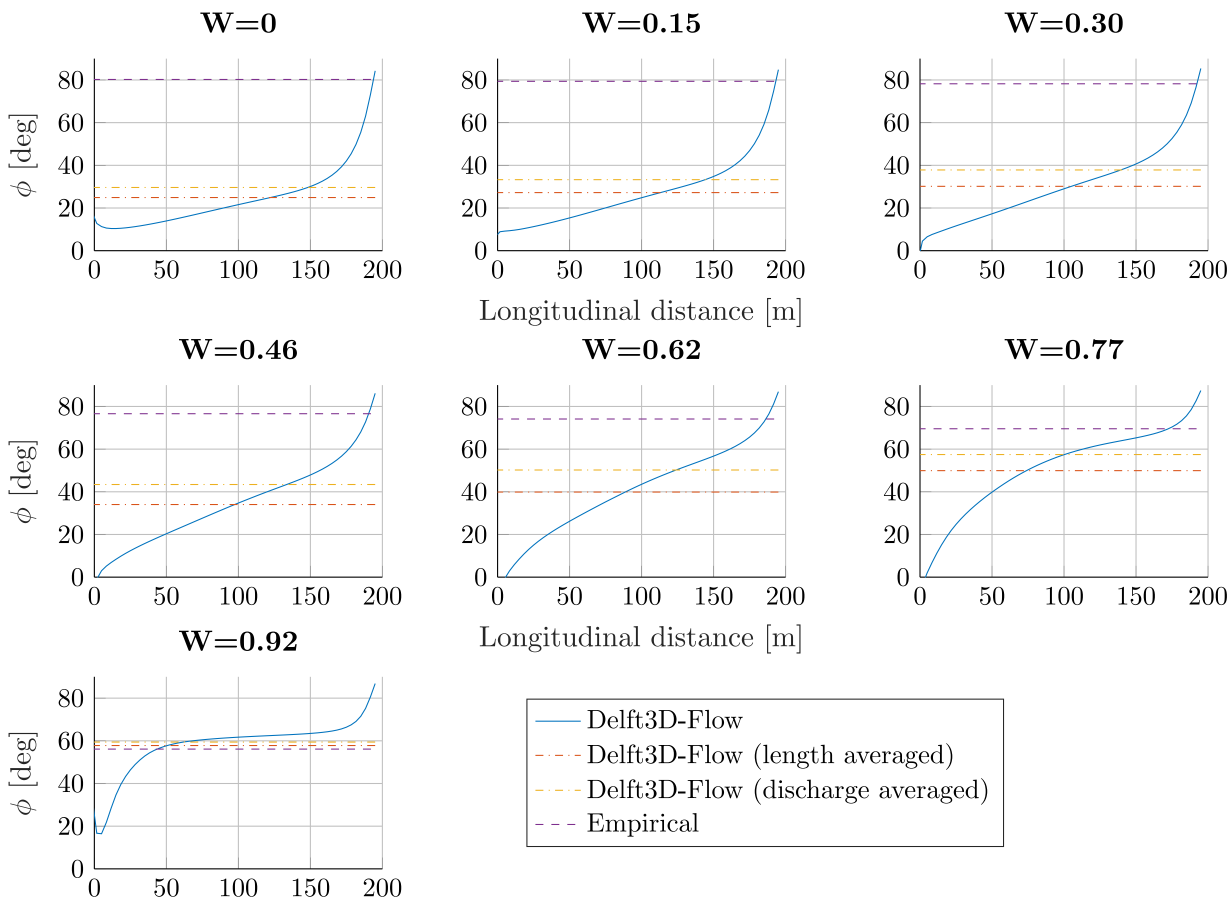

Figure 4.8: Flow angles atop the inlet for various dimensionless crest heights ($W = w/H$)

Velocity magnitude

The largest velocities are noticed above the inlet crest that reach maximum values of 1.6 m/s with a spike to 1.8 m/s at the downstream end at the side channel border. This spike in velocity magnitude is expected to be party numerical due to the sharp step-wise increase in bathymetry at the transition of the inlet and longitudinal training dam. Figure 4.9a shows the development of the transverse, lateral and total velocity magnitudes above the inlet crest in longitudinal direction for a dimensionless crest height of W=0.46 (w=3 m+bed level). The total velocity, as calculated by the two schematizations, rises considerably in downstream direction in the first quarter atop the crest. This is mostly due to the rapid widening at the upstream corner where water still needs to be accelerated by the main channel. The water is quickly accelerated in longitudinal direction. The longitudinal velocity magnitude reaches a relatively constant magnitude halfway along the crest after which it rapidly decreases again at the downstream end. In lateral direction, velocity magnitude slowly increases in downstream direction, reaching a maximum at the downstream end (see figure 4.9a). The transverse velocity magnitudes above the opening crests are very small ($\leq$ 0.1 m/s) compared to those found at the inlet. This can be explained by to the small discharge over the openings. The longitudinal velocity magnitude above the opening crests increases from 0 to roughly 0.6 m/s in downstream direction, see figures 4.9b and 4.9c. The flow in the channels around the openings id also not influenced much.

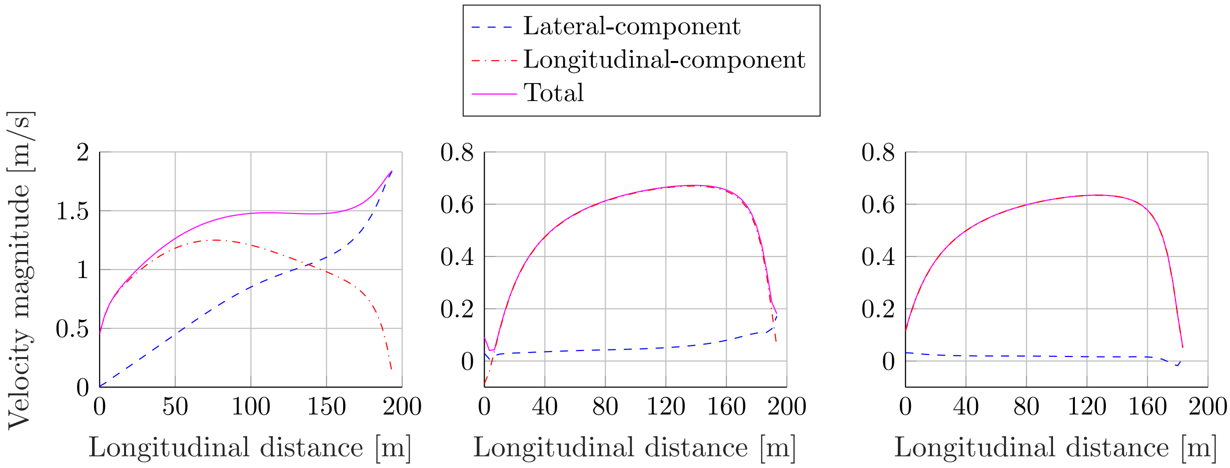

(a) Inlet

(b) First opening

(c) Second opening

Figure 4.9: Velocities magnitude atop the inlet and openings for specific dimensionless crest heights ($W_{inlet} = 0.46$, $W_{opening} = 0.92$)

4.4.3 Crest length

The influence of the crest length is modelled by several runs with different crest lengths. Figure 4.10 combines all discharge averaged flow angles atop the crest and its related deflection coefficient ($\sin(\phi)$). The discharge and not length averaged flow angle is used because thereby more weight is given to locations with a larger specific discharge. This is especially relevant for a future connection to sediment transport that is highly depended on the velocity magnitudes at the crest [Jammers, 2017].

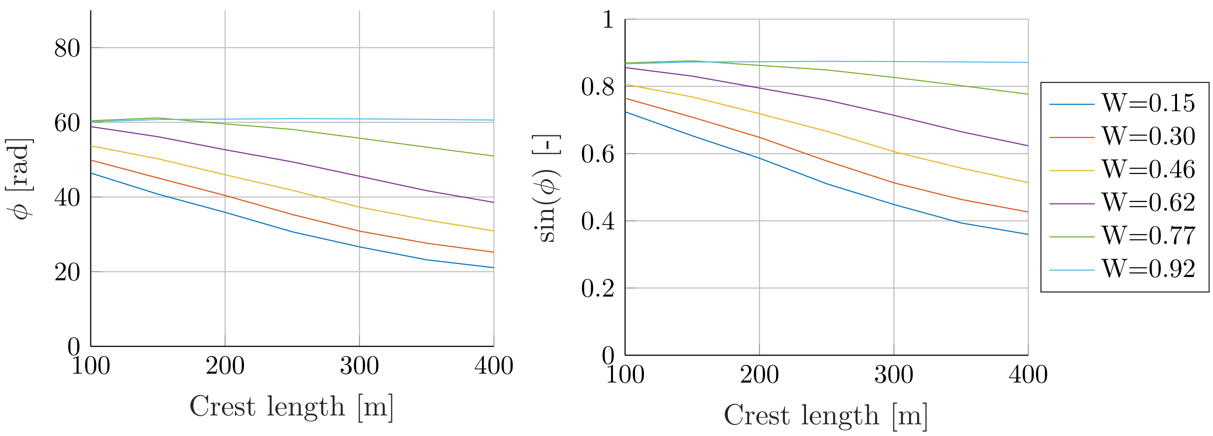

(a) Outflow angle (ϕ)

(b) Deflection coefficient ($\sin(\phi)$)

Figure 4.10: Influence of crest length (L_w) on the discharge averaged outflow angle (ϕ) and the corresponding deflection coefficient ($\sin(\phi)$)

The longitudinal variation of flow angles atop the crest is combined in figure 4.11. Under submerged conditions, the length averaged angles decrease up to 30 degrees when increasing the crest length. For crest heights inducing free-flowing conditions, the local flow angle atop the crest remains relatively constant. The lateral outflow angles as calculated by the empirical relationship (equation 2.14 by

Hager [1987]) are also plotted in the figure. Again, a slight underestimation is noticed in the order of 3 degrees for the calculated flow angles under free-flowing conditions by the empirical relationship. The submerged flow angles are not predicted well at all by the empirical relationship.

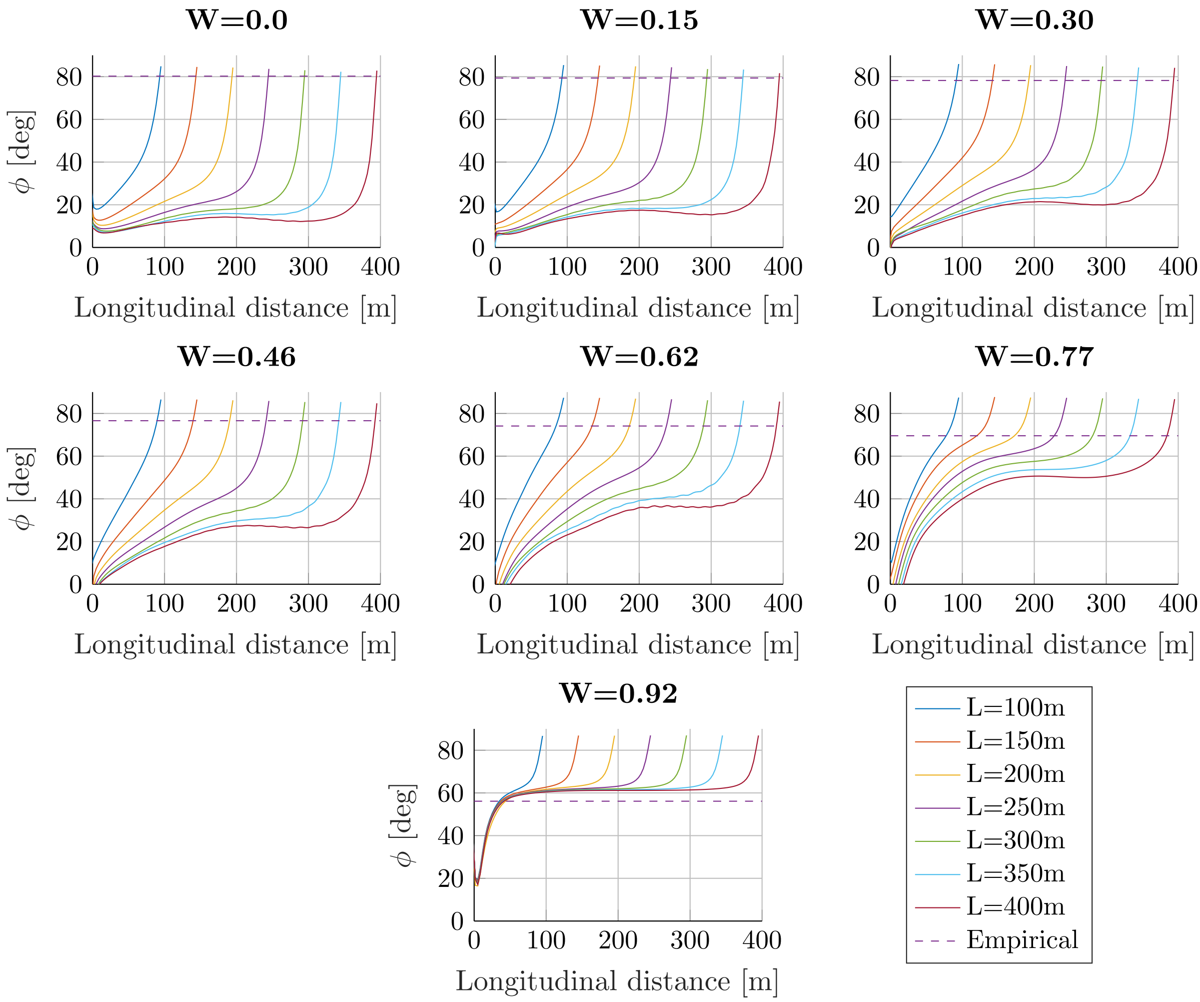

Figure 4.11: Flow angles atop the inlet for various crest lengths (L_w) and dimensionless crest heights ($W = w/H$)

Submergence coefficient for flow angles

The reason that the flow angles for submerged conditions are not calculated correctly can be explained by the fact that only free-flowing conditions are considered by Hager. Making use of the model results presented in figure 4.11, a submergence coefficients specifically for flow angles is determined. In figure 4.12, the resulting $C_{s,angle}$ is plotted for the model runs with various crest lengths and crest heights. The angle submergence coefficients are determined using the discharge averaged outflow angles. The $C_{s,angle}$ shows to decrease for increasing crest lengths. This is the results of the lower averaged flow angles atop the crest for increased lengths. The $C_{s,anlge}$ values also show to surpass a value of 1 for decreasing levels of submergence (S). This is the result of an underestimation of the free-flow lateral outflow angle by the formulation proposed by Hager (equation 2.14). This was also shown previously in figure 4.10. A relationship, in the same format as the general Villemonte or Ka-Leung side weir submergence formulas (equations 2.18 and 2.19), can be found by curve-fitting the data. Therefore, the coefficient a in the general Villemonte formula and coefficient b in the side weir formula by Ka-Leung are determined. Table 4.2 shows coefficients that were determined using a least root-mean-square error method. The R-square and root-mean-square error (RMSE) values are also added in the table.

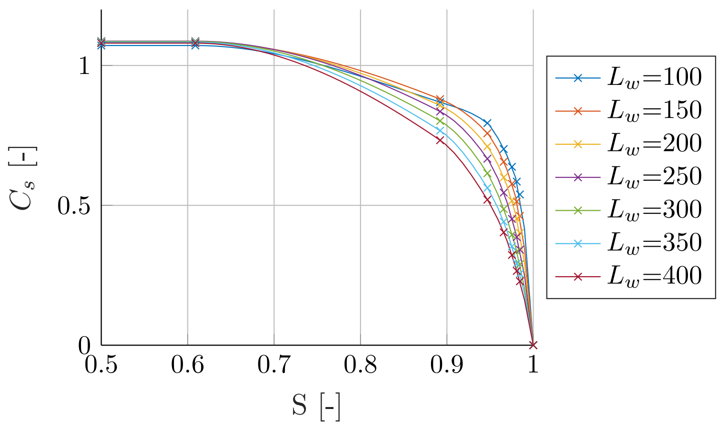

Figure 4.12: Angles submergence coefficient ($C_{s,angle}$) calculated from the Delft3D-Flow model runs for various crest lengths (L_w) and submergence factors (S).

Table 4.2: Determined angle submergence coefficients (a and b) for discharge averaged flow of different crest length (L_w) with corresponding root-mean-square error (RMSE)

Crest length	**General formula**			**Side formula**		
L_w [m]	a [-]	R-squared [-]	RMSE [-]	b [-]	R-squared [-]	RMSE [-]
100	19.66	0.979	0.0471	19.67	0.946	0.0755
150	15.55	0.984	0.0431	16.17	0.959	0.0682
200	12.26	0.984	0.0436	13.33	0.963	0.0669
250	9.73	0.982	0.0487	10.97	0.971	0.0617
300	7.79	0.978	0.0541	9.06	0.975	0.0580
350	6.48	0.975	0.0587	7.71	0.978	0.0553
400	5.59	0.973	0.0625	6.76	0.980	0.0530

The coefficients a and b show to be depended on both the submergence factor S and the crest length L_w. The crest length is non-dimensionalized by dividing by the main channel width. This results in the parameter L_w/B_{main} that was proposed by Rosier [2007] as being one of the controlling parameters for weir flow and introduced before in equation 2.9. The coefficients a and b as function of L_w/B_{main} that correspond best to the model runs are presented by equations 4.2 and 4.3.

$$Cs_{angle,1} = \sqrt{1 - S^a} \qquad \text{where } a = 9.14 * (\frac{L_w}{B_{main}})^{-0.84} \tag{4.2}$$

$$Cs_{angle,2} = 1 - \frac{1}{0.5^b}(S - 0.5)^b \qquad \text{where } b = 10.29 * (\frac{L_w}{B_{main}})^{-0.72} \tag{4.3}$$

The two equations (4.2 and 4.3) both compare well with the Delft3D-Flow model runs. The maximum difference between the equations and modelled C_s values is 13%. Comparison of the new angle submergence formulas with Delft3D-Flow model runs is shown in figure 4.13 for a crest length of 200 and 400 m. Equation 4.2 fits slightly better to the model runs showing a R-squared value of 0.98 (compared to 0.97). Equation 4.2 shows to better fit the data especially for very high submergence factors of $S > 0.9$, while equation 4.3 compares somewhat better for smaller S values ($S < 0.9$).

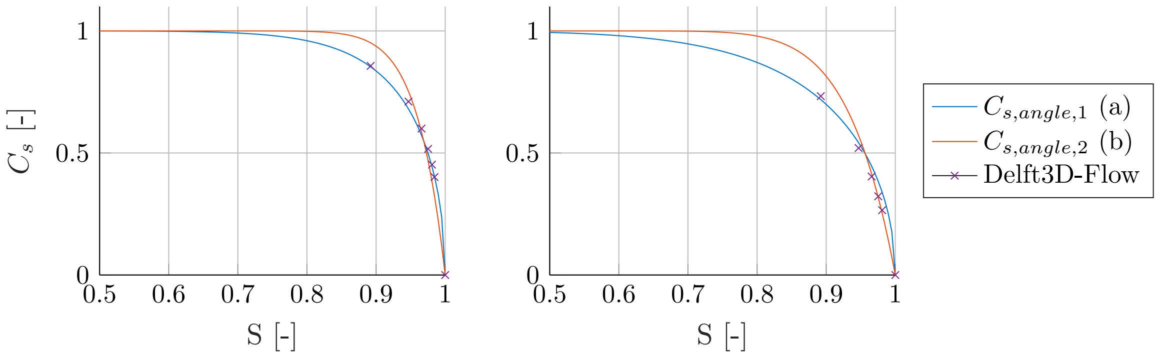

(a) $L_w = 200$ m **(b)** $L_w = 400$ m

Figure 4.13: Comparison of the new angle submergence coefficient formulas with the Delft3D-Flow model runs for $L_w = 200$ m

4.5 Modelling

The results of the model runs for the different schematizations in Delft3D-Flow, as summarized in tables 3.8c and 3.8c, are presented in this section.

4.5.1 Bed topography

Figures 4.14a, 4.14b and 4.14c show the evolution of the relative discharge toward the side channel, the depth average velocity and the flow angle atop the weir crest for different grid sizes respectively. The grid sizes are shown according to the refinement relative to a 10 by 10 m grid. The depth average velocity is considered at two-thirds of the side weir length, because it is expected that in the first section where flow diverts into te inlet, the sharp 90-degree angle will create some small numerical errors that will dissipate further downstream. Inconsistencies in this upstream section between numerical simulation and experimental data were also mentioned by Namaee [2016].

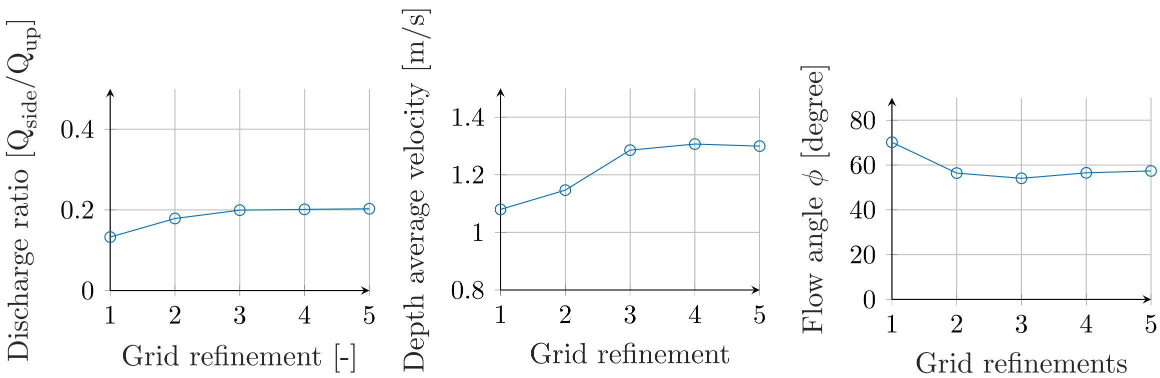

(a) Relative discharge **(b)** Depth average velocity **(c)** Flow angle

Figure 4.14: Model runs for different grid sizes relative to a 10 by 10 m grid (see table 3.8c)

As can be seen in figure 4.14, the considered variables all converge reasonably well at a grid refinement factor in the order of 3 or larger (grid sizes in the order of 3 by 3 m or smaller). For larger grid sizes, the model runs underestimate the discharge and flow velocities over the inlet. Figure 4.15 shows the discharge distribution towards the side channel for different crest height for each of the advection schemes. All schemes stay within a range of 5 % difference with each other. The flood and Waqua scheme show slightly larger discharge for smaller crest heights than the cyclic scheme.

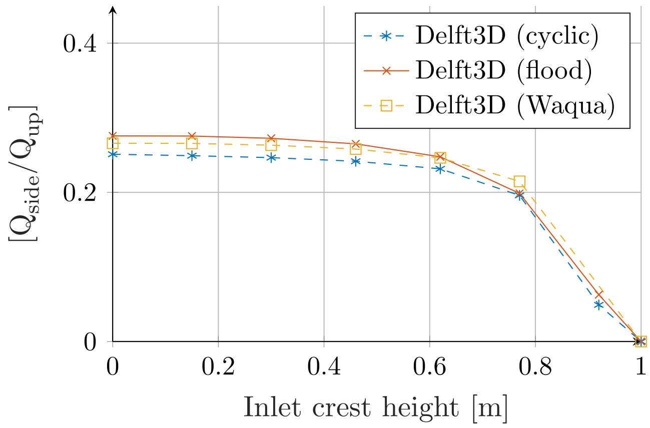

Figure 4.15: Comparison advection schemes

4.5.2 Subgrid weirs

Several model runs are performed with subgrid weirs in Delft3D-Flow model (see table 3.8). The results are presented below.

Discharge distribution

As mentioned previously, inconsistencies are found in calculating the discharge over subgrid weirs modelled in Delft3D-Flow. These inconsistencies are shown by the blue line in figure 4.16a. The crest height that is defined in the subgrid weir does not influence the discharge at all until it reaches critical flow conditions. After elaborate analysis and contact with Deltares experts, these inconsistencies are found to be related to the energy losses calculation. When using a Delft3D-Flow model N by M grid, flow in positive N-direction (from left to right) is considered positive and negative in the opposite direction (negative N-direction). Delft3D-Flow shows to only consider an energy loss for positive flow above a minimal critical velocity, while for flow in opposite direction the energy losses are not considered at all. When similar minimal critical velocities are applied for both positive and negative flow

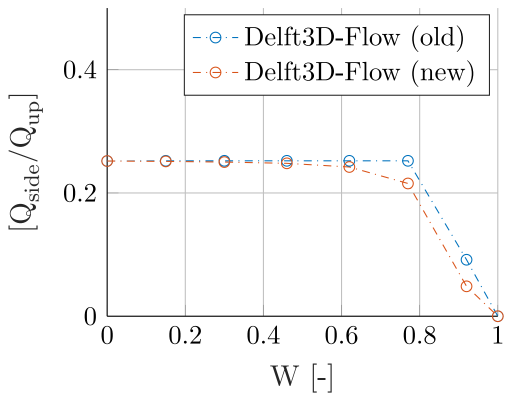

(a) Discharge distributions: Delft3D-Flow

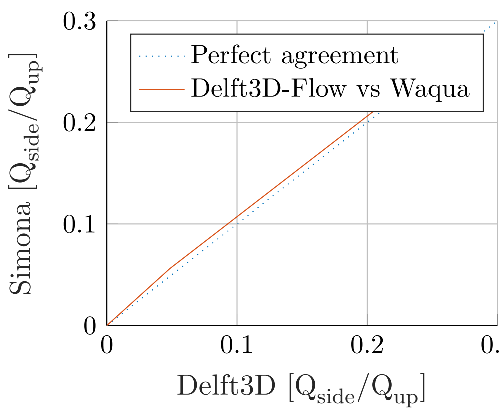

(b) Discharge distributions: Delft3D-Flow vs Waqua

Figure 4.16: Comparison of subgrid weirs in Delft3D-Flow and Waqua models

direction in the calculation of energy losses, the discharge over weir shows to be influenced by increasing crest heights again (red line in figure 4.16a). This adjustment is compared to the use of subgrid weirs in the modelling software Waqua in figure 4.16b and shows similar discharge. The adjustments will be included in the new Delft3D-Flow software release.

Comparing the calculated discharge over the inlet for schematization as part of the bed topography and subgrid weirs is shown in figure 4.17. The two methods compare relatively well (< 5 % difference), especially considering the completely different modelling approach.

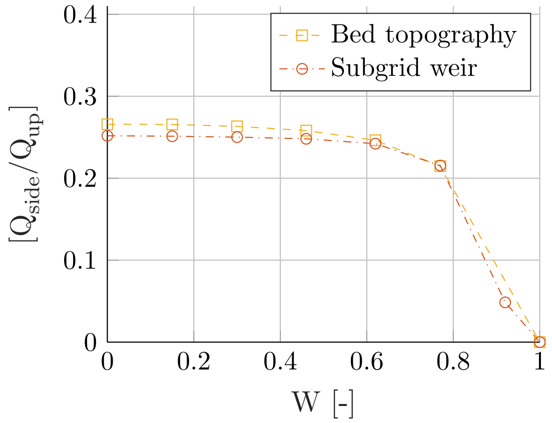

Figure 4.17: Comparison Delft3D-Flow bed topography and subgrid weirs runs

Grid size

The influence of using different grid sizes is analysed. Figure 4.18 shows the discharge distribution towards the side channel for the model runs as presented in table 3.8b. Decreasing the grid size from 3 by 3m to 10 by 10 m does not result in significantly different values. The maximum difference in calculated discharge distribution between the different grid size runs is 3%. This shows that model runs using larger grid sizes still calculate the discharge over weir-like structures relatively well.

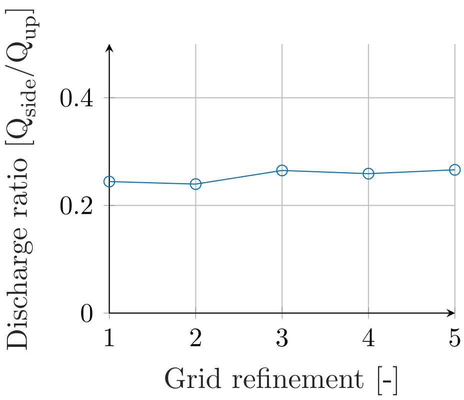

Figure 4.18: Discharge distribution of subgrid weir model runs for different grid sizes relative to a 10 by 10 m grid

Flow angles

The calculated flow angles above the inlet crest for three of the model runs, as presented in table 3.8c, are shown in figure 5.3. For reference, also the flow angles modelled by the bed topography runs are shown. The flow angles modelled by the subgrid weir runs are not influenced by different crest heights by more than 1 - 2 %. For all crest heights, the flow angles remain (almost) equal to that of a bed topography model run with a zero crest height ($W = 0$). The influence of the crest height on the flow angles is thus not included (or parameterized) in the calculations and results in an underestimation of the flow angles up to 40 degrees.

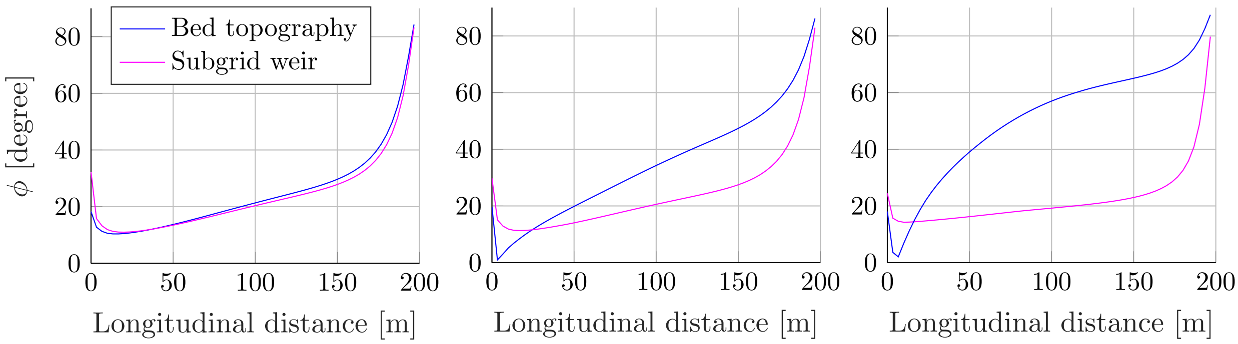

(a) $W = 0.0$ **(b)** $W = 0.46$ **(c)** $W = 0.77$

Figure 4.19: Flow angle atop inlet as function of longitudinal distance for subgrid weir runs for three dimensionless crest heights (W)

4.6 Control strategy

In this sections, the results from the one-dimension model runs are presented for parameters ranging according to table 3.9.

4.6.1 Impacts on discharge distribution

The impact of different design choices on the discharge distribution are shown in figures 4.20 and 4.21. The figures show the relative discharge to the main and side channel, shown by the blue and red line respectively for the different river section as shown in figure 3.1. Further discussion of these results is found in chapter 5.

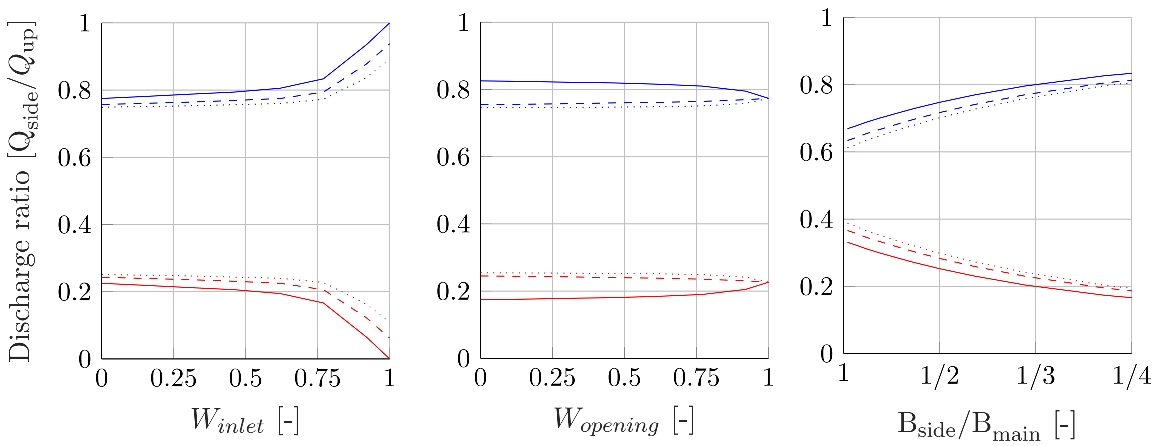

Figure 4.20: Influence of the dimensionless inlet and opening crest height ($W_{inlet,opening}$) on the discharge distribution towards the main (blue lines) and side channel (red lines)

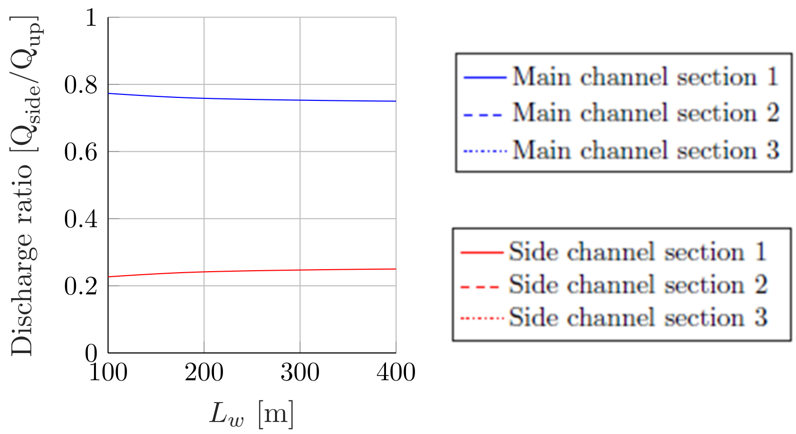

Figure 4.21: Influence of the width ratio (B_{side}/B_{main}) on the discharge distribution

4.6.2 Impacts on flow angles and velocity magnitudes

Impacts on the flow angles can be obtained from previously shown figures 4.7 and 4.8. The maximum velocity magnitudes and flow angles atop the crest are summarized in table 4.3, showing that both the velocity magnitudes and flow angles increase for increasing crest heights. The impact of the crest length on the flow angles and velocity magnitudes is discussed in detail in section 4.4.

Table 4.3: Overview of flow pattern characteristics for models runs with different dimensionless inlet crest heights ($W = w/H$)

Model run	**Crest height**	**Flow patterns**		**Width averaged velocities**	
	W [-]	$v_{1,max}$ [m/s]	ϕ_{160m} [deg]	v_{main} [m/s]	v_{side} [m/s]
B0	0.0	1.15 m/s	30 deg	0.90	1.2
B1	0.15	1.2 m/s	40 deg	0.90	1.2
B2	0.30	1.3 m/s	45 deg	0.91	1.19
B3	0.46	1.4 m/s	50 deg	0.92	1.18
B4	0.62	1.7 m/s	60 deg	0.92	1.1
B5	0.77	2.2 m/s	65 deg	0.94	0.9
B6	0.92	2.2 m/s	65 deg	1.0	0.3

4.6.3 Impacts on circulation cell

Starting with the model run representing a crest height of 0 m above bed level, the circulation cell in the side channel has a length scale around half the size of the inlet (in longitudinal distance). The cell circulates around a point that is located at around one-third the inlet length from the start of the inlet. The influence of different crest heights on the circulation cell at the inlet is summarized in table 4.4. Larger crest heights result in a steady but small increase in length scale to around two-thirds the inlet length. For the model run with a crest height nearly reaching the water level, the velocity magnitudes in the circulation cell decrease significantly and the length increases in longitudinal direction beyond that of the inlet dimensions. Only after around 220 m in longitudinal direction do the flow lines reattach to the shoreline in the side channel.

4.6.4 Various river discharges

Various model runs are performed using different upstream river discharges in the one-dimensional model. For river discharge below ±1800 m^3/s, the two opening crest heights emerge above the water

Table 4.4: Overview of circulation cell characteristics for Delft3D-Flow models runs with different dimensionless inlet crest heights ($W = w/H$)

Model run	**Crest height** W [-]	**Circulation cell** Length [m]	Centre point [m]
B0	0.0	120 m	80 m
B1	0.15	130 m	70 m
B2	0.30	140 m	60 m
B3	0.46	145 m	60 m
B4	0.62	150 m	70 m
B5	0.77	150 m	80 m
B6	0.92	220 m	150 m

level. Downstream of the inlet and openings, the discharge distribution to the side channel in percentage of the total upstream discharge stays relatively constant. However, a sudden change in location where water is directed towards the side channel is noticed when the openings become emerged. This can be seen in figure 4.22. During larger river discharge, the relative discharge towards the side channel slightly increases. This can be explained by the relative height of the weir to the water level decreasing ($h - w$ thus increases in equation 3.2). However, the influence on the discharge distribution is $< 2\%$ and thus considered small. Larger discharges are not evaluated as this will result in the emergence of the entire longitudinal training dams, which will not be modelled correctly by the one-dimensional model (see appendix B).

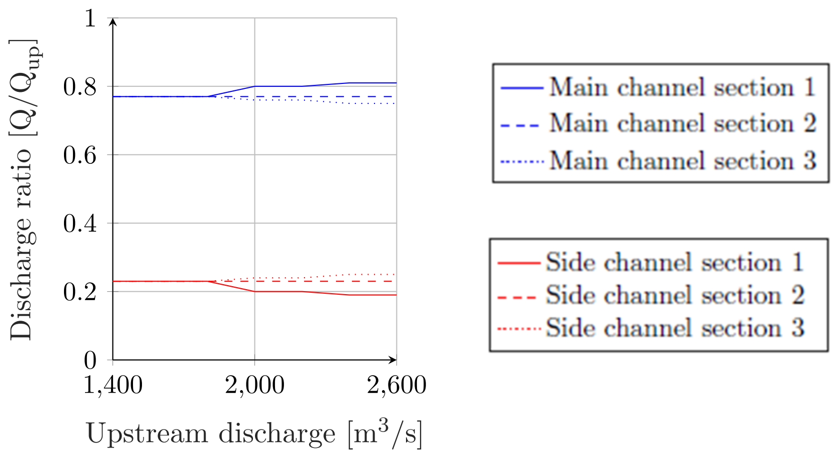

Figure 4.22: One-dimensional model runs for various upstream discharges ($W = 0.46$)

Chapter 5: Discussion

5.1 Introduction

The results presented in chapter 4 are discussed in this chapter. They are, again, treated in order of the research questions as presented in chapter 1. The one- and two-dimensional models are discussed further in appendices B and C. In the last two sections, a reflection on the river functions and the accuracy and uncertainties of this research is given.

5.2 Mechanisms and factors

The one-dimensional model runs with different mechanisms and factors, as presented in the previous chapter, show that the influence of the transverse slope, secondary flow and porous discharge on the discharge distribution is relatively small. The transport of water seems to be mainly controlled by the equilibrium water depth in the two channels. This complies with the general theory of river bifurcations that discharge distributions depend on downstream conditions, with hardly any influence from the local flow field. As shown by equation 2.1, the equilibrium water depth is influenced by a combination of the specific discharge, bed resistance, and bed slope. It is therefore very interesting to evaluate the difference between the specific discharges in the two channels. As shown in table 5.1, the specific discharge in the side channel is considerably lower than in the main channel. Looking at the different sections, it can be seen that the specific discharge in both channels is almost equal in the last river section (downstream of the last opening).

Table 5.1: Specific discharge in different river sections for dimensionless inlet and opening crest heights of $W = 0$

Channel	**Section 1** [m^2/s]	**Section 2** [m^2/s]	**Section 3** [m^2/s]
Main	6.14	5.77	5.72
Side	4.47	5.54	5.68

Crest length
This would suggest that longer inlet or opening crests (in combination low crest heights, equal bed levels, and channel roughness) result in the specific discharge in the channels converging to an equal value. It can thus be argued that the inlet is not long enough to direct sufficient water towards the side channel to result in an equal specific discharge. By performing an additional model run with equal channel widths and zero crest height (see table B.2), the specific discharge is shown to converge to (almost) equal values for larger inlet lengths. This verifies the assumption that a long enough crest length results in an equal specific discharge distribution and also the idea that the crest length plays an important role in the different equilibrium water depths in the two channels.

Bend radius
The bed slope is influenced mostly by the decrease of side channel length for decreasing river bend radius ($\frac{ib_{side}}{ib_{main}} \propto \frac{L_{main}}{L_{side}}$). The difference in length between the channels is found to be equal to the difference in bend radius (see equation 2.2) and can be expressed by the transverse distance between the center lines of the two channels. As the ratio of transverse distance over bend radius is small, also the bed slope difference is small (5%). The corresponding impact on the discharge distribution

is much smaller (≪1%, see figure 5.1a). Looking at other impacts of the bend radius, the difference in discharge distribution resulting from enabling or disabling the transverse slope is in the order of 10^{-2}%. The impact of increased transverse velocity by secondary flow in the calculations is even smaller ($< 10^{-3}$%) as shown in table 4.1. The discharge distribution, thus, shows not to be influenced much by the placement of the longitudinal training dams in a river bend. A nearly straight channel, neglecting all bend effects, still results in a similar discharge distribution. This is supported by the model runs for different bend radius values in the one-dimensional model, see figure 5.1a.

For larger weir heights, the influence of the bend radius on the discharge distribution increases but only becomes significant for crest heights approaching values very near the water level (see figure 5.1b). Similarly, for a wider channel, the influence of the bend radius is argued to increase somewhat due to a larger effect of the transverse water level slope. A reason for still placing the longitudinal training dams in a river's inner bend is that also in periods with a low river discharge, even though the effect on the bed is small, water is still being drawn towards the side channel. This would, for instance, not be the case in an outer main channel bend.

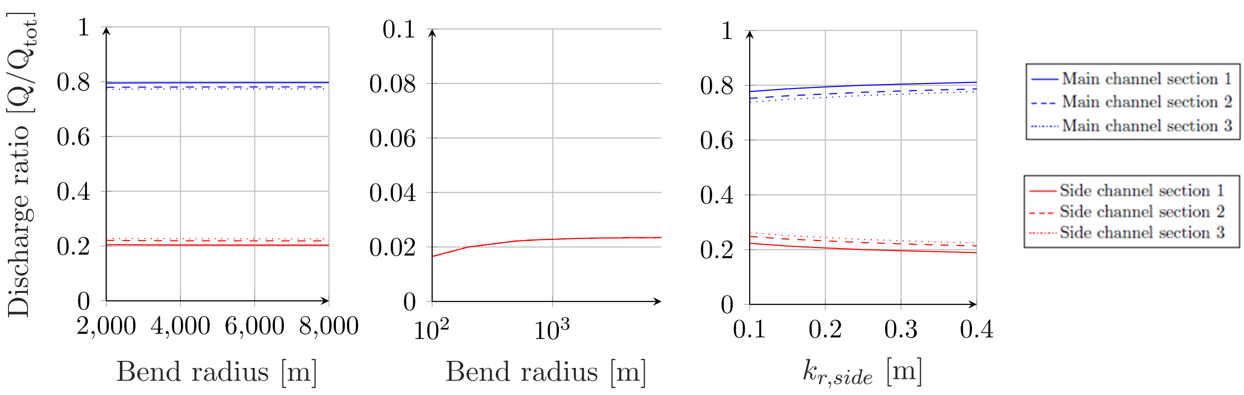

(a) $W = 0.45$ (b) $W = 0.95$ (c) Nikuradse side channel

Figure 5.1: Discharge distribution for different bend radius and side channel bed friction values

Bed resistance

Relative to the bend radius, the one-dimensional model shows a larger influence on the discharge distribution by an increase in bed resistance in the side channel, relative to the main channel. Figure 5.1 shows that the discharge towards the side channel decreases in the order of a few percent (3-5 %) for larger bed friction values in the side channel. This can be explained by the fact that a larger bed friction (larger bed roughness height) 'blocks' water in the side channel. This will result in increasing water levels in the side channel, thereby decreasing the difference in water level between the two channels that drive discharge over the inlet and openings.

When changing the crest height of either the inlet or the openings, some of the mechanisms and factors positively influence the discharge towards the side channel. For an increasing crest height, the longitudinal water level slope difference between the two channels also increases. This is noticed by a decreasing level of submergence as shown in figure 4.16. An explanation for this is given by the decrease in specific discharge and thus a lowering of the water level in the side channel. The lower submergence level thus partly compensates the decrease in water depth above the weir crest $(h - w)$ for increasing crest levels.

5.3 Flow patterns

In chapter 4 it was discussed that for increasing crest heights the flow eventually becomes critical atop the crest (see figure 4.5). The categorization by Borghei [2003], that distinguishes short- from broad-crested weirs, seems to very well predict the crest heights at which this occurs. For an inlet in submerged condition, the specific discharge atop the crest increases in downstream direction (figures 4.7 and 4.8). For free-flowing conditions ($Fr_1 > 1$), both the specific discharge and the flow angles show to remain relatively constant in downstream direction (with exception of the most upstream and downstream edges).

The submergence coefficient from Ka-Leung Lee [2002] shows to predict the discharges in submerged conditions well but cannot be used to predict the flow angles in submerged conditions (figure 4.8). The coefficient a in the Villemonte [1947] formula and the coefficient b in the formula by Ka-Leung Lee [2002] have been calibrated specifically for the flow angles. This is done with help of the Delft3D-Flow model runs are presented in chapter 3. The newly found formulas and their coefficients a and b are found to depend on the submergence factor (S) and the crest length (L_w) that is made nondimensional by division by the main channel width (B_{main}). The newly proposed equations and corresponding coefficients are presented below.

$$Cs_{angle,1} = \sqrt{1 - S^a} \qquad \text{where } a = 9.14 * (\frac{L_w}{B_{main}})^{-0.84} \tag{5.1}$$

$$Cs_{angle,2} = 1 - \frac{1}{0.5^b}(S - 0.5)^b \qquad \text{where } b = 10.29 * (\frac{L_w}{B_{main}})^{-0.72} \tag{5.2}$$

The newly proposed parameterization for flow angles is an improvement over the existing submergence formulas that do not predict the angles well. Figure 5.2 compares the new coefficients for several submergence factors with the existing parameterization that predict the discharge in submerged conditions (equation by Ka-Leung Lee [2002] and Villemonte [1947]). It can be seen that for a submergence factor (S) larger than 0.8, the newly proposed $C_{s,anlge}$ differs considerably from the C_s relationships. For increasing S values the difference between the proposed $C_{s,angle1}$ or $C_{s,angle,2}$ equations and C_s increases to an order of 60 %.

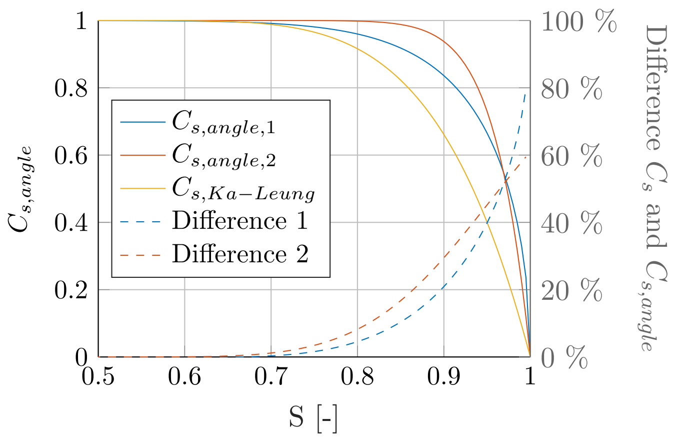

Figure 5.2: Comparison of newly determined parameterization for flow angles ($C_{s,angle}$) with parameterization for discharge from literature (C_s) including the relative difference

The general Villemonte formula with the newly determined coefficient a slightly better estimates the submergence coefficient, according to the calculated total root-mean-squared-error value (RMSE). Therefore, the use of this formula is preferred and the implementation of this parameterization into Delft3D-Flow subgrid weirs is suggested. It must be noted, however, that this new relationship is only fitted for submergence factors that are determined at one location: at the start of the inlet in upstream direction. For implementation in Delft3D-Flow or other modelling software, it is advisable to analyse the data again for each grid cell individually. The local submergence factor (S) and the discharge at each grid cell containing a subgrid weir can be determined, thereby calculating a flow angle for each grid cell instead of determining an averaged flow angle atop the entire weir crest. Secondly, equation 5.1 is determined for the specific dimensions as given by table 3.1 with varying inlet crest heights and crest lengths. This means that situations with a different upstream discharge, channel widths or bed elevation in the side channel are not included. The effect of a different upstream discharge is expected to not change the above-found relationship for flow angles significantly. This is motivated by figure 4.22 that already showed that different upstream discharges only affect the discharge distribution in the order of 1-3 % and the upstream discharge mainly influences the water level and energy head. This effect is already included in the submergence factor (S). A larger main channel width is also expected to not result in different flow angles as the flow in the main channel opposite the inlet and openings already flows parallel to the right river bank. If the main channel width will be decreased, it is, however, expected that flow over the entire channel width is affected by the inlet or openings. This will possibly significantly influence the flow angles atop the inlet or opening crests.

5.4 Modelling

When looking at the possible schematizations of the system of longitudinal training dams in large river models, the schematization with help of bed topography and subgrid weirs are compared. As shown in figure 4.17, both methods provide similar discharges over the inlet or openings. When schematizing the inlet or openings in the bed topography, small enough grid sizes are required to produce numerically converged discharges and velocities (in the order of 3 by 3 metre or smaller as previously shown in figure 4.14). The use of subgrid weirs does not require such small grid sizes (figure 4.18). The computation time required to perform both types of calculations thus differs considerably as a result of the different grid sizes required. When only interested in the discharge distribution between the two channels, it is thus preferable from a computation efficiency point of view to use the subgrid weirs.

However, when also velocity magnitudes or flow angles are important parameters, large differences are found between the two methods. This is shown in figure 5.3. The flow angles atop the crest in subgrid weir runs do not change for different crest heights and remain (nearly) equal for all performed model runs from table 3.8c. The flow angles are (very) similar to the angles resulting from bed topography runs with zero crest height ($W = 0$). This is explained by the lack of parameterization of flow angles within Delft3D-Flow and Waqua. According to literature, and as found using the bed topography model runs, different crest heights should result in increased flow angle (figures 2.9 and 2.10). It is thus expected that subgrid weirs, as currently implemented in Delft3D-Flow or Waqua, are not applicable when (besides water levels and discharge distribution) also velocity magnitudes and flow angles are of importance. This is the case for sediment transport calculations in morphological models. In such cases, the use of bed topography schematization for the inlet en openings should be used. Below, a number of additional comments are made on the use of either of the schematization methods.

5.4.1 Bed topography

When the longitudinal training dams are schematized as part of the bed topography, small enough grid sizes (see figure 4.14) produce numerically converged discharges and velocities. Larger grid sizes underestimate the discharge over an inlet or opening in the order of 30 % and increasing for grid sizes of 10 m and larger. Small grid sizes (<5 m) are expected not to be feasible in larger river models that usually have grid sizes in the order of 10 to 20 m. This will thus require the use of locally decreased grid sizes in order not increase the computational time to unrealistic large durations. There are several ways to locally decrease the grid sizes, including the use of flexible grids. Other than showing that small grid sizes are required, these grid size reduction techniques have not been treated in this research. From a computation efficiency point of view, it would be interesting to evaluate techniques in more detail.

As can be seen in figure 4.15, the Waqua scheme results in slightly more discharge towards the side channel then the Cyclic scheme. This can be related to the friction terms in both schemes, where the friction term in the Waqua scheme is smaller compared to the cyclic scheme [Stelling, 1983]. As previously shown in figure 5.1, less friction results in more discharge towards the side channel. The flood scheme shows results fairly similar to the Waqua scheme. The cyclic scheme differs in the order of $5-10\%$ with the Waqua and flood advection scheme. The flood advection scheme is expected to produce the most accurate discharge distribution between the channels. This is because the flood scheme takes into account the local characteristics of the flow such as flow contraction and expansion, that require a different modelling approach as is treated in appendix C (see figure C.6).

Although the flood scheme is expected to be the most accurate, due to the combination of conservation of energy and momentum, the flood scheme also shows to become unstable for too large time steps in combination with crest heights inducing supercritical flow (W>0.9). This is explained by the large velocity changes atop the inlet or opening crest as previously shown in chapter 4 (figure 4.5). The use of the flood scheme, therefore, results in large computational times (dt=0.005 min instead of dt=0.02 min) for such large crest heights. Therefore, it is advisable to use the Waqua scheme when modelling longitudinal training dams.

5.4.2 Subgrid weirs

The inconsistencies found in the calculated discharge over subgrid weirs in Delft3D-Flow has minimal influence for small crest heights (see figure 4.16a). However, for larger crest heights, the impact of not including the energy losses over the weirs results in significant differences (>10% difference). The adjustment that has been made in the Delft3D-Flow software regarding the energy loss calculation will be incorporated in the new software release of Delft3D-Flow. Waqua shows not to experience the above-mentioned inconsistencies. The corrected Delft3D-Flow and Waqua models have been compared and are shown to provide similar discharge distributions, see figure 4.16b. One must thus be careful when using the subgrid weirs in older versions of Delft3D-Flow.

Additionally, schematization with the help of subgrid weirs shows to be less influenced by increasing grid sizes (smaller grid refinement). This is shown in figure 4.18 in chapter 4. The calculated discharge distribution towards the side channel remains relatively equal with a difference in the order of 5-10 % for grid size decreasing from 10 to 3 m (this is in the order of 30 % when using bed topography schematization).

Regarding the flow patterns, the inclusion of a new parameterization to adjust for the effects of increased crest heights on the flow patterns is advisable. Without this parameterization, the error made in the modelled flow angle is especially high in the downstream section of the inlet and openings and can reach as high as 40 degrees. By inclusion of the parameterization, figure 5.3 shows the adjusted flow angles in longitudinal direction. Using a length averaged parameterization still results in some errors in the upstream section but reduces the error in downstream direction significantly. The downstream section conveys the largest discharge towards the side channel end is thus also of main importance when considering future sediment transport and morphodynamic calculation.

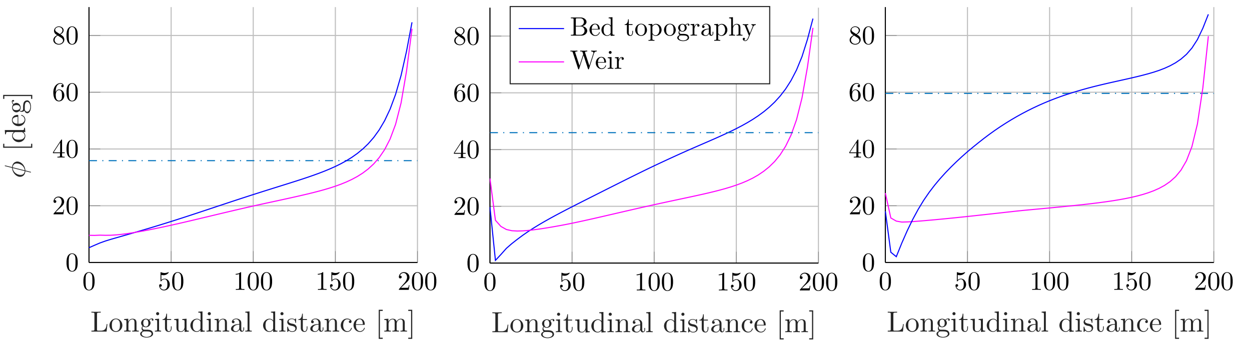

(a) $W = 0.15$ (b) $W = 0.46$ (c) $W = 0.77$

Figure 5.3: Flow angle atop inlet as function of longitudinal distance for weir structures for schematization in bed topography (plus discharge averaged) and as subgrid weir

5.5 Control strategy

In the construction process of the longitudinal training dams, several design choices were made. Some of the design choices result in the inclusion of regulatory dimensions such as the inlet and opening crest heights that provide an adaptable control strategy. As a second considered type of design choice, the side channel width can vary over time due to maintenance dredging activities or morphological development in the river section. Possibly by adjusting the crest height, the sediment transport into the side channel can be controlled, which is studied in more detail by Jammers [2017]. Other design choices include permanent dimensions such as the crest width and position of inlet and openings. Such permanent dimensions are not included in this research but, from a hydraulic and sediment transport point of view would be very interesting to investigate in further studies. The one-dimensional model is used to assess the impact of the crest heights and side channel width on the discharge distribution between the main and side channel. The two-dimensional model is used to determine the impacts on local flow patterns.

5.5.1 Inlet crest height

Influence on discharge distribution

At first, changing the inlet height does not show a large effect on the discharge distribution. The decreasing water depth above the weir crest $(h - w)$ is (partly) compensated by a decreasing level of submergence. A lower submergence factor means a larger water level (or pressure) difference over the inlet crest that thus limits the decrease in discharge. After the dimensionless crest height reaches a value of roughly 0.9 or larger (corresponds to broad-crested categorization by Bos [1976]), the side channel discharge decreases significantly towards zero when the water level is below the crest. Such a dimensionless crest height corresponds to the Froude number above the crest reaching 1. The flow and weir type then change to free-flowing and broad-crested respectively. This means that for dimensionless crest heights above 0.9, the discharge over the inlet or openings is no longer influenced by conditions in the side channel and thus neither by the level of submergence. Therefore, the discharge distribution sharply decreases beyond this point.

Secondly, lowering the crest height results in a more equal specific discharge distribution in longitudinal direction at the inlet or openings, as shown in figure 5.4. This means that also the depth average velocities in two channels slowly convergence to similar magnitudes when the inlet crest height is lowered.

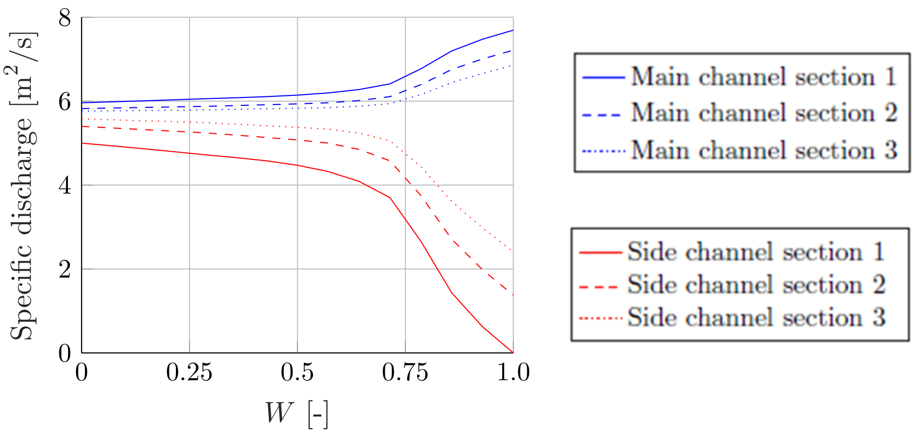

Figure 5.4: Specific discharge in both channels for different dimensionless inlet crest heights ($W_{inlet} = w/H$) and constant opening crest heights ($W_{opening} = 0.92$)

Influence on flow patterns

As can be seen in figure 5.5, the lateral outflow angle at the inlet increases for increasing crest heights. For high crest heights, where flow is in super-critical condition (see figure 4.5), the lateral flow angles remain nearly constant in longitudinal direction. Secondly, it can be seen that for larger crest heights, the flow angle at the upstream side is negative. This indicates that flow is directed from the side towards the main channel and the secondary circulation cell thus protrudes onto the crest.

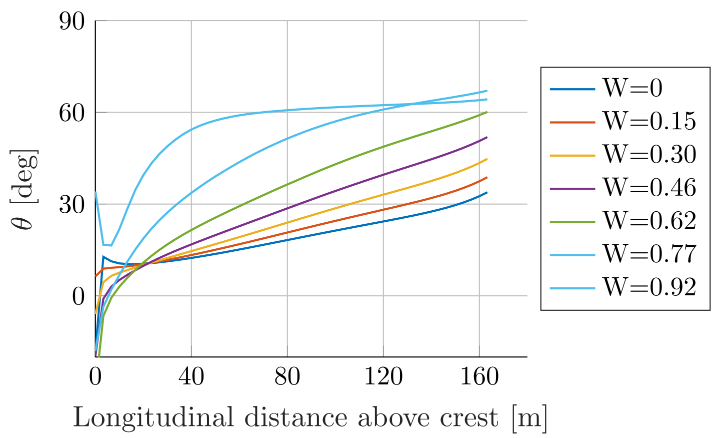

Figure 5.5: Comparison of flow angles (ϕ) in longitudinal direction atop the inlet for different dimensionless crest heights ($W = w/H$)

Characteristics of the circulation cell can be found in table 4.3 for different inlet crest height. It is seen that the circulation cell increases in length and intensity for larger crest heights. This can be explained by the larger velocities and smaller discharges over the inlet, resulting in higher velocity gradients while the amount of discharge over the inlet does not suppress the circulation cell growth.

5.5.2 Opening crest height

Changing the crest height of the openings between the longitudinal training dams has some influence on the discharge ratio in the sections upstream of the opening (O(5%)). Smaller opening crest heights force a larger discharge over the opening, while at the same time they result in less discharge being drawn at the inlet. Altogether, the discharge ratio in the sections downstream of the openings is not influenced much (O(1%)) by the opening crest heights.

5.5.3 Channel width

Increasing the side channel width (or in dimensionless term the ratio between the main- and side channel width) can influence the discharge ratio in the order of 30%. Even a relatively small change in side channel width of 10 m thus shows to have a rather large influence on the amount of discharge towards the side channel (10%). This can be explained by the change in conveyance area that results in more or less water being able to flow through the respective channel. The specific discharge in the side channel stays nearly the same, but not the total discharge. This means that with a constant main channel width, the specific discharge and also the water levels in the main channel decrease considerably. With help of figure 5.6, a side to main channel width ratio can be determined for a given discharge distribution.

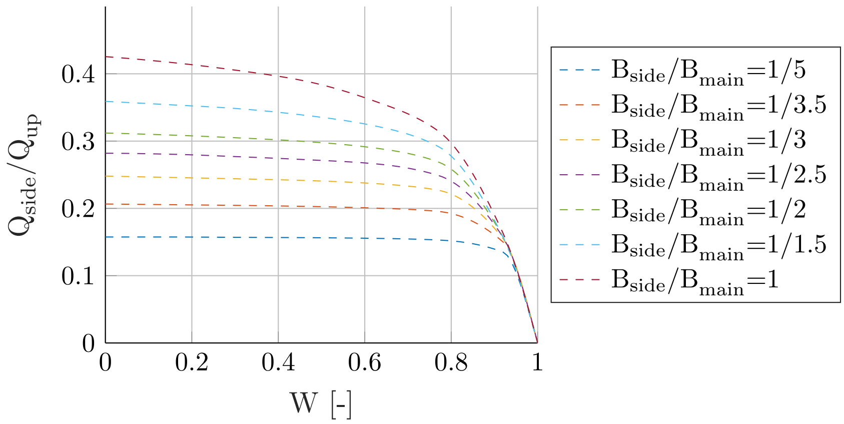

Figure 5.6: Combined influence of dimensionless crest height (W) and side channel width B_{side} on the discharge distribution

5.5.4 Crest length

In some conditions, not the total discharge but rather the specific discharge in the side channel is an important design criterion. For instance, from an ecological point of view, the averaged velocity magnitudes are influenced by the specific discharge. Not the side channel width, but the combination of crest height and crest length provides better control of this. Figure 5.7 shows the influence of different crest heights and lengths on the specific discharge in both channels that can be used in designing towards a particular specific discharge in the side channel. As the dimensionless crest height greatly varies for different river discharges, the crest length could provide more stable control over a large range of river discharges.

5.6 River functions

The pilot project longitudinal training dams in the Waal has been initiated to improve several river functions. This has previously been discussed in chapter 1. In this section, the hydraulic conditions as investigated in this research are used to reflect on these river functions. It must be noted again that knowledge on the sediment transport and morphological development is crucial to understanding the impacts on the river functions. The sediment transport at longitudinal training dams is treated in research by Jammers [2017]. Combining the findings by Jammers and this research can be used to reflect on - or perform calculations of - the morphological development. This integration, however, is not performed in this research. In the sections below a selection of river functions are discussed separately with help of the found hydraulic conditions. However, a full translation to the river functions is not possible due to the lack of knowledge on the morphological development. A reflection on the combination of several river functions is made in the last section.

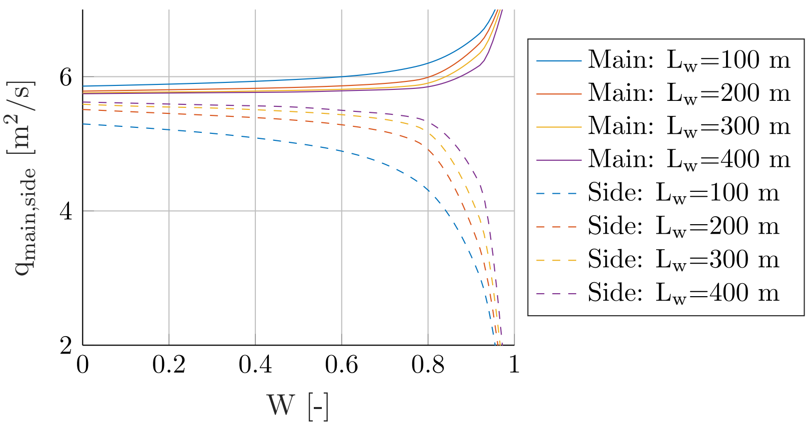

Figure 5.7: Combined influence of dimensionless crest height (W) and inlet crest length L_w on the specific discharge in both channels

5.6.1 Flood protection

The flood protection is mainly influenced by conveyance area and associated average water levels on a spatial scale of the longitudinal training dams or larger. The water levels, in turn, are largely influenced by the discharge distributions between the two channels. This means that local flow angles or velocity magnitudes at the scale of an inlet or opening are not very relevant. Due to the interaction of the system of longitudinal training dams with a great many other river interventions, the level of flood protection is often calculated using larger river models. In such two-dimensional models, schematization of the inlet and openings with help of subgrid weirs is advisable from a computational efficiency point of view.

As a first evaluation, the influence of different crest heights on the water levels evolution in the main channel is considered. This is done for the river discharge of 2000 m^3/s that is used throughout this research. A larger river discharge is not considered as the longitudinal training dams will then be fully submerged, which is not modelled correctly as this can no longer be schematized as a two channel system. The longitudinal water level evolution along the dams for different inlet crest heights, as calculated with help of the two-dimensional Delft3D-Flow model, are presented in figure 5.8. Increasing the dimensionless inlet crest heights from $W = 0$ (zero metres above bed level) to $W = 0.77$ has very limited influence on the water levels in the main channel (order of 0.01 m). A fully closed inlet crest height ($W = 1$) results in an increasing water level in the order of 15 cm with respect to a fully open condition ($W = 0$). A comparison with the original situation of groyne fields is not made here.

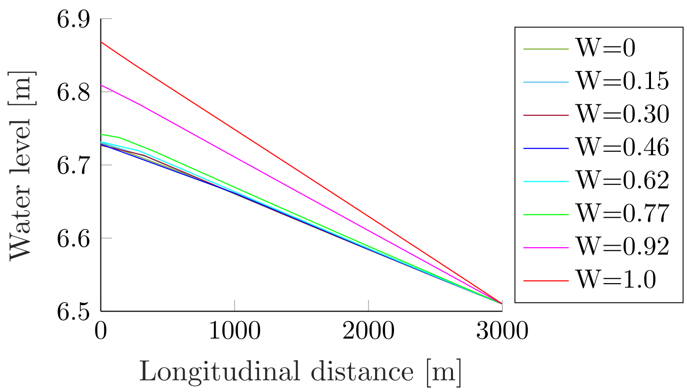

Figure 5.8: Water level in longitudinal direction along training dams for various dimensionless crest heights ($W = w/H$)

5.6.2 Navigation

Navigation in the river is mainly influenced by the dimensions of the navigational channel and the transverse velocity magnitudes around the inlet and openings in the navigational channel. From this research, no statements can be made on the influence of longitudinal training dams on the bed levels and thus the depth criteria in the navigational channel. This will require information of the morphological development that is not treated here. With help of research by Jammers [2017], this could be investigated in the future. The transverse velocities can be investigated with help of this research and will require the use of the two-dimensional model. Schematization with help of bed topography will be required due to the interest in velocity magnitudes and flow angles around the inlet and openings. These are not modelled correctly by the subgrid weirs.

The velocity magnitudes and directions have previously been visualized in figure 4.6 and the transverse velocities around the inlet are magnified in figure 5.9. This figure shows the specific cases of $W = 0$, $W = 0.30$ and $W = 0.77$ as these show the reduction of transverse velocities for increasing crest heights. The largest velocity magnitudes in transverse direction are found for the lowest crest height. Looking specifically at the magnitudes of transverse velocities in the navigation channel, that is situated between the black lines, maximum values of 0.2 m/s are noticed around the inlet for lower crest heights. This is right around the allowable 0.15 - 0.3 m/s as determined by Rijkswaterstaat. Maximum values of 0.15 and 0.30 m/s for the transverse velocities extend to around 20 and 70 m respectively into the main channel.

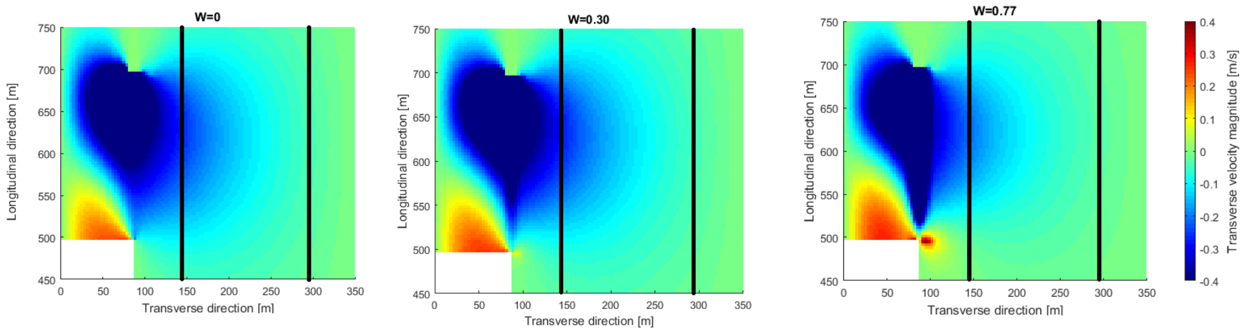

(a) $W = 0$ **(b)** $W = 0.30$ **(c)** $W = 0.77$

Figure 5.9: Top view of transverse velocity magnitude at the inlet for different dimensionless crest heights ($W = w/H$)

5.6.3 Ecology

The most important aspects from an ecological point of view are the average and fluctuating components of the velocity magnitudes. Small average velocities are important to provide sheltered and calm locations for ecological development on the river bed. Low velocity fluctuations provide a more stable environment that shows to have a positive effect on the ecological development [Collas, 2016]. The largest velocity fluctuations are the result of waves and water level variations induced by passing ships. The ecological development in the side channel is thus very much influenced by the extent to which the velocity magnitudes and flow angles created at the inlet and openings penetrate into the side channel. This means a two-dimensional bed topography model is essential to properly analyse the influence of a system of longitudinal training dams on the ecological development. Due to the lack of correct flow angles and velocity magnitudes, the use of subgrid weirs will not suffice.

The blocking effect of the inlet and openings on ship waves has not been analysed. This is the result of the static model runs with constant river discharge used in this research, that does not include time-dependent boundary conditions. The averaged velocity magnitudes and flow angles in both channels can be computed with help of the extended Delft3D-Flow model. Table 5.2 presents the width averaged velocity magnitudes for a variation of inlet crest heights. The velocity magnitude in the side channel is considerably lower than in the main channel and decreases further for increasing crest heights. High inlet and opening crest heights show to result in the smallest depth-averaged velocities in the side channel. Also, higher opening crest heights show to result in the smallest velocity magnitudes penetrating into the side channel.

Table 5.2: Overview of the velocity magnitudes in the two channels for different dimensionless inlet crest heights ($W/w/H$)

Model run	**Crest height** W [-]	**Crest velocity** $v_{1,max}$ [m/s]	**Width averaged velocities** v_{main} [m/s]	v_{side} [m/s]
B0	0.0	1.15 m/s	0.90	1.2
B1	0.15	1.2 m/s	0.90	1.2
B2	0.30	1.3 m/s]	0.91	1.19
B3	0.46	1.4 m/s	0.92	1.18
B4	0.62	1.7 m/s	0.92	1.1
B5	0.77	2.2 m/s	0.94	0.9
B6	0.92	2.2 m/s	1.0	0.3

5.6.4 Designing for multiple river functions in an integral way

The longitudinal training dam pilot project in the Waal was initiated as a possibility to not only make improvement for a single river function individually but provide a combined effect on different functions simultaneously. Design considerations or maintenance strategies should thus include all aspects and consider an integral way to include all intended river functions without having to treat each river function individually.

The different river functions each require other areas of attention (water depths, water levels, transverse velocity). Finding a combination that fits all criteria is the ultimate goal. An increased inlet crest height is both favourable from a navigation and ecological point of view (less transverse velocities and lower specific discharge and fluctuations). However, increasing the inlet crest height does result in the side channel not receiving any water at all during periods with very low river discharge. From a flood protection point of view, larger crest heights mean an increasing water level in the main channel. However, this is the case for small river discharge and this effect greatly reduces for an increasing river discharge. The water level corresponding to an extreme river discharge of 10.000 m^3/s is $h \approx 10$ m +NAP according to Rijkswaterstaat [2016b]. The dimensionless inlet crest height then becomes W=0 or W=0.55 for a completely open or closed inlet respectively. Therefore, it is expected that for such high river discharges, the inlet crest height only marginally influences the distribution of discharge between the two channel. Although, for such conditions, a true discharge distribution is not reached anymore as the longitudinal training dams will be completely submerged. It must be noted that in this consideration the influence of increased flow angles on the sediment transport and resulting morphological development on the river functions is not included (different bed levels or channel widths). The morphological development is expected to have a large impact on the river functions, possibly larger than the hydraulic conditions, and should thus be investigated in more detail. When only considering the hydraulic impacts, the suggestion is made to optimize the inlet crest height to a higher crest level while still keeping the inlet in submerged conditions for most of the year (prevent too frequent cut off from the river).

From a modelling point of view, making use of the available modelling tools to determine the impact on river functions simultaneously would also be very beneficial. If subgrid weirs in their current form are used to schematize longitudinal training dams, the flow patterns and velocity magnitudes atop and around the crest are not modelled correctly. As long as parameterization for flow angles (as suggested in this research) is not included, the use of subgrid weirs is not useful to analyse the impact of a system of longitudinal training dams on the combined river functions. Besides the flow angles not being modelled correctly, no parameterization has been included yet in subgrid weirs for modelling the sediment transport into the side channel for a full morphodynamic calculation. Therefore, schematization of the inlet and openings within the bed topography is required using a small enough grid size (order of 3 m) and a Waqua or flood advection scheme.

5.7 Accuracy and uncertainties

"A natural river system is subject to uncertainties that are inherent to spatial and temporal processes in nature" [Vuren, 2005]. In combination with a -by definition- imperfect schematization of reality and the use of error-sensitive input parameters, the descriptive accuracy of (computational) models such as those used in this research become subject of discussion. In other words, the real world can be approached by scientific models but stays fundamentally unpredictable and always shows to be richer and more complex than we can comprehend. The inherent uncertainties, that includes "the realisation of the [natural] stochastic process in the future" is not discussed in this research and reference is made to Vuren [2005]. The parameter and model uncertainties are discussed in the sections below. The sensitivity analysis that is discussed in appendix B.5.2 provides a first inside in the level of uncertainty of the model results, provided the (in)accuracy of the input parameters. However, this analysis only covers the uncertainties in the bend radius, bed friction, and permeability of the inlet and openings. Variations in other input parameters, such as the upstream river discharge, crest widths, weir coefficients, and other parameterization coefficients have not been analyzed.

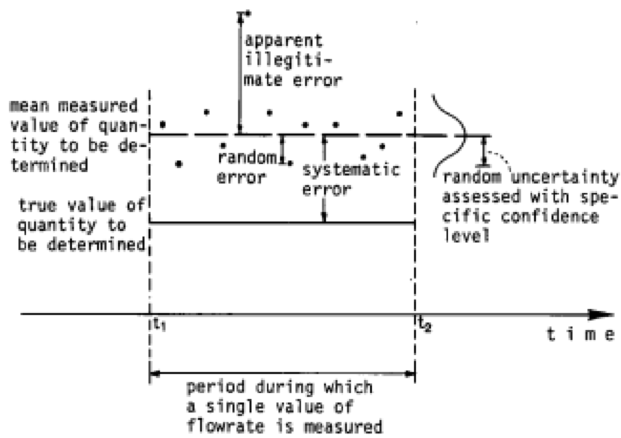

Figure 5.10: Nature of errors from parameter measurements [Bos, 1976]

5.7.1 Parameter uncertainty

There are three basic types of possible errors resulting from parameter use that should be considered in hydraulic research [Bos, 1976]. These are: spurious errors (caused by human mistakes), random errors (caused by experimental and reading errors), and systematic error (caused by a mean deviation). Figure 5.10 presents the last two types of errors in an illustrative form. The relative error X_i is used to describe and compare the different errors and is calculated by the ratio of the uncertainty Δi over the actual value of parameter i. Considering the discharge calculated by the empirical weir formula ($Q_w = \omega c C_{d0} C_s \sqrt{2g}(H-w)^{3/2} L_w$), each of the parameters can be identified as a source of error. The relative errors of the following parameters should thus be taken into account:

1. **Discharge coefficients** ($X_d = \frac{\Delta C_d}{C_d}, \frac{\Delta\omega}{\omega}$)

   The relative error resulting from C_d and ω can be considered constant and systematic (when considering the indirect errors from h to be neglectable). Bos [1976] argues that in general the error in discharge coefficient for broad-crested weirs is depended on the energy head H_1 to crest width B_w factor with a minimum of 4 % error. Bos deduced equation 5.3.

   $$X_c = \pm(3[\frac{H_1}{B_w}^{1.5} + 4]) \tag{5.3}$$

   where X_c is the error in the discharge coefficient. A value of $X_c = 3\%$ has been found when comparing the empirical relationship of Hager [1987] with the Delft3D-Flow modelling results (see figure 4.1b).

2. **Submergence coefficient** ($X_s = \frac{\Delta C_s}{C_s}, \frac{\Delta C_{s,angle}}{C_{s,angle}}$)

   The error in the submergence coefficient (X_s) is considered a combination of systematic and random errors due to the strong correlation with the input of the energy level ($C_s = f(S)$). The newly determined formula for the flow submergence coefficients shows a maximum relative error of $\leq$13 % with the discharge averaged flow angles from the Delft3D-Flow models for various crest lengths. This is still a rather large relative error compared to the previously discussed errors but already a huge improvement to the relatively error of up to 600 % for low dimensionless crest heights (see figure 4.11).

3. **Dimensional parameters** ($X_b = \frac{\Delta B_w}{B_w}, \frac{\Delta L_w}{L_w}$)

   The errors in the dimensional parameters in field measurements, especially crest width and length, are considered to be of systematic nature. The stones that make up the inlet and openings are basically loose rouble, resulting in varying crest width. For instance, an error of 10 % in crest width can, in turn, results in a $\pm$1.5 % error in C_d (see figure 2.7). The crest length, that also depends on the water level at the time of measuring (see the difference between L_w and $L_{w,effective}$ in figure 2.6b), is expected to result in a similar order of error. Both are considered neglectable with the respect to the other errors.

4. **Energy level and river discharge** ($X_h = \frac{\Delta h}{h}, \frac{\Delta Q_up}{Q_up}$)

   The relative error in energy and water levels is comprised of a random and systematic error [Bos, 1976] but will not be treated in more detail. Enough literature is available on the errors in determining water levels and discharge measurements, see Bos [1976] and Thomas [1957].

   The impact of a different upstream discharge is not expected to change the general findings on flow patterns or discharge distribution from this research. This is motivated by the fact that the upstream discharge mainly influences the water level and energy head that both are included in the submergence factor (S). The use of the dimensionless weir crest height (W) and submergence factor (S) allows for more generally applicable results. Secondly, figure 4.22 shows that different upstream discharges only affect the discharge distribution in the order of 1-3 %.

Combining the different parameters can result in the propagation of errors. The resultant of the various errors can be "based on the standard deviation of the errors" [Bos, 1976], but this is not done in this research due to a lack of statistical data. Using the standard deviations as proposed by Bos [1976], the combined propagating error of the discharge calculated with the weir formula is in the order of 5-30 %, depending on the energy level magnitude and submergence. The newly proposed

$C_{s,angle}$ has an error of $\leq$13 %, resulting in an even larger propagating error for the calculated flow angles when the contribution of other parameters (X_s) is included. Including spatial (longitudinal) variation of the flow angles by calibrating coefficient a for submergence factors at individual grid cells is expected to greatly reduce the error.

5.7.2 Model uncertainty

Both models make several assumptions in the schematization of the system of longitudinal training dams as a system of lines and nodes, schematization in the bed topography or the use of subgrid weirs. Thereby, different levels of simplifications are made that are, on the one hand (often) justifiable when considering the relative difference to not applying the simplification (being as low as possible). On the other hand, the simplifications induce errors that, all combined, can result in the model producing significantly different outcomes than found in the real world.

The Delft3D-Flow model is expected to be reasonably accurate for the modelling of a river system with a system of longitudinal training dams. A very rough estimation of the accuracy of the one-dimensional model is made by comparison to the Delft3D-Flow model. Both the one-dimensional model (using the empirical relationships) and two-dimensional schematization model similar discharge over the inlet and openings. This provides some confidence in the accuracy of the models, however, a true validation is missing and should still be performed with the help of physical scale model tests and field data. Scale tests can be performed in the laboratory in Wageningen in order to validate the empirical relationships by Hager [1987] and Ka-Leung Lee [2002] and the Delft3D-Flow model schematization. A scale model is being built at the moment of writing this thesis although no tests have been done yet. In addition to physical model tests, field data should be used in order to capture the influence of uncertainties that are not captured in scale tests.

One-dimensional model
Many assumptions are made by the one-dimensional model that all contribute to the model uncertainty. The different assumptions are summarized in appendix B.5.2. Those include the basic assumptions of constant energy head along the crests as this forms the basis of the side weir formulation as discussed by Hager [1987]. The use data from the scale test or field data can help to determine the accuracy of these assumptions and validate the one-dimensional model. The required data is the average energy head and water levels alongside the weir in both channels and the velocity magnitudes in transverse and longitudinal direction. The method for validating the weir coefficients in the one-dimensional model is described by De Marchi [1926]. The method is explained in more detail in section A.4.2. Field data will be most useful to analysis the application in a nature system. When measuring or obtaining experimental or field data, one should be aware of the overall accuracy of the measurements. The section on parameter uncertainty describes the propagation error resulting from the use parameter error in combination with the empirical weir formula in the one-dimensional model.

Two-dimensional model
The use of bed topography schematization and subgrid weirs in Delft3D-Flow and Waqua has been tested and validated in previous studies for a large variety of plain weir configuration [Deltares, 2008]. It must be noted though, that no validation tests are found that specifically validate the use of Delft3D-Flow or Waqua on side weirs. Also, the data from the 'Tabellenboek' [Deltares, 2008] as used in Delft3D-Flow and Waqua to calculate the energy loss over a subgrid weir does not distinguish specific weir types, such as side or oblique weirs. Only plain weirs are considered in one flow direction. The investigate the uncertainties, the scale model can be used to compare the Delft3D-Flow model results. Special attention should be put to the spatial variation of flow angles and velocity magnitudes atop the crest. The downstream end is the most interesting part, as there the largest specific discharges are found towards the side channel.

Chapter 6: Conclusions and recommendations

This chapter presents the answers to the research questions and several recommendations.

6.1 Conclusions

1. **What mechanisms and factors influence the discharge distribution at longitudinal training dams?**

The transport of water between the two channels at longitudinal training dams is mainly controlled by a different longitudinal water level slope between both channels. This is mostly affected by the fact that the channels have a different equilibrium water depth and the inlet and openings are too short to direct enough water towards the side channel to result in equal specific discharges. The discharge distribution shows to not be influenced significantly (<1% difference) by the placement of the longitudinal training dams in a river bend or by any of the bend related mechanisms.

2. **What are the local flow patterns at the inlet and openings and how can these be parameterized?**

Under submerged conditions, the specific discharge and flow angles atop the inlet increase in downstream direction. The transition to free-flow conditions atop the crest is shown to be well approximated by the categorization by Bos [1976]. In such free-flowing conditions, the specific discharge and flow angles are nearly constant in downstream direction. The free-flowing conditions in the Delft3D-Flow runs are well described by the empirical relationship by Hager [1987] ($\leq$3 degrees difference), and submerged conditions are modelled well by the addition of the submergence coefficient by Ka-Leung Lee [2002]. However, lateral outflow angles under submerged conditions are not modelled correctly and an additional angle submergence coefficient is suggested. This new parameterization is based on the Villemonte submergence formulas and is a function of the submergence factor and the dimensionless crest length. The new formula compares well to data obtained from the performed two-dimensional model runs with a R-squared value of 0.97.

3. **How can the system of longitudinal training dams best modelled in existing larger river models?**

When only interested in discharge distribution, schematization of longitudinal training dams with help of subgrid weirs is recommended. Schematization of the inlet and openings as part of the bed topography and as subgrid weirs both provide similar discharges, but far smaller grid sizes (order of 3 m or less) are required for schematization in the bed topography. Subgrid weirs, however, should only be used in the latest Delft3D-Flow version as only there the inconsistency found in the energy-loss calculation are resolved. When velocity magnitudes and lateral outflow angles are of interest as well, schematization with subgrid weirs shows inconsistent results with respect to the bed topography runs. Differences in flow angles up to 40 degrees are found. This is explained by the implementation of subgrid weirs in the two-dimensional modelling software, which is focused on correctly simulating the discharge over weirs. The subgrid weirs are not designed or calibrated to model velocities and flow angles at side weirs with large crest heights. Adding the suggested parameterization for flow angles atop the weir crest will provide results that are more consistent with bed topography model runs.

4. **How can control strategies and the design of longitudinal training dams influence the discharge distribution and flow patterns?**

For a given crest width of 2 m and an upstream river discharge of 2000 m^3/s, varying the inlet crest height from fully open to nearly closed provides a reduction in discharge towards the side channel by 5-10%. Only for crest heights nearly reaching the water level does the side channel discharge reduce more than 10%. Increasing the crest height does greatly influence the specific discharge in the side channel and the flow angles atop the crest up to 40 degrees. The opening crest heights do not influence the discharge distribution more than 1%. The side channel width shows to be the most dominant parameter for the discharge distribution. A side channel width reduction in the order of 10 m reduces the side channel discharge by ± 10%. The inlet crest height and crest length together provide a good design instrument to optimize the specific discharge in the side channel and flow patterns around the inlet and openings.

6.2 Recommendations

1. **Control strategy**
   Adjusting the inlet and opening crest heights provide only a limited influence on the discharge distribution between the two channels. Only for crest heights nearly reaching the water level, does the discharge distribution drop considerably. In submerged conditions, the inlet crest height does reduce the specific discharge in the side channel, limits the transverse velocities in the main channel, and greatly influence the flow angles (order of 20-40 degrees and thus influence the sediment transport). An optimization is therefore suggested for the pilot project longitudinal training dams by raising the inlet crest while preventing too frequent emerging of the inlet crest or negative effects on flood protection. In the design strategy of future longitudinal training dams, the crest length and side channel width should be included in the design or control strategy of future longitudinal training dams, as they greatly influence the hydraulic conditions.

2. **Schematization of the inlet and openings**
   From a computational efficiency point of view, the use of subgrid weirs in river models (Delft3D-Flow or Waqua) is highly favourable over schematization of the inlet and openings in the bed topography. However, the subgrid weirs show several inconsistencies in the modelling of flow angles. Therefore, when only modelling the averaged water levels or general discharge distribution at the longitudinal training dams, it is recommended to make use of the updated subgrid weirs. They result in similar discharge but can be modelled using a far larger grid size. When also the local velocity magnitudes, flow angles, or the sediment transport are of importance, schematization by subgrid weirs no longer suffices and the inlet and opening should be schematized as part of the bed topography. The reason for this is that subgrid weirs only include a parameterization for the discharge and not for the flow angles nor velocity magnitudes, specifically atop the crest. This requires grid sizes in the order of 3 metre or smaller. The use of the flood scheme is expected to be most accurate but requires small time steps (dt=0.005 min). Therefore, it is advisable to use the Waqua scheme the results in similar discharge with a time step of dt=0.02 min.

   Considering the combination of different river functions, where for some the flow patterns are of great importance, an integral modelling approach will require schematization as part of the bed topography. Due to the small grid size required, the use of flexible mesh type of approaches should be explored to limit the computational times.

3. **Combine hydraulic conditions with sediment transport**
   The combination of this thesis and research by Jammers [2017] provides most tools to start performing morhological model runs. The two-dimensional model from this research can be extended with (findings of) the sediment transport model created by Jammers [2017]. As a

start, the first morphological models could be run with a constant river discharge, similar to the approach used in this research. In a later stage, the morphological development of the system of longitudinal training dams can be modelled using a full hydrograph to include a full cycle of high and low river discharges. Provided such newly obtained knowledge on the morphological development, a translation to the actual influence on the river functions can be made.

4. **Validation of discharge and submergence coefficients**
   It is highly recommended to validate the side weir discharge formulation by Hager [1987] and the side weir submergence coefficient from Ka-Leung Lee [2002] in a physical scale model. The reason is that the weir type (side weir) and inlet dimensions deviate from previous Delft3D-Flow or Waqua validation tests found in literature [Deltares, 2008]. Such model tests can be performed in the scale model in Wageningen that is being built at the moment of writing this thesis. The required data from these scale model runs are the average energy head and water levels alongside the weir in both channels and the velocity magnitudes and flow angles atop the crest. The method for validating weir coefficients was first introduced by De Marchi [1926]. The method is explained in more detail in section A.4.2. In this scale model, also the assumptions that form the basis of the side weir formulation should be evaluated.

   Similarly, for the newly found flow angle submergence coefficient the flow angles atop the crest from the Delft3D-Flow model are used. The new coefficient should still be validated with a scale model first. For this, it is recommended to collect detailed data on the precise longitudinal variation of discharge and flow patterns at the inlet of longitudinal training dams. It is shown that the largest flow angles occur at the most downstream point atop the inlet and openings. Because larger flow angles are of great importance to the sediment transport, focus should thus be put in the downstream part of the inlet.

5. **Validation with field data** Besides validation of the different empirical coefficients, a proper validation of the one- and two-dimensional models and natural variability found in nature are also still missing. This should be performed with the help of field data collected in the Waal. Field data should be used in order to capture the influence of uncertainties and mechanisms that are not captured in scale tests. The recommended data to collect is the average energy head and water levels alongside the inlet and openings in both channels and the velocity magnitudes and flow angles atop the crest. The data should be collected simultaneously at the different location to ensure an equal river discharge during the measuring duration. In addition, the data should be repeated during several different river discharges to validate the conclusions from this research for a wider range of discharge found throughout the year.

6. **Implementation of angle submergence coefficient in Delft3D-Flow**
   By introducing the suggested angle submergence coefficient in the momentum equation over a subgrid weir in Delft3D-Flow, the relative flow angle error can be reduced considerably from $\approx 600\%$ to 13%. The submergence factor S that is required as input for the suggested angle submergence coefficient can easily be determined from the energy level above the crest $(H - w)$ in the upstream and downstream water level points on either side of the subgrid weir. Additionally, in the current situation, the momentum equation between two grid cells does not have any information on the total inlet or opening length (L_w). Therefore, the crest length should be requested as an additional input parameter when assigning a subgrid weir or it should be calculated by the model itself. This can then be used in the parameterization for flow angles in the model calculations.

   It should be noted that the coefficient a that is determined in this research is fitted using only a single submergence factor (S) that is determined at the most upstream point of the inlet. To include a spatial (longitudinal) variation of the flow angle, the coefficient a needs to be redetermined for S values at individual grid cells at the upstream and downstream water level points on either side of the subgrid weir. This is expected to greatly reduce the maximum error of 13% found for the angle submergence coefficient.

7. **Include velocity and water level fluctuations**
   In order to better determine the impacts of longitudinal training dams on the ecological development, the velocity and water level fluctuations induced by ships should be included. This has not been considered in this research but could fairly easily be done by applying a temporarily lowering of the downstream water level boundary. With the help of such a model run, the focus should be laid on the variations in water levels, velocity magnitudes, and flow direction at the openings. Combining such findings with the knowledge gained from research by Collas [2016] will allow optimization in the longitudinal distance between openings at longitudinal training dams.

Bibliography

Ackers, P., White, W., Perkins, J., and Harrison, A. (1978). *Weirs and flume for flow measurement.* John Wiley and Sons Ltd., Bath.

Agaccioglu, H. and Yksel, Y. (1998). Side-weir flow in curved channels. *Journal of Irrigation and Drainage Engineering*, pages 163–175.

Aichel, O. (1953). Abflusszahlen fur schiefe wehre (discharge ratios for oblique weirs). *Z. VDI.*, 95(1):26–27.

Ali, S. (2013). *Flow over weir-like obstacles.* Doctoral thesis, Delft University of Technology.

Azami, A. H. (2009). Discharge characteristics of weirs of finite crest length. *Journal of Hydraulic Engineering*, 2009(12):1081–1085.

Baek, K. and Seo, I. (2009). Equation for streamwise variation of secondary flow in sinuous channels. *Proceedings of 16th IAHR-APD Congress and 3rd Symposium of IAHR-ISHS*, Advances in Water Resources and Hydraulic Engineering:580 – 585.

Bern, M., Flaherty, J., and Luskin, M. (1999). Grid generation computational mechanics. *The Institute for Mathematics and its Applications, Springer-Verlag, New York, NY*, 113(Am. Soc. Mechanical Engineers: New and adaptive algorithms).

Borghei, S. (2003). Oblique rectangular sharp-crested weir. *Proceedings of the Institution of Civil Engineers - Water and Maritime Engineering*, 156:185–191.

Bos, M. (1976). Discharge measurement structures. Report ISBN 90 70754 15 O, WUR.

Bradley, J. N. (1978). Hydraulics of bridge waterways. Report, FHWA.

Breienthal, R. (1981). Structure in turbulent mixing layers and wakes wing a chemical reaction. *Journal of Fluid Mechaniscs*, 109:1–24.

CCNR (2016). Navigation channel clearances of the Rhine.

Cheong, H. (1991). Discharge coefficient of lateral diversion from trapezoidal channel. *Journal of Irrigation and Drainage Engineering*, 117(4):461 – 475.

CIRIA (2007). *The Rock Manual.* version 2007. CIRIA.

Collas, F. (2016). *Langsdammen Waal: resultaten vismonitoring 2016.* Radboud University, Deltares, and Bureau Waardenburg. Institute for Water and Wetland Research, Radboud University, Nijmegen.

Cushman-Roisin, B. (2014). Environmental fluid mechanics. Report, John Wiley and Sons, Inc.

De Marchi, G. (1926). Saggio di teoria del funzionamento degli stramazzi laterali. *L'Energia Elettr.*, pages 849–860.

Delkash (2012). An examination of rectangular side weir discharge coefficient equations under subcritical condition. *International Journal of Hydraulic Engineering*, 3(1):24–34.

Deltares (2008). Validation document Delft3D-Flow. Report, Deltares.

Deltares (2014). Delft3D-Flow user manual. *Version: 3.15.*

Frazer, W. (1957). The behavior of side weirs in primatic rectangular channel. *ICE- Civil Engineering*, Vol 6:305–327.

Haddadi, H. (2012). A discharge coefficient for a trapezoidal broad-crested side weir in subcritical flow. *Flow Measurement and Instrumentation*, 26:63–67.

Hager, W. (1982). Die hydraulik von verteilkanaelen. *Versuchanstalt fur Wasserbau, Hydrologie und Glaziologie.*

Hager, W. H. (1987). Lateral outflow over side weirs. *J. Hydraulic Engineering*, 113(4):491–504.

Herik, V. d. and Boskalis (2014). Ontwerpnota langsdam Wamel. Report.

Honar, T. and Javan, M. (2007). Discharge coefficient in oblique side weirs. *Iran Agricultural Research*, 25(2).

Jammers, S. (2017). Sediment transport over longitudinal training dam sills. *MSc Thesis*, Delft University of Technology.

Jansen, P., Van Bendegom, L., Van den Berg, J., De Vries, M., and Zanen, A. (1979). *Principles of River Engineering: The non-tidal alluvial river.* Delftse Uitgevers Maatschappij, Delft.

Ji, U., Kim, S., and Yoon, B. (2013). Analytical and experimental investigation of a side-weir detention basin in flood-level reduction in the main channel. *Journal of Irrigation and Drainage Engineering*, 139(8):663–671.

Ka-Leung Lee, E. H. (2002). Physical modeling for side-channel weirs. Report, Center for Research in Water Resources.

Keshavarzi, K. (2014). Discharge coefficient of sharp-crested side weir in trapezoidal channel with different side-wall slopes under subcritical flow conditions. *Journal of Irrigation and Drainage*, 63:512522.

Kirkil, G. (2015). Detached eddy simulation of shallow mixing layer development between parallel streams. *Journal of Hydro-environment Research*, 9(2):304–313.

Kolkman, P. (1989). *Discharge relations for hydraulic structures and head losses from different components.* WL— Delft Hydraulics.

Liefveld, W. M., Emond, D., and van der Valk, M. (2011). Kribverlaging Waal fase 3 en langsdammen Wamel en Ophemert. Report rapport nr. 11-093, Bureau Waardenburg bv.

Merwade, V., Maidment, D., and Hodges, B. (2005). Geospatial representation of river channels. *Journal of Hydrologic Engineering*, 10(3):243–251.

Mosselman, E. (2001). Morphological development of side channels. Report, IRMA-SPONGE en Delft Cluster.

Namaee, M. (2013). Discharge coefficient of a broad crested side weir in an earthen channel. *Water science and technology*, 13(1):166–177.

Namaee, M. (2016). Numerical modeling of flow over two side weirs. *Arab J Sci Eng*, 41:1495–1510.

Njanga (2012). Secondary current and classification of river channels. *Applied Mathematics*, 4:70–78.

Prooijen, B. C. v. and Uijttewaal, W. S. J. (2002). A linear approach for the evolution of coherent structures in shallow mixing layers. *Physics of Fluids*, 14(12):4105–4114.

Raju, K. R., Prasad, B., and Gupta, S. (1979). Side weir in rectangular channel. *Journal of the Hydraulics Division*, 105(5):547–554.

Ramamurthy, A. and Carballada, L. (1980). Lateral weir ow model. *Journal of the Irrigation and Drainage Division*, 106:9–25.

Rijkswaterstaat (2011). Integraal ontwerp pilot langsdammen Waal. Report, Rijkswaterstaat - Oost Nederland.

Rijkswaterstaat (2012). Users guide WAQPRE. Report, Rijkswaterstaat.

Rijkswaterstaat (2016a). Duurzame vaardiepte Rijntakken (DVR2). Report, Rijkwaterstaat - Oost Nederland.

Rijkswaterstaat (2016b). *Waternormalen.* Rijkswaterstaat, https://waterinfo.rws.nl.

Roads, B. and Sukhodolov, A. (2004). Spatial and temporal structure of shear layer turbulence at a stream confluence. *Water resources research*, 40(W06304).

Rosier, B. (2007). Interaction of side weir overflow with bed-load transport and bed morphology in a channel. Report, Ecole Polytechnique Fdrale de Lausanne.

Rozovskii, I. (1957). *Flow of water in bends of open channels.* Academy of Sciences of the Ukrainian SSR, Kiev.

Singh, R., Manivnnan, D., and Satyanarayana, T. (1994). Discharge coefficient of rectangular side weirs. *Journal of Irrigation and Drainage Engineering*, 120(4):814–819.

Stelling, G. (1983). On the construction of computational methods for shallow water flow problems. *Doctoral Thesis*, Delft University of Technology.

Subramanya, K. and Awasthy, S. (1972). Spatially varied flow over side-weirs. *Journal of Hydraulic Div.*, 98:1–10.

Swamee, P. K., Pathak, S., and Ali, M. S. (1994). Side-weir analysis using elementary discharge coefficient. *Journal of Irrigation and Drainage Engineering*, 120(4):742–755.

Tanguy, J. (2009). *Physical Processes and Measurement Devices: Environmental Hydraulics.* John Wiley and Sons, London.

Thomas, C. (1957). Common errors in measurement of irrigation water. *Journal of Irrigation and Drainage*, 83(2):1–24.

Tracy, H. (1957). *Discharge characteristics of broad-crested weirs.* Geological survey Circular 397, U.S. Department of the Interior, Washington, D. C.

Tynes, K. (1989). Hydraulics of side-channel weirs for regional detention basins. *M. S. Thesis*, Dept. of Civil Engineering, University of Texas.

Uijttewaal, W. (2015). *Turbulence in hydraulics, Lecture notes (CT5312).* Delft University of Technology, Delft.

Uijttewaal, W., Lehmann, D., and Mazijk, A. v. (2001). Exchange processes between a rivebend its groyne fields: model experiments. *Journal of Hydraulic Engineering*, 127(11):928–936.

Verhagen, H. and d'Angremond, K. (2009). *Breakwaters and Closure Dams.* Delft University Press.

Vermaas, H. (1987). *Energylosses due to weirs.* Techical Report Q92. Delft Hydraulics, Delft, The Netherlands.

Villemonte, J. (1947). Submerged weir discharge studies. *Engineering News Record 193*, pages 866–869.

Vuik, V. (2010). Numerical modeling of sediment transport over hydraulic structures. *MSc Thesis*.

Vuren, S. v. (2005). Stochastic modeling of river morphodynamcs. *Doctoral Thesis*, Delft University Press (ISBN 90-407-2604-3).

Weitbrecht, V., Socolofsky, S., and Jirka, G. (2008). Experiments on mass exchange between groin fields and main stream in rivers. *Journal of Hydraulic Engineering*, 134(2):173–183.

Zijlema, M. (2014). *Computational Hydraulics, Lecture notes (CT5315)*. Delft University of Technology, Delft.

Appendix A: General equations

A.1 Fluid mechanics

The basic equation described in this chapter give an theoretical background to better understand the flow characteristics in rivers. All equations are taken from the general text book on the non-tidal alluvial river by Jansen et al. [1979].

A.1.1 Conservation of mass

By considering conservation of mass it is simply stated that the accumulation over time of mass $\rho A dx$ inside the slice of length dx is caused by a possible difference between the amount of mass $\rho A u$ that enters per time at position x and the amount that leaves per time at position $x+dx$ [Cushman-Roisin, 2014]. The conservation of mass thus becomes:

$$[\rho A dx]_{t+dt} = [\rho A dx]_t + ([\rho A u]_x - [\rho A u]_{x+dx}) \tag{A.1}$$

For an infinitely small time step dt and considering three dimensional flow the equations for conservation of mass becomes:

$$\frac{\partial \rho A}{\partial t} + \frac{\partial \rho A_x u}{\partial x} + \frac{\partial \rho A_y v}{\partial y} + \frac{\partial \rho A_z w}{\partial z} = 0 \tag{A.2}$$

In a control volume of 1 by 1 by 1 meter the equations for conservation of mass, also known as the continuity equations, becomes:

$$\frac{\partial \rho}{\partial t} + \frac{\partial \rho u}{\partial x} + \frac{\partial \rho v}{\partial y} + \frac{\partial \rho w}{\partial z} = 0 \tag{A.3}$$

When assuming a one dimensional river system (integrating over the y and z-direction) and assuming incompressible water ($\rho = constant$), the mass conservation for a undefined control volume can be greatly simplified to:

$$\frac{\partial A}{\partial t} + \frac{\partial A u}{\partial x} = 0 \tag{A.4}$$

The cross-sectional area A of a rectangular river is equal to the width times the water depth ($A = W * h$). For a river with a constant width (W=constant) the equation above reduces to:

$$\frac{\partial h}{\partial t} + \frac{\partial h u}{\partial x} = 0 \tag{A.5}$$

When considering steady flow, the water level (h) or flow velocity at location x_1 can be calculated when the water level and flow velocity at location x_0 are known:

$$h_0 u_0 = h_1 u_1 \tag{A.6}$$

A.1.2 Conservation of momentum

By considering conservation of mass it is simply stated that the time rate of change of momentum inside our slice of river is the momentum flux entering upstream, minus the momentum flux exiting downstream, plus the sum of accelerating forces (acting in the direction of the flow), and minus the sum of the decelerating forces [Cushman-Roisin, 2014]. The three dimensional conservation of momentum in three directions for a control volume of 1 by 1 by 1 m are:

$$\frac{\partial \rho u}{\partial t} + \frac{\partial \rho uu}{\partial x} + \frac{\partial \rho vu}{\partial v} + \frac{\partial \rho wu}{\partial z} - [\frac{\partial \tau_{xx}}{\partial x} + \frac{\partial \tau_{xy}}{\partial y} + \frac{\partial \tau_{xz}}{\partial z}] = -\frac{\partial \partial p}{\partial x} + \rho f v + F_x \tag{A.7}$$
$$\frac{\partial \rho v}{\partial t} + \frac{\partial \rho uv}{\partial x} + \frac{\partial \rho vv}{\partial y} + \frac{\partial \rho wv}{\partial z} - [\frac{\partial \tau_{yx}}{\partial x} + \frac{\partial \tau_{yy}}{\partial y} + \frac{\partial \tau_{yz}}{\partial z}] = -\frac{\partial \partial p}{\partial y} + \rho f u + F_y$$
$$\frac{\partial \rho w}{\partial t} + \frac{\partial \rho uw}{\partial x} + \frac{\partial \rho vw}{\partial y} + \frac{\partial \rho ww}{\partial z} - [\frac{\partial \tau_{zx}}{\partial x} + \frac{\partial \tau_{zy}}{\partial y} + \frac{\partial \tau_{zz}}{\partial z}] = -\frac{\partial \partial p}{\partial z} - \rho g + F_z$$

where the first terms, the time derivatives, represents acceleration of the fluid. The second to fourth terms represent advection. The terms containing τ represent shear force gradients and diffusion. The right-hand sides represent the forces in and on the fluid. From left to right the pressure forces containing p, the Coriolis forces containing f, the gravity force containing g and other forces denotes by F.

In river systems a few term in the momentum equations can (sometimes) be neglected. The gravitational force can often be neglected as a river system is usually not several kilometres in width. In some cases the shear (of viscosity) term can be neglected as turbulent stresses are often much more important. Thirdly, the density can be considered constant and in rivers flow where vertical accelerations are negligible (which is blunt assumption especially in river bends and flow over obstacles) the momentum equation in z-direction can be simplified to a balance between the gravitational forces and pressure forces:

$$\frac{\partial p}{\partial z} = \rho g \tag{A.8}$$

When applying all simplifications mentioned above, the momentum equations simplify to the equations below:

$$\frac{\partial u}{\partial t} + \frac{\partial uu}{\partial x} + \frac{\partial vu}{\partial y} + + \frac{\partial wu}{\partial z} = -g\frac{\partial Z_w}{\partial x} \tag{A.9}$$
$$\frac{\partial v}{\partial t} + \frac{\partial uv}{\partial x} + \frac{\partial vv}{\partial y} + + \frac{\partial wv}{\partial z} = -g\frac{\partial Z_w}{\partial y}$$

A.1.3 Conservation of energy

To calculate flow over and obstacles, use can be made of the principle of conservation of energy or conservation of momentum. When no energy is supplied or lost (frictionless fluid) in a control volume, the equation for conservation of energy can be applied. The assumption of conservation of energy (no energy loss) is useful for quick one-dimension calculations but it can become difficult in more detailed calculations when it become difficult assessing how much energy is lost in a river system with many friction losses. When calculating the energy levels in a system, different forms of energy are present (work done by moving the fluid into the domain, the kinetic energy and the potential energy) that can be combined to a total energy available energy:

$$Totalenergy = pAL + \frac{1}{2}\rho A u^2 L + \rho A z L g \tag{A.10}$$

where p is the pressure, A is the cross-sectional area, L is the section length, ρ is the density, z is the vertical elevation and g is the gravitational constant. Equations A.10 assumes a constant energy level among stream lines. When converting the equation above to total energy per unit weight by dividing by ρALg, the Bernoulli equation is conceived for the total energy head H:

$$H = \frac{p}{\rho g} + \frac{u^2}{2g} + z \tag{A.11}$$

$$\begin{aligned} \text{where } \frac{p}{\rho g} &= d = \text{pressure head,} \\ \frac{u^2}{2g} &= \text{velocity head,} \\ z &= \text{potential head,} \\ h = d + \frac{u^2}{2g} &= \text{hydraulic head} \end{aligned}$$

When considering a rectangular open channel ($Q = uA$) with a hydrostatic pressure distribution ($p = h\rho g$), the velocity head can be rewritten in terms of specific discharge. The energy balance becomes:

$$H = z + d + \alpha_0 \frac{Q^2}{2gA^2} \tag{A.12}$$

where α_0 is the kinetic energy correction factor [Ali, 2013]. When differentiating equation A.12 over longitudinal direction (x), the following equation yields:

$$\frac{\partial H}{\partial x} = \frac{\partial z}{\partial x} + \frac{\partial d}{\partial x} + \alpha_0 \left(\frac{Q}{A^2 g}\frac{\partial Q}{\partial x} - \frac{Q^2}{A^3 g}\frac{\partial A}{\partial x}\right) \tag{A.13}$$

When considering an uniform channel (B = uniform) and re-writing for the water level change results in the "dynamic equation for spatially varied flow with decreasing discharge" Rosier [2007]:

$$\frac{\partial d}{\partial x} = \frac{\frac{\partial z}{\partial x} - \frac{\partial H}{\partial x} - \frac{\alpha_0 Q}{gA^2}\frac{\partial Q}{\partial A}}{1 - \frac{\alpha Q^2 B}{gA^3}} \tag{A.14}$$

A.2 Plain weirs

Many studies and experiments have been conducted to determine the discharge over weirs for a large variety of weir-like structures and flow types that will be discussed below. The general equations for flow over weirs can be derived from the energy conservation equation of spatially varied flow. A derivation of the equation from the general conservation equations is found in appendix A where equation A.14 presents the energy conservation equation of spatially varied flow. When assuming a constant specific energy ($\frac{dH}{dx} = \frac{dz}{dx}$), this equation converts to:

$$-\frac{dQ_w}{dx} = q_w = C_d\sqrt{2gd}d = C_d\sqrt{2g}d^{3/2} \tag{A.15}$$

where Q_w is the total discharge and q_w is the specific discharge over the weir, x is the longitudinal distance and C_d is a newly introduced weir discharge coefficient that accounts for the combination of contraction and friction losses of the weir.

Flow regimes

Flow over weirs can roughly be distinguished in three types of flow regimes as classified by Kolkman [1989] and shown in figure A.2:

1. **Free flow:** Flow is governed only by upstream boundary conditions
2. **Transitional flow:** A transitional phase between submerged and free-flow
3. **Submerged flow:** Flow is governed by upstream and downstream boundary conditions

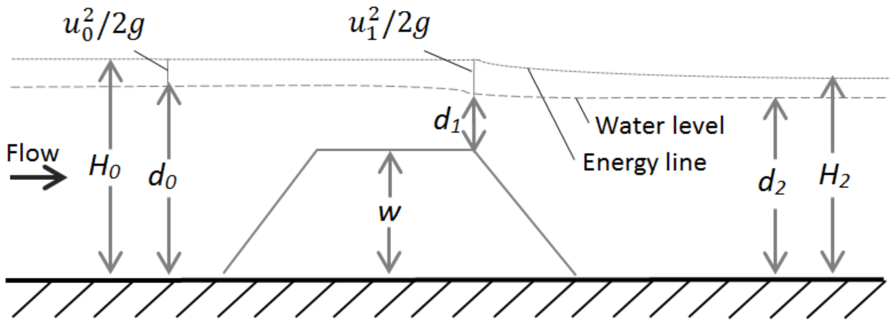

Figure A.1: A sketch of the energy levels along a plain weir [Ali, 2013]

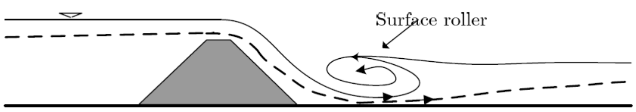

(a) Free flow

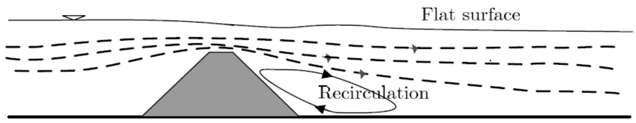

(b) Transitional flow

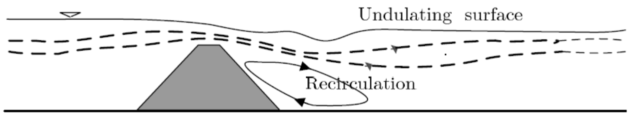

(c) Submerged flow

Figure A.2: Flow types over a plain weir [Ali, 2013]

The transition from sub-critical to super-critical is depended on the weir height and the water levels upstream and downstream of the weir. If the weir crest height is increased or the water level decreased, flow will eventually become critical. The water depth above the weir crest, corresponding to the moment flow becomes critical, is referred to as the critical water depth. The ratio of upstream energy level to the crest water depth at which this occurs is called the modular limit (ML). According to Ka-Leung Lee [2002], the modular limit is effected by the ratio of the weir height in relation to the water level downstream of the weir. As a general rule of thumb, the modular limit is given by $d_{downstream}/H_{upstream} = \frac{2}{3}$ [Verhagen and d'Angremond, 2009]. When the weir height is increased or the downstream water level is decreased further, the discharge over the weir will not be depended on downstream conditions anymore and becomes critical.

Similar to the type of flow over a weir, also the weir itself can be categorized. It seems to be useful to divide weirs onto three categories were depending on the accurance of the above stated critical flow and the curvature of streamlines above the crest. The three weir types are sharp-crested, short-crested and broad-creasted and are shown in figure A.3.

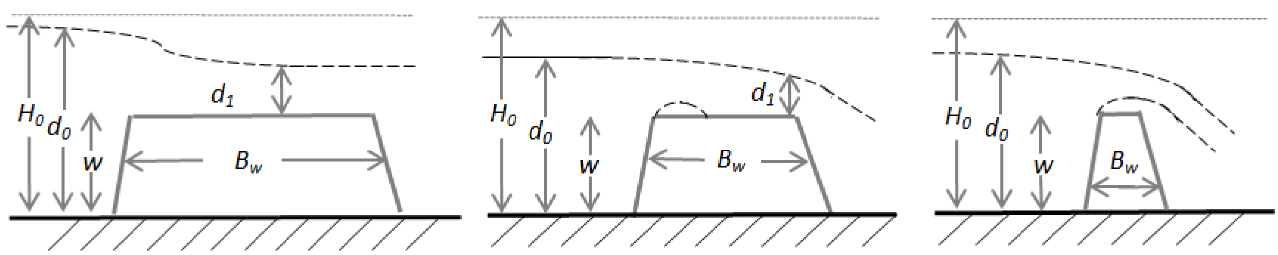

Figure A.3: Schematization of (a) broad-, (b) short- and (c) sharp-crested weirs

The categorization of broad-crested weirs refers to situations where flow line run parallel over the weir and therefore the "deviations from a hydrostatic pressure distribution may be neglected" Bos [1976]; Azami [2009]. For weirs with a shorter water depth $(d - w)$ to crest width (B_w) ratio, flow lines will not run parallel any more but remain curvilinear instead. This means that no hydrostatic pressure distribution can be assumed and this is referred to as short-crested weirs. Depending on the upstream edge, the flow will separate from the edge in smaller or larger amounts. In case of weirs with very short crest lengths, separated flow does not reattach any more and these weirs are referred to as sharp-crested. The ratio of water level over the weir crest $(d - w)$ to the crest length L seems to determine the weir type Borghei [2003]. Table A.1 shows the values for the different classifications.

Table A.1: Categorization of weir types Bos [1976]

Type	$(H - w)/B_w$
Sharp-crested	$(H - w)/B_w > 15$
Short-crested	$15 > (H - w)/B_w > 1/3$
Broad-crested	$(H - w)/B_w < 1/3$

For different flow regimes, the discharge over a weir can depend either on just the upstream flow depth (free-flow), or on the upstream flow depth in combination with generated energy loss (submerged flow). The transitional regime is shown to depend on a combination of the upstream and downstream flow depth, as shown in figure A.4.

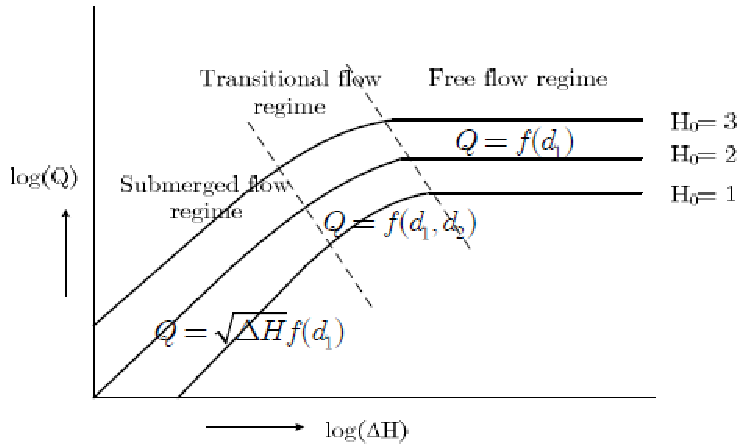

Figure A.4: Relation between weir discharge and energy loss [Kolkman, 1989]

Free flow

For free-flow conditions, water on the weir crest becomes critical and reaches, what is referred to as, the critical depth. This corresponds to the ratio of upstream energy head to water depth above the crest reaching the modular limit, $d_1 = \frac{2}{3}H_0$, where the factor $\frac{2}{3}$ is the modular limit as explained before. In this case, the weir discharge is only depended on upstream flow conditions. The discharge coefficient representing the modular limit is called the modular discharge coefficient and denoted by $C_{d,0}$. This results in the general equation for the specific discharge for the free-flow regime:

$$q_w = cC_{d,0}\frac{2}{3}\sqrt{2g}(H_0 - w)^{3/2} = C_d\sqrt{2g}(H_0 - w)^{3/2} \tag{A.16}$$

where C_d is the discharge coeffiecient, c is a geometry correction factor, and $C_{d,0}$ the modular discharge coefficient for plain weirs. The proposed formulation of the discharge coefficient by Raju et al. [1979] for weirs becoming broad-crested is:

$$C_d = 0.8(1 + \frac{H_0 - w}{8 * B_w})C_{d,0} = c * C_{d,0} \tag{A.17}$$

where C_d is the general discharge coefficient, $C_{d,0}$ the modular plain weir coefficient for sharp-crested weirs, B_w the crest width, and c is the geometry correction factor. Figure A.5 shows the theoretical evolution of C_d for different values of B_w. A constant value for $C_{d,0}$ of 0.61 is used that was found by Subramanya and Awasthy [1972] and is in good agreement with Ackers et al. [1978] and Borghei [2003].

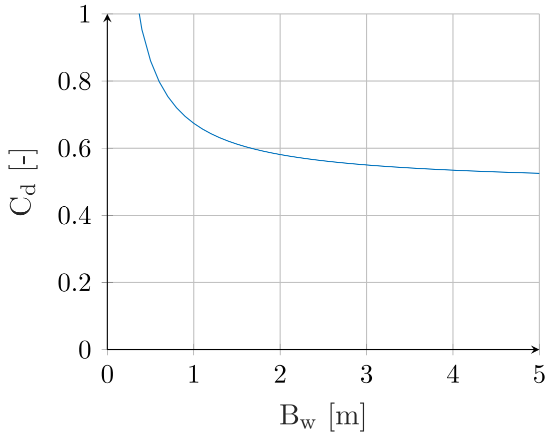

Figure A.5: Theoretical discharge coefficient (C_d) for different crest widths (B_w) for $H_0 = 6.5$ and $w = 3$ m

When not considering downstream energy losses, and thus only using an energy conservation, the equation above can be rewritten to express the discharge coefficient as a relation of the flow conditions at the weir. For this purpose, the energy head can be rewritten as follows:

$$H = h + \frac{u^2}{2g} = h(1 + \frac{Fr^2}{2}) \tag{A.18}$$

Substituting above relationship into equation A.16 results in the expression for the discharge coefficient as given by equation A.19. For convenience $\widetilde{H_1} = H_1 - w$ and $\widetilde{h_1} = h_1 - w$. The variation of C_d for different Froude numbers is shown in figure A.6. "Owing to the pressure and velocity distributions above the weir crest, the discharge coefficient (C_d) of a short-crested weir is larger than that of a broad-crest weir" Bos [1976]. For flow reaching critical velocities (Fr=1), the discharge coefficient converges to the modular discharge coefficient and the geometry correct factor thus becomes 1.

$$C_d = \frac{q_w}{C_{d,0}\sqrt{2g}(\widetilde{H_1})^{3/2}} = \frac{u_1 h_1}{C_{d,0}\sqrt{2g}(\widetilde{h_1})^{3/2}(\frac{2+Fr_1^2}{2})^{3/2}} = \frac{Fr_1}{C_{d,0}1/3\sqrt{1/3}(2 + Fr_1^2)^{3/2}} \tag{A.19}$$

Transitional flow

When the water on the downstream side of the weir becomes large enough compared to the water level on upstream side, flow is influenced by both upstream and downstream boundary conditions (sub-critical flow). In the case of sub-critical (or submerged) flow conditions, an additional coefficient C_s was introduced by (Villemonte 1947) to be added to general weir equation (equation A.16) to account for submergence:

$$q_w = C_s C_d \sqrt{2g}(H_0 - w)^{3/2} \tag{A.20}$$

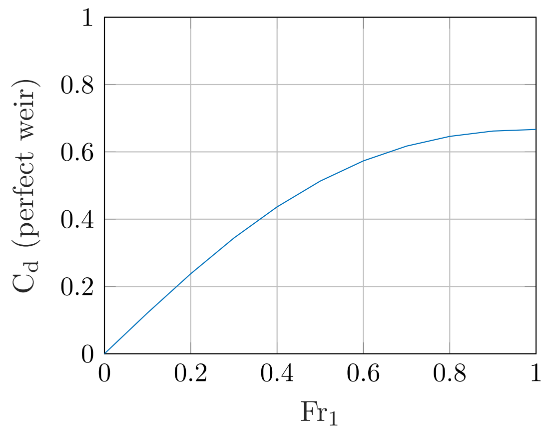

Figure A.6: Relation between C_d and Froude number for a perfect plain weir

A general form for a submergence factor C_s was introduced for flow in the transitional regime by Villemonte [1947]. In the generalized form, the submergence factor is influenced by the channel geometry and the level of submergence as shown by equation A.21

$$C_s = \sqrt{1 - S^P} \tag{A.21}$$

$$\text{where } S = \frac{H_2 - w}{H_0 - w} \tag{A.22}$$

were P is an empirical coefficient that is influenced by the channel geometry and S is the submergence factor. The relation between the submergence factor S and the submergence coefficient C_s, provided equation 2.4.2, is presented in figure A.7 for different values of P. It can be noted that for larger values of S, the submergence coefficient starts to greatly influence the weir discharge. The value of P also greatly influences the development of C_{sub} for large S values (up to a factor 2 difference for $S = 0.9$). According to research by Ali [2013], the type of vegetation on weirs also influences the value of P. This influence is also implemented in modelling program such as the Waqua. This is not considered in more detail and reference is made to the doctoral thesis by Ali [2013] or the WAQPRE User's guide [Rijkswaterstaat, 2012].

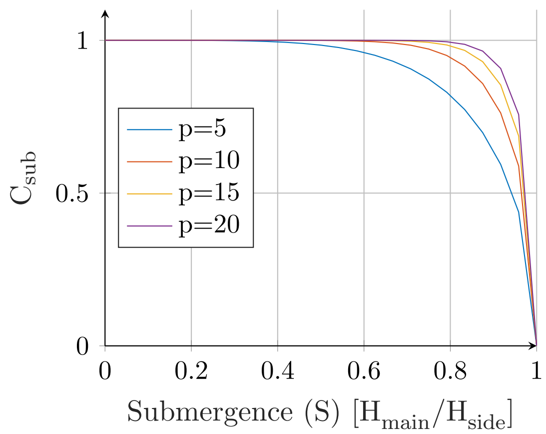

Figure A.7: Relation between submergence factor S and submergence coefficient C_s

Submerged flow

Considering fully submerged flow, an energy conservation equation can be used between the section upstream of the weir and downstream of the weir (section 0 and 2 in figure A.1). The result is given by equation A.23.

$$q_w = C_d\sqrt{2g}(H_2 - H_0)^{3/2} \tag{A.23}$$

A.3 Oblique-weirs

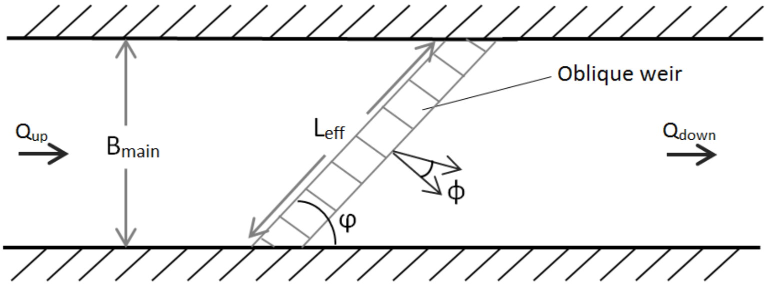

Figure A.8: Schematization of an oblique weir

Introduced by Aichel [1953], the obliqueness (φ) of a weir can be included through an increased weir length that influences the discharge (see figure A.8). The discharge is influenced due to an increased crest length per unit of length perpendicular to the incoming stream lines. The factor that accounts for the increased crest length is:

$$C_{obl} = (1 - \beta_A \frac{d_0 - w}{w}) \tag{A.24}$$

where d_0 is the water depth upstream of the weir, w is the weir height and β_A is a coefficient that depends on the obliqueness. The specific discharge over an oblique weir ($q_{w,L}$) can be calculated by multiplying the specific discharge for a plain weir of equal type (for instance, sharp-crested) with the crest length factor:

$$q_{w,L} = C_{obl}q_w = (1 - \beta_A \frac{d_0 - w}{w})q_w \tag{A.25}$$

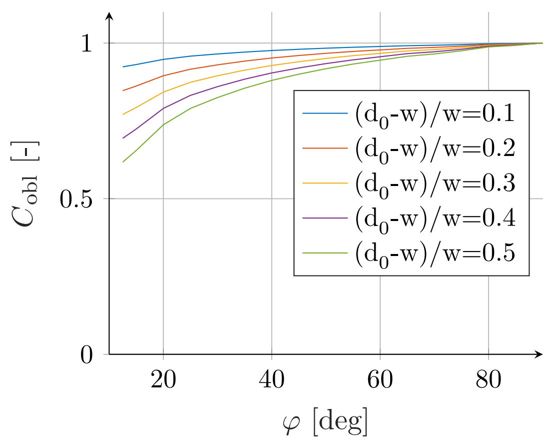

Figure A.9: Values for the oblique reduction factor as function of the obliqueness

Values for β_A are depended on the angle of obliqueness and can be obtained from literature. Using the β values obtained from Bos [1976], the relationship between the obliqueness and the reduction oblique factor can be found as shown in figure A.9. It can be seen that an angle of 90 degree results in a $C_{obl} = 1$ thus resembles a plain weir.

As a result of the obliqueness, flow atop the weir will start to bend and deviate from straight flow lines as found upstream (outside of the influence of the weir). This is different from the straight flow lines that can be found at plain weirs (where φ= 90 deg). The flow angle atop the crest is expressed by θ, where $tan(\theta) = \frac{u_l}{u_p}$. When mass conservation is assumed for flow over the ($q_0 = q_1$), the relation between obliqueness and flow angle can be expressed by the Froude number ratio upstream and above the weir as show below.

$$\frac{q_1}{q_0} = \frac{u_1 h_1}{u_0 h_0} = \frac{Fr_1 \sqrt{g} h_1^{3/2}}{Fr_0 \sqrt{g} h_0^{3/2}} = 1 \tag{A.26}$$
$$\frac{Fr_1}{Fr_0} = (\frac{h_0}{h_1})^{3/2}$$

When including the definitions of φ, θ, and mass conservation ($u_0 h_0 = u_1 h_1$), the above relationship can be rewritten to equation A.27. Figure A.10 shows the theoretical flow angle as a function of the relative Froude number and for different obliqueness values.

$$tan(\theta) = (\frac{Fr_0}{Fr_1})^{2/3} tan(\varphi) \tag{A.27}$$

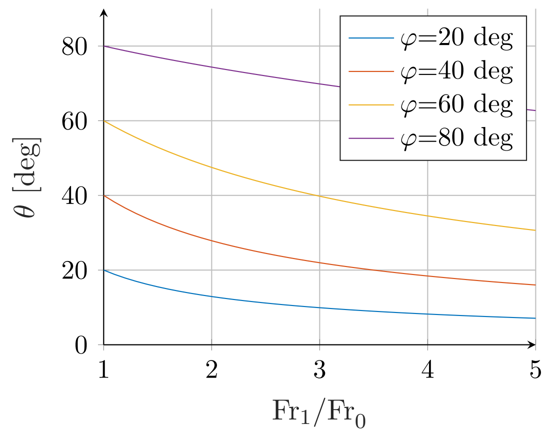

Figure A.10: Theoretical flow angles as function of relative Froude number for oblique weirs

Similarly to plain weirs, a C_s coefficient can be determined for oblique weirs specifically. Borghei [2003] found that besides the submergence factor S, the C_s coefficient for oblique weirs is also depended on the channel width (B_{main}) to crest length (L_w) ratio and concluded the relationship a shown in equation A.28. This relationship was determined for submergence factors (S) between 0.2 and 0.8 and it can be seen that in formula C_s does not converge to zero for $S \rightarrow 1$. This formula can thus only be used for oblique weirs with a limited range of submergence factors.

$$C_s = [0.008\frac{L_w}{B} + 0.985 + (0.161\frac{L_w}{B} - 0.479)S^3]^2 \tag{A.28}$$

A.4 Side weir flow

The main difference between a general plain or oblique weir, and the side weir, is the fact that conservation of mass does not require all upstream discharge to flow over the side weir. In the case of side weirs, only part of the water mass flows over the weir. Specific configurations could result in no water flowing over the side-weir (too large weir crest) or even in reversed flow (negative water level gradient).

Flow regimes

Flow characteristics alongside a free-flowing side weir can evolve in several distinct ways that are characterized according to different flow regime stages. Figure A.11 shows the flow regimes in the main channel along the side weir. The stages are similarly to those found for plain weir, as discussed appendix A and shown in Figure A.2. Research by De Marchi [De Marchi, 1926] showed that for supercritical (free) flow, the water depth is decreasing in downstream direction while the opposite is the case for sub critical flow. This behaviour is noticeable in low, medium and high overflow rates, as can be seen in Figure A.11. This effect can be explained by the effect of secondary flow due to lateral flow near the downstream end of a side-weir [Agaccioglu and Yksel, 1998].

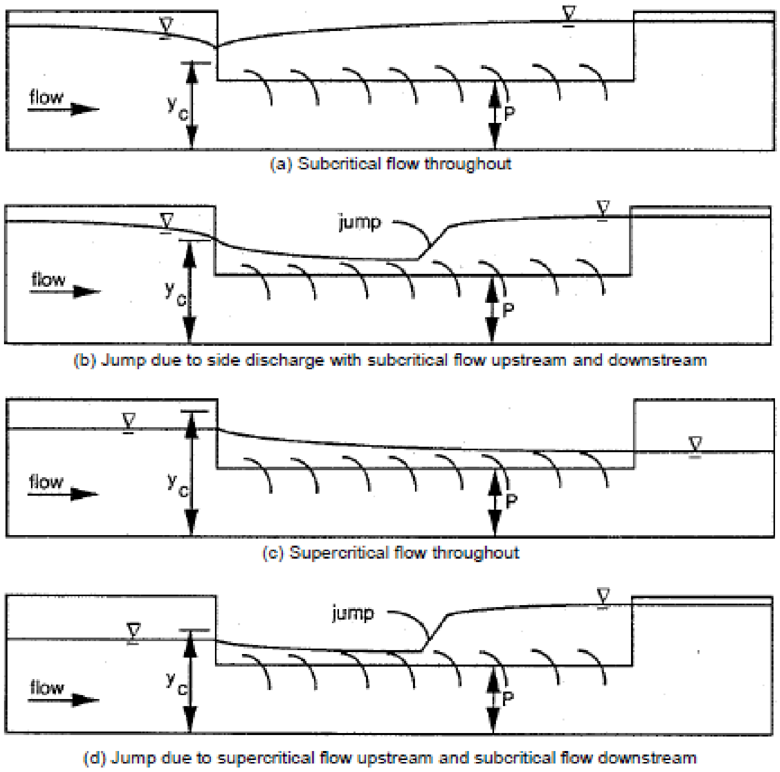

Figure A.11: Flow types of side-weir [Ka-Leung Lee, 2002]

Additionally, also a difference is noticed in equations used to described submerged flow for plain- and side weirs. In the case of side-weirs, a submergence factor is used to calculate the discharge for submerged side-weir flow in contrary to equation A.23 for plain weirs. The result is a submerged side-weir equation similar to equation A.20 with a submergence factor for side weirs and shown in equation A.29.

$$q_w = \frac{2}{3} C_s C_d \sqrt{2g} (H - w)^{3/2} \tag{A.29}$$

.

A.4.1 Standard De-Marchi weir-equation

De Marchi tried to solve the side weir discharge coefficient analytically by assuming that the energy head along the side-weir can be considered constant and ignoring friction. The standard weir-equation, as given by equation A.16 and repeated below, was combined with the equation for constant specific energy ($E = d + \frac{Q^2}{2B^2gd^2}$) resulting in:

$$q_w = \frac{2}{3}C_d\sqrt{2g}(H)^{3/2} \tag{A.30}$$

$$\frac{\mathrm{d}E}{\mathrm{d}x} + (\frac{Q^2}{gB^2d^2} - 1)\frac{\mathrm{d}d}{\mathrm{d}x} = \frac{2Q}{3gB^2y^2}C_d\sqrt{2g} \tag{A.31}$$

where E is the specific energy along side weir, B is the channel width and h the water level. By evaluating the specific energy in a channel, the discharge for any given section can also be computed:

$$Q = Bd\sqrt{2g(E-d)} \tag{A.32}$$

By combining equations A.31 and A.32, and assuming constant specific energy (E), De Marchi found:

$$C_d = \frac{3}{2}\frac{B_{main}}{L_w}\Phi + c \tag{A.33}$$
$$\text{where } \Phi = \frac{2E-3w}{E-w}\sqrt{\frac{E-h}{h-w}} - 3sin(\sqrt{\frac{E-h}{E-w}})^{-1}$$

A.4.2 Discharge Coefficients

In has been concluded that a "complete analytical solution" of equation A.31 is not yet possible and "only approximate methods have been suggested" [Honar and Javan, 2007]. There are two approaches to approximate the discharge coefficient:

1. The discharge coefficient of a similar plain weir can be reduced by correction factor representing the lateral flow conditions, as used by Hager [1987].

2. The discharge coefficient can be obtained from (experimental) data on specific channels shapes and weir types ([Ali, 2013; Subramanya and Awasthy, 1972; Raju et al., 1979; Cheong, 1991; Singh et al., 1994; Swamee et al., 1994; Borghei, 2003]).

Hager side-weir equation
In his analysis of lateral flow over side weirs [Hager, 1987], considered the flow conditions of a plain-weir as described by the standard weir equation. He adjusted for the impacts of the approach velocity, weir shape, lateral outflow angle and flow depth on the side-weir discharge. The resulting equation is given by equation A.34 that is the result of all correcting factors that are described in more detail below.

$$q_{w,side} = \omega * q_{w,plain} \tag{A.34}$$

where $q_{w,side}$ is the discharge over a side weir, $q_{w,plain}$ the discharge over a plain weir and ω the lateral flow coefficient. The lateral flow coefficient includes the effects of the lateral velocity U, lateral angle Θ and lateral outlfow depth h and can be respresented by: $\omega = \omega_U + \omega_\Theta + \omega_h$. The different coefficients will be discussed in more detail below. The combination of all lateral flow coefficients results in the following equation:

$$\omega = (y-W)^{\frac{3}{2}}[\frac{1-W}{3-2y-W}]^{\frac{1}{2}}(1-(\theta+i_b)[\frac{3(1-y)}{y-W}]^{\frac{1}{2}}) \tag{A.35}$$

where y is the relative water level ($y = h/H$), W is the relative weir height ($W = w/H$), θ is the tangent of the width contraction angle and i_b is the bed level gradient.

Flow depth

Figure A.12 shows a comparing of flow over a plain weir and a side weir with equal weir height w and flow depth h. The water depth h near the left boundary of the side weir case is nearly equal to the energy head H of the plain weir (considering $\frac{V_1^2}{2g} \to 0$). Considering the nearly horizontal water profile, Hager assumed the flow depth of a side-weir equal to the energy head of plain weir. This transforms equation A.16 from being depended on the energy head $(q_w(H))$ to depending on the water level $(q_w(h))$. This results in a correction factor given by:

$$\omega_h = (y - W)^{\frac{3}{2}} \tag{A.36}$$

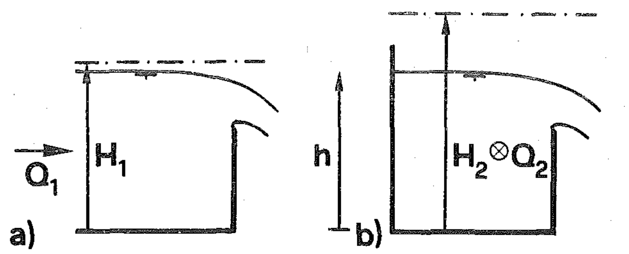

Figure A.12: Comparison of weir flow of (a) a plain-weir and (b) a side-weir [Hager, 1987]

Approach velocity

Looking at figure A.12, the two weirs have different flow velocities, namely $u_1 = sqrt(2g(H_1 - w))$ and $u_2 = sqrt(2g(H_2 - w))$. As explained previously, Hager assumed $H_1 \to h$ and $H_2 \to H$. The effect of the different velocities is then captured in the factor:

$$\frac{u_2}{u_1} = \frac{(H - w)}{(h - w)}^{\frac{1}{2}}$$

re-writing the above factor into the variables relative water level $(y = h/H)$ and dimensionless crest height $(W = \frac{w}{H})$ results in:

$$\omega_U = \frac{u_2}{u_1} = \frac{(H - w)}{(h - w)}^{\frac{1}{2}} = \frac{1 - W}{y - w}^{\frac{1}{2}} \tag{A.37}$$

Lateral outflow angle

Hager considered the outflow discharge over a side-weir to be influenced by the lateral outflow angle ϕ through the factor $sin(\phi)$. The definition of lateral outflow angle is shown in figure A.13. By assuming the average channel velocity u to be equal to the axial component of the lateral outflow velocity $u_{w,axial} = u_w * cos(\phi)$, Hager could approximated the lateral outflow angle:

$$u = u_w * cos(\phi) \tag{A.38}$$

$$cos(\phi) = \frac{u}{u_w}$$

$$sin(\phi) = [1 - \frac{u}{u_w}^2]^{\frac{1}{2}} \tag{A.39}$$

When considering equal energy heads in the centre of the river and at the weir, Bernoulli's equation

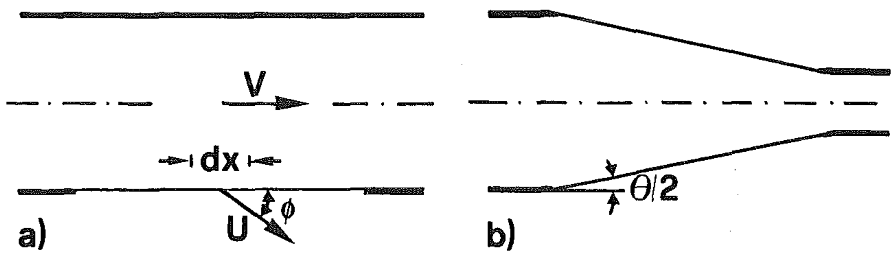

Figure A.13: Definition sketch of (a) lateral outflow angle ϕ and (b) channel contraction angle Θ [Hager, 1987]

can be used to re-write equation A.39 into the following equation:

$$H = h + \frac{u^2}{2g} = w + \rho(h - w) + \frac{u_w^2}{2g} \tag{A.40}$$

Re-writing the above equations results in two formulas for the two velocities:

$$\begin{aligned} u^2 &= (H - h)2g \\ u_w^2 &= ((H - w) - \rho(h - w))2g \end{aligned} \tag{A.41}$$

Inserting A.41 in A.39 results in:

$$\begin{aligned} \frac{u}{u_w}^{2} &= \frac{H - h}{(H - w) - \rho(h - w)} \\ &= \frac{1 - y}{(1 - w) - \rho(y - W)} \\ &= \frac{1 - y}{1 - \rho y - (1 - \rho)W} \end{aligned} \tag{A.42}$$

$$\begin{aligned} sin(\phi) &= (1 - \frac{u}{u_w}^{2})^{\frac{1}{2}} \\ &= [1 - \frac{1 - y}{1 - \rho y - (1 - \rho)W}]^{\frac{1}{2}} \\ &= [\frac{1 - \rho y - (1 - \rho)W}{1 - \rho y - (1 - \rho)W} - \frac{1 - y}{1 - \rho y - (1 - \rho)W}]^{\frac{1}{2}} \\ &= [\frac{1 - \rho y - W(1 - \rho) - (1 - y)}{1 - \rho y - (1 - \rho)W}]^{\frac{1}{2}} \\ &= [\frac{y - \rho y - W(1 - \rho)}{1 - \rho y - (1 - \rho)W}]^{\frac{1}{2}} \\ &= [\frac{y(1 - \rho) - W(1 - \rho)}{1 - \rho y - (1 - \rho)W}]^{\frac{1}{2}} \end{aligned} \tag{A.43}$$

Hager [1987] considered $\rho = \frac{2}{3}$ and inserted this in the above equation. This resulted in the following equation for the lateral outflow angle ϕ:

$$\omega_U = sin(\phi) = [\frac{y - W}{3 - 2y - W}]^{\frac{1}{2}} \tag{A.44}$$

Channel shape

Hager argued that a channel contraction angle Θ, as shown in figure A.13, also results in an increasing lateral outflow discharge. Similarly, Hager argues that the bed level gradient also effects the outflow discharge. The resulting modification factor ω_Θ is:

$$\omega_\Theta = (1 - (\theta + i_b)[\frac{3(1-y)}{y-W}]^{\frac{1}{2}}) \tag{A.45}$$

Experimental data

A large number of these experiments have been conducted that try to determine the relation of the discharge coefficient C_d for various flow conditions. One of the first comprehensive investigations of the discharge coefficient C_d was done by Frazer [1957]. Frazer's experiments on lateral outflow over side-weirs in a rectangular channel found the discharge coefficients to be dependent on the upstream Froude number (Fr):

$$C_d = 0.78 - \frac{0.23H_0}{d_0} - \frac{0.017H_0}{L} \tag{A.46}$$

Several years later, experiments performed by Subramanya and Awasthy [1972] also found a being depended on the upstream Froude number. The newly proposed relationship for the discharge coefficient of sharp-crested weirs under free-flow conditions was different from the one proposed by Frazer. Subramanya argued that the different weir discharge between a plain and side weir can be explained by a later outflow angle that can be expressed by the Froude number. The experiments also showed a dependency on the upstream Froude number (Fr) according to equation A.47 and neglected other flow conditions.

$$C_d = 0.611\sqrt{1 - \frac{3Fr^2}{2 + Fr^2}} \tag{A.47}$$

Raju et al. [1979] included the effects of lateral outflow in a 90 degree side channel that was previously not included. In addition to sharp crested side-weirs, he also found that C_d for broad-crested side-weirs the side-weir crest width played an role.

$$C_d = (0.81 - 0.6Fr)(0.8 + 0.1\frac{d-w}{B_w}) \tag{A.48}$$

Thereafter, Ramamurthy and Carballada [1980] analysed side-weir flow by considering the outflow jet velocities and its related outflow angle. The main parameters influencing C_d were found to be the ratio of average channel velocity/jet velocity and L_d/B. The interesting aspect of this research is the validation for very long side weirs, which is not the case for the previous C_d factors.

Later research by Hager [1987], similar to Subramanya investigated the impact of the lateral outflow angle, as well as several other lateral flow coefficient. Hager included a spatial variation of the Froude number of the side weir and rewrote the lateral flow coefficients to be depended on the dimensionless crest height ($W = w/H$) and dimensionless water depth ($y = h/H$). He included several lateral flow characteristics for side-weirs, including the approach velocity, lateral outflow angle and flow depth. The combination of a weir shape coefficient for plain weirs and these lateral coefficients provided an generalized weir coefficient for side weirs. This new side weir equation is treated more extensively in the next paragraph as this method provides useful general insights in the hydraulic properties of side weirs.

In 1994, research conducted by Singh et al. [1994] concluded a dependence on other parameters besides the Froude number. Singh concluded the dependence on weir heigh Δ and the upstream flow depth d_0:

$$C_d = 0.33 - 0.18Fr + 0.49(\frac{w}{d_0}) \tag{A.49}$$

Agaccioglu and Yksel [1998] conducted research on side-weirs in a 180 degree river bend for which they found a stagnation zone in the inner bend. They also found a reverse flow for low Froude numbers ($Fr < 0.3$) that disappeared if the Froude number is increased, see Figure A.14.

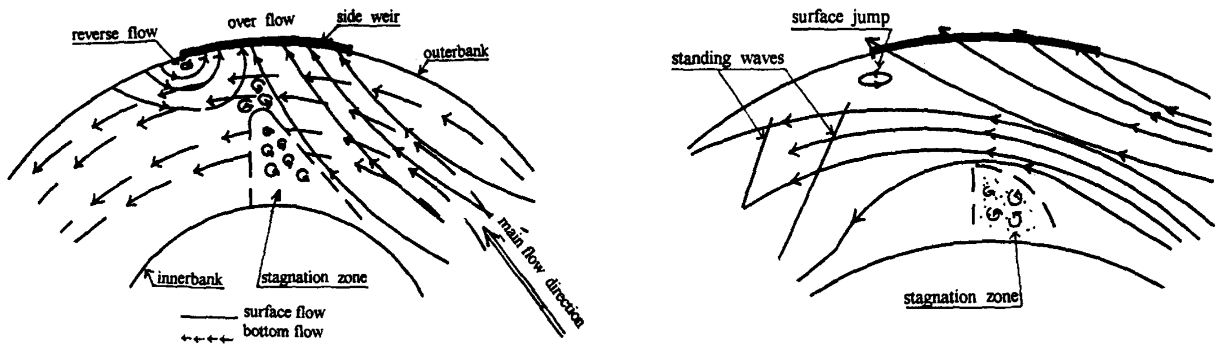

Figure A.14: Flow patterns of side-weirs in a curved channel [Agaccioglu and Yksel, 1998]

Research conducted by Swamee et al. [1994], similar to Raju et al. [1979], investigated flow over a 90 degree side channel restricted by a wall in the side channel. The relationship for C_d he came up with is not only related to the upstream Froude number but also ratio energy head above the weir and width of the weir H_0/B_w:

$$C_d = 0.447 + 0.1\left(\frac{\frac{H_0}{B_w}^{1.79} + 0.05\frac{0}{B_w}^{1.69}}{1 + 2.9\frac{H_0}{B_w}^{0.02}}\right) \tag{A.50}$$

One of the most recent experiments on sharp-crested side-weirs was conducted by Keshavarzi [2014]. His experiments were conducted for sharp-crested side-weirs in trapezoidal channels for different side wall slide. It was concluded that for a trapezoidal channel shape, an increasing side slope (Z) decreases the discharge coefficient. The following relationship was determined:

$$C_d = 0.7 - 0.452Fr - 0.157 * \frac{w}{h_0} + 0.045Z \tag{A.51}$$

where Z is the channel side wall slope. Table A.2 shows a comparison of the most important coefficient equations discussed above. It can be seen that the equations differ considerably, which has been discussed by [Namaee, 2013; Delkash, 2012] who argue that the difference can be contributed to the many different experimental conditions. Figure A.15 shows the variations in discharge coefficients as function of the Froude number. The coefficients are shown as a function of the Froude number as most equations are, at least, depended of the Froude number. Also the formula by Hager as presented in equation 2.17 can be rewritten to a function of the Froude number for a given height ($H = h(1 + Fr^2/2)$). Rewriting Hager's equation for a crest height of zero ($W = 0$), similar to for instance Subramanya, results in the following discharge coefficient [Hager, 1987].

$$C_{d,hager} = 0.485 * \frac{2 + Fr^2}{2 + 3Fr^3}^{0.5} \tag{A.52}$$

Submergence Coefficient

Similar to weir-flow over plain weirs, also side-weirs can experience submerged flow that can be included in the general weir equation with help of a submergence coefficient C_s, as shown by equation A.20. A number of different formulations for the submergence coefficients are available that all are dependent on the submergence factor S. Research conducted by Bradley [1978] on the relationship of the submergence coefficient and the weir discharge for side weirs showed that for side weirs the submergence factor also plays an important role. Bradley's investigation of flow over roadways resulted in figure A.16 that can be used to determine the submergence facto for side weirs. An example of research that uses these factors is the analytical and experimental research by Ji et al. [2013].

Table A.2: Overview of side-weir discharge coefficient (C_d) formula's

Source	**Formula**	**Weir type**	**Channel shape**	**Flow condition**	**Year**	**factor**
Frazer	$C_d = 0.78 - \frac{0.23E}{d_0} - \frac{0.017E}{L}$	Sharp	Rectangular	Free	1957	
Subramanya and Awasthy	$C_d = 0.611\sqrt{1 - \frac{3Fr^2}{2+Fr^2}}$	Sharp	Rectangular	Subcritical	1972	2/3
Ranga Raju	$C_d = (0.81 - 0.6Fr)(0.8 + 0.1\frac{d-w}{B_w})$	Broad	Rectangular	Free 90 deg side channel	1979	2/3
Singh	$C_d = 0.33 - 0.18Fr + 0.49(\frac{w}{d_0})$	Sharp	Rectangular	Subcritical	1994	2/3
Keshavarzi	$C_d = 0.7 - 0.452Fr - 0.157 * \frac{w}{h_0} + 0.045Z$	Sharp	Trapezoidal	Subcritical	2014	2/3

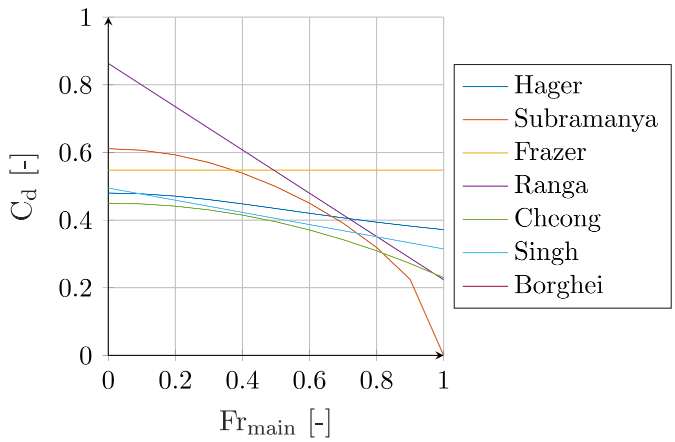

Figure A.15: Comparison of weir discharge obtained from different weir coefficients [S=0.5, h_0=8 m,]

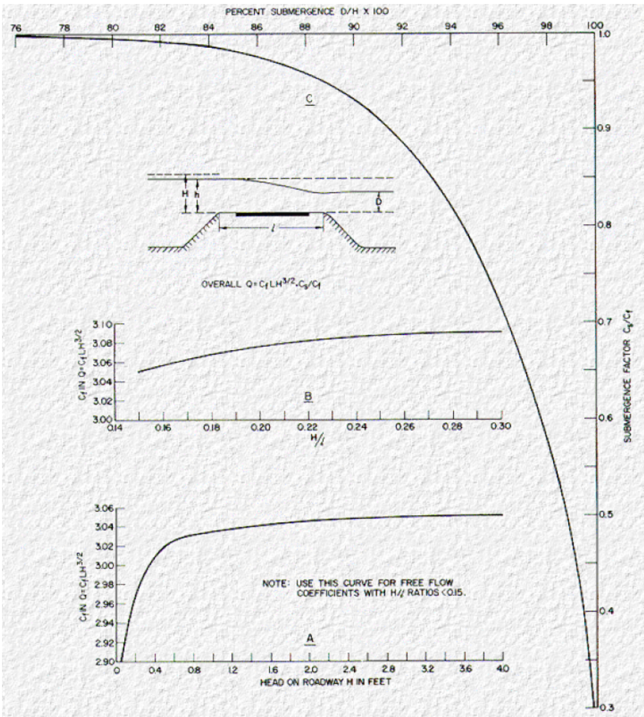

Figure A.16: Submergence coefficients for flow over roadway embankment [Bradley, 1978]

Another example of the determination of the submergence factor C_s is the tests performed by Ka-Leung Lee [2002] where the submergence coefficient for side weirs was determined by thirty-five tests. The following relationship was determined:

$$
\begin{aligned}
C_s &= 1 && \text{for } 0.0 < S < 0.5 \\
C_s &= 1 - 28.84(S-0.5)^{4.85} && \text{for } 0.5 < S < 1.0
\end{aligned}
\tag{A.53}
$$

A.4.3 Conclusion

The difficulty in determining the lateral outflow over side-weirs is the determination of the required discharge coefficients. A large number of discharge coefficient formulations have been derived for side-

Table A.3: Overview of side-weir submergence factor (C_s) formula's

Source	Formula	Weir type	Channel shape	Flow condition	Year
Villemonte	$C_s = \sqrt{1 - S^P}$	plain	rectangular	$0.0 < S < 0.5$	1947
Borghei	$C_s = [0.008\frac{L_w}{B_{main}} + 0.985 + (0.161\frac{L_w}{B} - 0.479)S^3]^2$	oblique	rectangular	0.2¡S¡0.8	2003
Ka-Leung Lee	$C_s = 1$	side	rectangular	$0.0 < S < 0.5$	2002
	$C_s = 1 - 28.84(S - 0.5)^{4.85}$			$0.5 < S < 1.0$	

weir flow that each apply to very different experimental conditions with largely varying relationships as a result. This it very difficult to determine the right formulation to be used. Secondly, from the literature review on side-weir flow it can be concluded that very limited (to no) research is available on side-weir flow between two parallel channels in combination with the effect of a river bend.

A.5 Turbulence

The turbulent transport processes have shortly been evaluated in this research, but not in enough detail to draw conclusions from. To show the possibilities of including these processes, an overview of the relevant literature on turbulent mixing layers is presented in this section. In appendix B.3.1 the implementation in the one-dimensional model is discussed.

A.5.1 Shear layers and wakes

When two parallel channels with a different velocity connect, a shear layer is formed as is shown in figure A.17a. When the two connecting channels have equal velocities, a wake is formed instead. Depending on the thickness of the separating 'splitter plate', figure A.17b or A.17c shows the formed wake.

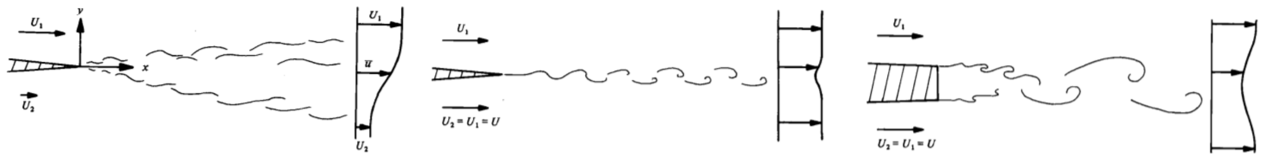

(a) Plain shear layer **(b)** Plain wake: thin trailing edge **(c)** Plain wake: thick trailing edge

Figure A.17: Types of shear layers and wakes [Breienthal, 1981]

A.5.2 Turbulent mixing layer

At the interface between two channels, a shear layer or wake is formed depending on the velocities in both channels. In both cases a mixing layer can be observed. A mixing layer is, for instance, present at river confluences where two rivers merged under an angle but can also be found at the interface between two parallel streams. The suspended sediment flux at the mixing layer between the two channels can be approximated by the entrainment flux (F_e) of the mixing layer. The entrainment flux can be estimated with the help of a simple turbulent diffusion model:

$$F_e = AD_t \frac{\partial C_s}{\partial y} \tag{A.54}$$

where A is the area, D_t is the turbulent diffusivity and $\frac{\partial C_s}{\partial y}$ is the gradient in suspended sediment concentration between the two channels. The turbulent diffusivity can be estimated with the help of a velocity and length scale $D_t \sim u'l$. Because turbulence is non-isotropic (not equal in all directions), it can be expected that the turbulent diffusion is not either ($D_{t,x} \neq D_{t,y} \neq D_{t,z}$).

Looking at the lengths scales, a range of scales can be considered. Large-scale coherent turbulent structures develop that in groyne fields result in large exchange of mass and momentum (Uijttewaal et al. [2001], Weitbrecht et al. [2008], [Kirkil, 2015]). In the case of well defined large-scale turbulent structures, large bundles of unmixed fluid are transported across the mixing layer without being mixed. Actual mixing only takes place at when these large scale structures have been broken down to a much smaller scale. This process of large-scale turbulent structures breaking down to smaller scales is called the Kolmogorov (energy) cascade. Figure A.18 presents this cascade with on the horizontal axis the length scale k in m^{-1} and on the vertical axis the amount of energy E within that length scale.

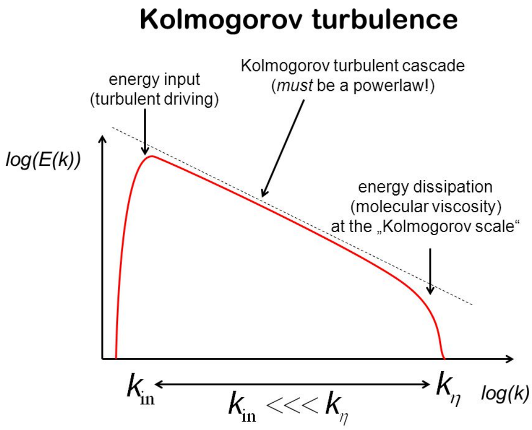

Figure A.18: Kolmogorov turbulent energy cascade [Prooijen and Uijttewaal, 2002]

Considering the mechanisms involved in the turbulent flows, different length and velocity scales play a role. The governing length scale is considered the mixing layer thickness δ (not the depth d). The turbulent diffusivity D_t can be based on the large-scale motion and be determined by the mixing layer thickness δ and the velocity difference over the mixing layer Δu:

$$F_{e,a} = AD_t \frac{\partial u}{\partial \delta} \tag{A.55a}$$

$$D_t \sim \Delta u \delta \tag{A.55b}$$

The local mixing layer thickness can be defined in a number of ways. In this case the following definition is chosen: "the ratio of the velocity difference Δu and the lateral gradient of the velocity in the centre" [Prooijen and Uijttewaal, 2002], as is shown in figure A.19:

$$\delta = \frac{\Delta u}{\frac{\partial u}{\partial y}_c} \tag{A.56}$$

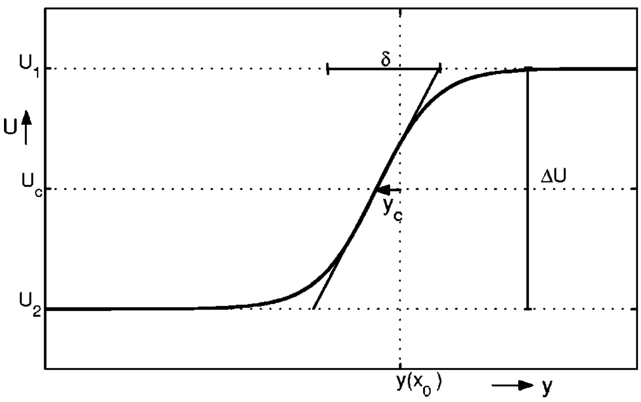

Figure A.19: Sketch of the lateral profile of the stream wise velocity [Prooijen and Uijttewaal, 2002]

A characteristic of mixing layers is that generally the thickness increases in downstream direction from the point of first contact [Roads and Sukhodolov, 2004]. The increase of thickness (δ) seems to depend on the velocities difference in the mixing layer through the following relationship:

$$\frac{d\delta}{ds} = \alpha 2\lambda \tag{A.57}$$

where $\frac{\partial \delta}{\partial x}$ is the growth rate of the mixing layer in streamwise direction, λ is a mixing layer parameter that is given by $\lambda = \frac{u_1 - u_2}{u_1 + u_2}$ and $\alpha \approx 0.085$ is an empirically determined entrainment coefficient.

When considering a self-preserving mixing layer, the mixing layer thickness δ as a function of the streamwise direction can be rewritten by using the momentum balance in streamwise direction to substitute the velocities in equation A.56. After integrating over s, the following relationship is found [Prooijen and Uijttewaal, 2002]:

$$\delta(s) = \alpha \frac{\Delta u_0}{u_c} \frac{d}{c_f}(1 - exp(-\frac{c_f}{d}x)) + \delta_0 \tag{A.58}$$

where u_0 is the initial velocity difference over the mixing layer, u_c is mean velocity of the two channels, C_f is the bed friction coefficient and δ_0 is the initial boundary layer thickness.

Appendix B: One-dimensional model

The one-dimensional model is a schematization of longitudinal training dams in a river section. This model can be used to determine the discharge distribution between the main- and side channel that are created by the longitudinal training dams. This model is used to evaluate the longitudinal trainings dams in the project area near Wamel in the Rhine between river kilometre 911.5 and 914.7.

B.1 Model set-up

Figure B.1 shows the schematized model used in the one dimensional numerical model. The model is bounded in upstream direction (left in figure B.1 by a single river channel. The river then bifurcates at the position of the side channel inlet. Thereafter, the main channel twice more at the positions of the two openings. Directly downstream in the side channel a weir is located at the inlet and both the openings, depicted by the purple line. At the downstream end, the two channels are bounded by a water level. The general river dimensions and longitudinal training dam dimensions are defined according to figures B.2 and B.3.

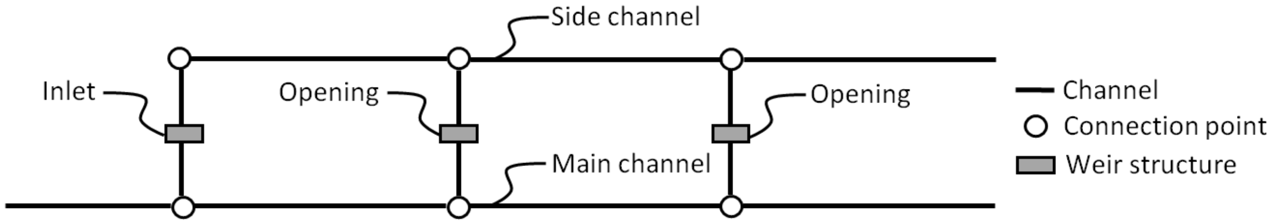

Figure B.1: Overview of one dimensional Matlab schemetization including inlet

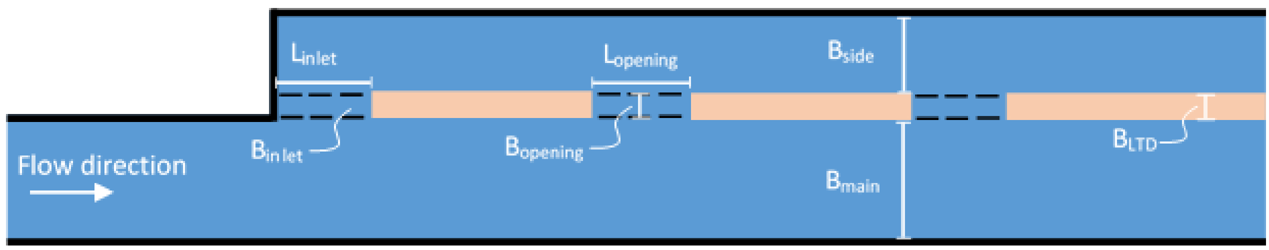

Figure B.2: Definition sketch of one dimensional Matlab schemetization (topview)

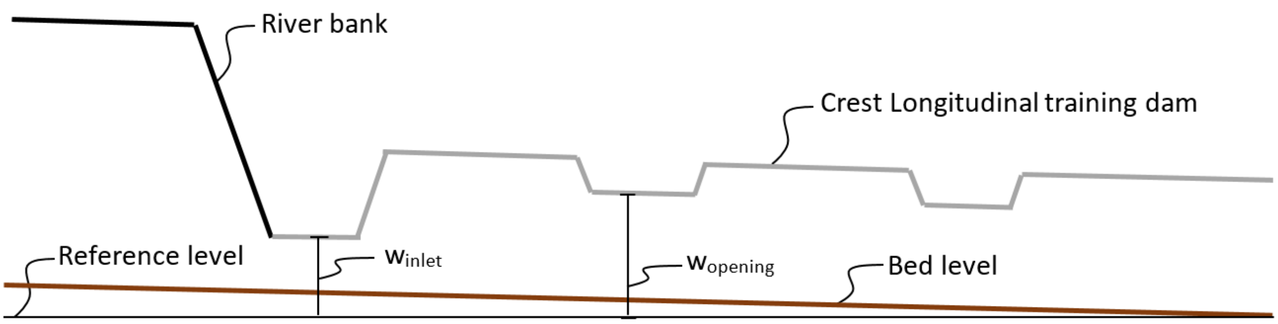

Figure B.3: Definition sketch of one dimensional Matlab schemetization (sideview)

B.1.1 Input parameters and pre-processing

At first the model required the input of several user specified parameters. These include the channel dimensions, such as the length, width and curvature, and other river parameters (bed roughness values and bed level gradient). Figure B.4 shows the created graphical user interface in which the most important parameters can be defined. These parameters are described by one value for an entire branch. The bed level in the channels is not, by definition, equal in each separate channel. A value can be defined that uniformly elevates the bed level in one river branch. In addition, the number and dimensions of the different openings need to be defined. For the discharge calculations, the appropriate weir coefficients and permeability can be defined. Also, several parameters can be adjusted that influence the numerical, iteration and convergence calculations. At last, the different mechanisms and factors can be included or excluded in the calculation and the initial conditions need to be defined. At the upstream boundary, a constant discharge is imposed. At the downstream end, a constant and equal water level is imposed on both river branches. The water level is determined with help of the given discharge and the known discharge to water level relation in the Waal at St Andries Rijkswaterstaat [2016b]. All vectors required in further calculations are then pre-allocated to improve computation time, and the coordinate system is defined. The model uses a polar coordinate system to ensure correct representation of a river bend. The boundary and initial conditions are then imposed onto the coordinate system.

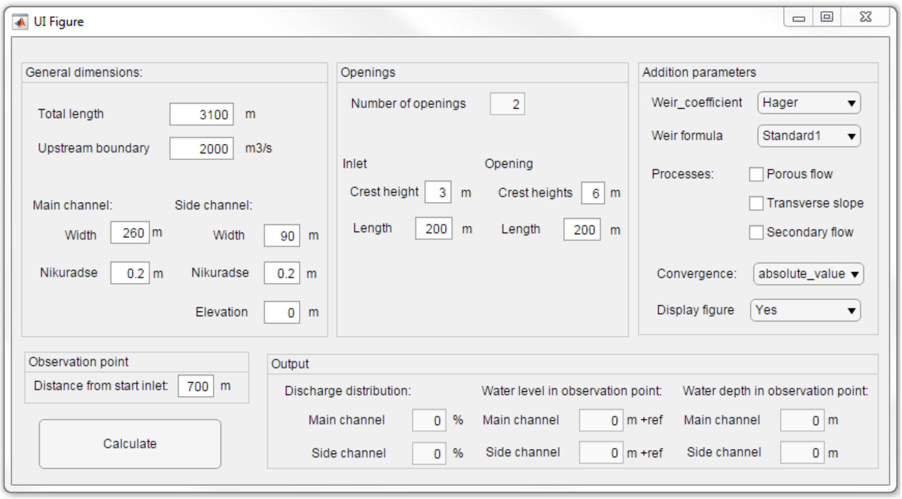

Figure B.4: GUI design of one-dimensional model

Boundary conditions

The boundary conditions are chosen with help of the known discharge to water level relation in the Waal at St Andries. The discharge to water level relation uses the known discharges in the Rhine at Lobith. Table B.1 gives an overview of the discharge - water level relation in the Waal at the city of St Andries (just downstream of the pilot project longitudinal training dams) [Herik and Boskalis, 2014]. The columns 'Waal discharge' and 'Water level' from table B.1 will be used as upstream and downstream boundary conditions respectively [Rijkswaterstaat, 2016b].

Table B.1: Discharge-waterlevel relation St Andries

Upper-Rhine discharge [m3/s]	**Waal discharge** [m3/s]	**Water level** [m +NAP]	**Flow velocity Waal** [m/s]
15.000	10.000	9.90	2.3
12.600	8.400	9.00	2.0
12.320	8.213	8.90	2.0
9.670	6.447	8.10	2.0
6.800	4.533	6.90	1.5
5.800	3.867	6.40	1.2
2.200	1.467	3.00	<1.0
1.985	1.323	2.70	<1.0
984	656	1.50	<1.0

An average ratio of $\frac{2}{3}$ has been used to convert the Rhine discharge at Lobith to the discharge in the Waal. This fraction is the distribution that is strived towards and is roughly found in Rhine-Waal discharge relations such as shown in figure B.5.

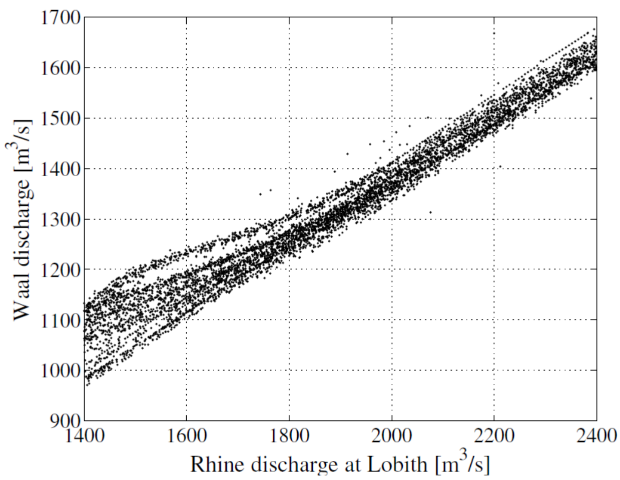

Figure B.5: Waal discarge as a function of the Rhine discharge Vuren [2005]

A best fit curve is plotted through the data given in table B.1 to obtain values for other discharge to water level relations as shown in figure B.6.

B.2 Calculations

B.2.1 Backwatercurves

The backwater curves can be calculated in a number of ways that include the use of the Bresse equation and a numerical approximation. The bresse equation is a difficult equation that can be approximated by an empirical fit as given in equation B.1.

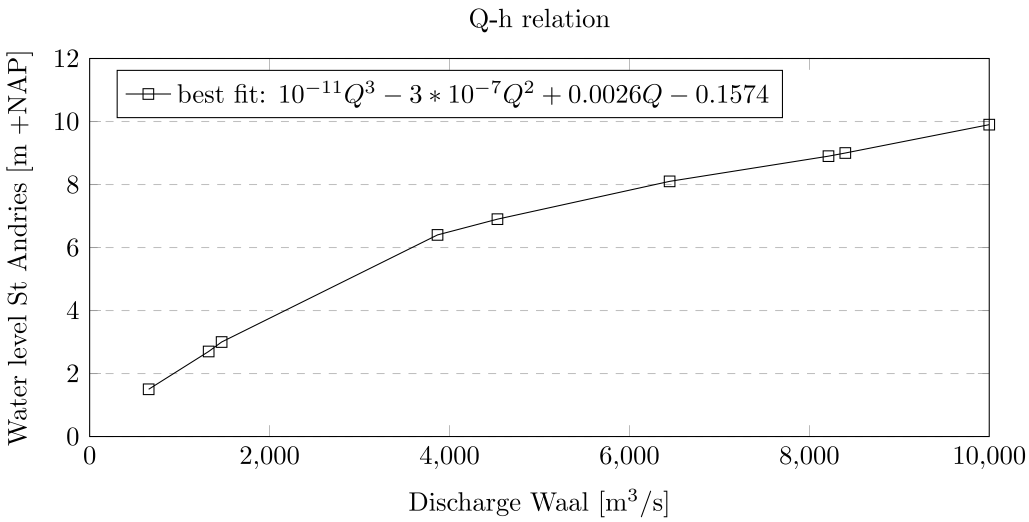

Figure B.6: Discharge to water level relation St Andries

$$d(s) = d_e + (d_o - d_e)2^{\frac{s-s_0}{L_{0.5}}} \tag{B.1}$$
$$L_{0.5} = 0.24\frac{d_e}{i_b}(\frac{d_0}{d_e})^{\frac{4}{3}}$$

$$\text{where } d_e = (\frac{c_f q^2}{i_b g})^{\frac{1}{3}}$$
$$d_0 = \text{downstream boundary condition}$$

A numerical approximation can be calculated with a number of different schemes. An implicit predictor-corrector scheme results in the most stable solution and is given by equation B.2

$$d_{x+1} = d_x - 0.5 * (\frac{\mathrm{d}d}{\mathrm{d}x}_{pred} + \frac{\mathrm{d}d}{\mathrm{d}x}_{corr}) * \mathrm{d}x \tag{B.2}$$

$$\text{where } \frac{\mathrm{d}d}{\mathrm{d}x}_{pred} = \frac{i_b - \frac{q^2}{C^2 d_x^3}}{1 - \frac{q^2}{9.81 d_x^3}}$$
$$d_{pred} = d - \frac{\mathrm{d}d}{\mathrm{d}x}_{pred}\mathrm{d}x$$
$$\frac{\mathrm{d}d}{\mathrm{d}x}_{corr} = \frac{i_b - \frac{q^2}{C^2 d_{pred}^3}}{1 - \frac{q^2}{9.81 d_{pred}^3}}$$

where and d_{x+1} are the water depth at location x and $x + 1$, $\mathrm{d}h/\mathrm{d}x$ is the water level gradient, and $\mathrm{d}x$ is the space step. The difference between the backwater curves in the main and side channel are calculated by the Matlab script and plotted as shown in figure B.7. Comparing the two different backwater curve methods shows that both result in almost identical backwaters. Due to the similar computation time and expected higher accuracy from the numerical method, the numerical predictor-corrector scheme will be used to calculate the backwater curves.
The backwater curves are calculated per river section, as shown in figure B.1, starting from the most downstream section in upstream direction. The downstream boundary condition (h_0) for the first

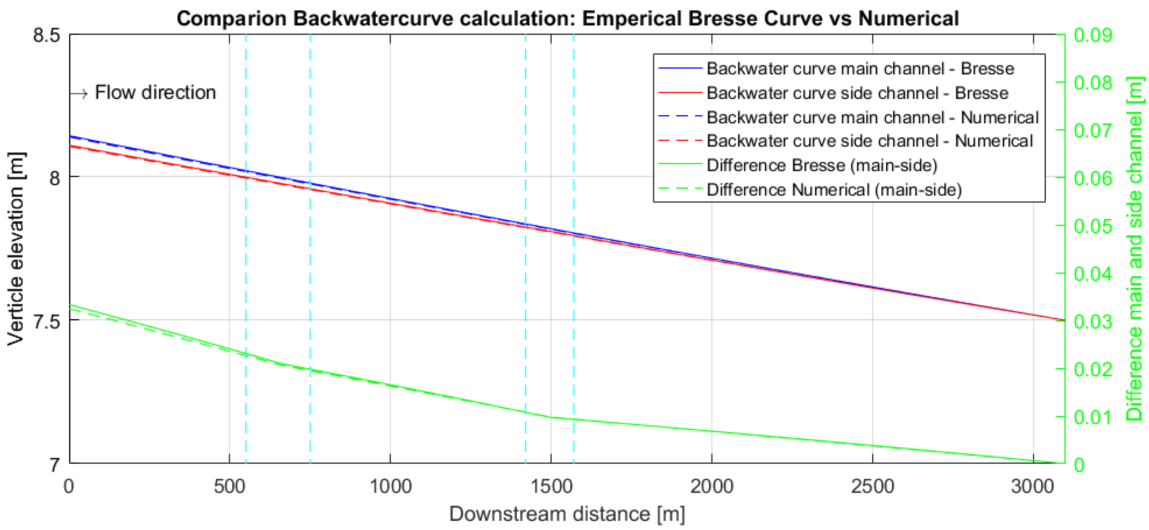

Figure B.7: Comparison of backwater curve with the emperical fit to bresse and predictor-corrector numerical scheme

river section has to be specified. The boundary conditions for the calculation of backwater curves in the following river section is given by the neighbouring water level from the downstream section.

B.2.2 Weir-formula

In order to calculate the discharge over the openings as a result of the difference in water level between the main and side channel, use if made of the side-weir equations as discussed in chapter 2. Most of the literature found on side-weir flow uses the standard side weir with De Marchi's assumption of constant specific energy (see equation A.20 in chapter 2). A large range of discharge coefficient formulas can be used as discussed in given by equations A.46 until A.51).

As discussed by Namaee [2013], the difference between different weir formula and weir coefficients can be related to the large range of experimental conditions used in the determination of these formulas. Namaee [2013] concluded that for broad-crested side weirs, most discharge formula's including the formula proposed by Cheong [1991] and Raju et al. [1979] present too low discharge coefficients. The experimental conditions from Haddadi [2012] also showed these lower values that both Cheong and Rang. Haddadi's proposed formula is expected to best described the trapezoidal weir shape and long side-weir length to channel width ratio of the longitudinal training dams. Therefore, the Haddadi weir-coefficient formula will be used for calculating the discharge over the openings.

B.2.3 Steady-state solution

The matlab model will run several iteration loops ($i = 1 : \mathbf{nr}_{\text{iterations}} + 1$) in order to converge towards a steady state solution for the discharge in the main and side channel. The discharges are converged towards a discharge ratio such that the water level in the main and side channel at the upstream inlet (upstream of the inlet weir) are equal. This is the point where the side channel bifurcates from the main channel. The discharge in the first river section is iterated in several time steps towards this equilibrium. The discharge in the following river sections for the next time step ($Q_{i+1,s}$) is calculated by subtracting the side-weir discharge and the porous flow through the openings ($Q_{w,i,s}$ and $Q_{p,i,s}$)

from the discharge at the upstream section ($Q_{w,i,s-1}$).

$$Q_{main(i+1,s)} = Q_{main(i+1,s-1)} - Q_{w(i,s)} - Q_{p(i,s)} \tag{B.3a}$$
$$Q_{side(i+1,s)} = Q_{side(i+1,s-1)} - Q_{w(i,s)} - Q_{p(i,s)} \tag{B.3b}$$

where $Q_{(i+1,s)}$ is the discharge in a section s in a river branch at iteration step $i+1$, $Q_{(i+1,s-1)}$ is the discharge in the upstream river section, Q_w is the calculated weir discharge and Q_p is the calculated porous discharge. To check whether the simulation is converged towards a steady state solution, the water levels in both channels are considered. For a given side channel discharge ($Q_{side,i,s}$), the expected water level in the main at the upstream side of the opening can be calculated by re-writing the side-weir equation to equation B.4.

$$h_{main,up,2} = \frac{Q_{side}}{2/3 L_w \omega C_d C_s \sqrt{2*g}}^{2/3} + w \tag{B.4}$$

where $hm_{up,2}$ is the expected water level in the main channel just upstream of the inlet or opening for a given side-weir discharge, L_w the crest length, C_d the weir discharge coefficient, C_s the weir submergence coefficient and $w_{opening}$ the crest height. It must be noted that $hm_u p$ is implicitly depended on the water levels in the main (hm_{up}) and side channel (hs_{up}) through the weir submergence coefficient. When the expected water level in the main channel ($hm_{up,2}$) and the actual calculated water level (hm_{up}) is less than a minimal convergence value (e.q. 0.005 m), the simulation is considered to be in equilibrium.

B.3 Mechanisms and factors

Lateral water level gradient

The impacts of a lateral water level gradient has been included in the one-dimensional model through an increased water level level in the inner bend (see equation 3.6). The influence can be estimated with help of the general weir formula as shown below.

$$\frac{\mathrm{d}Q_w}{\mathrm{d}r} \sim \frac{\mathrm{d}[h_{trans}]^{\frac{3}{2}}}{\mathrm{d}r} = \frac{\mathrm{d}[h - \frac{u^2B}{2gr}]^{\frac{3}{2}}}{\mathrm{d}r} = \frac{3}{2}\sqrt{h - \frac{u^2B}{2gr}}\frac{u^2B}{2gr^2} \tag{B.5a}$$
$$O(\frac{\mathrm{d}Q_w}{\mathrm{d}r}) \sim \frac{3}{2}\sqrt{O(10^1) - \frac{O(10^0)^2 O(10^2)}{2 10^1 O(10^3)}}\frac{O(10^0)^2 O(10^2)}{2 10^1 O(10^3)^2} \approx O(10^{-5}) \tag{B.5b}$$

It can be seen that the values from the one-dimensional model (4.1) and the order of magnitude estimation compare relatively well. The influence of the transverse gradient that is created in a river bend increases with larger inlet or opening crest height. This is can be explained by an increasing ratio of lateral water level difference to water depth above the crest.

Secondary flow

Because the transverse flow velocity is of second order smaller than the longitudinal flow velocity (see equation 2.5), a first estimate would suggests that the secondary flow will have a very limited to negligible effect on the flow patterns around longitudinal training dams. Similar to the effects of the transverse gradient, an order of magnitude can for the influence can be estimated as shown below. The estimate influences is two orders larger than calculated with the one-dimensional model, but is still very small. The difference could be explained by the rough overestimation that follows from assuming the transverse velocities to be of second order smaller than the longitudinal flow velocities.

$$O(\frac{\mathrm{d}Q_w}{\mathrm{d}v}) \sim \frac{3}{2}\sqrt{O(10^1) + (1/2)\frac{O(10^0)^2}{10^1} + (1/2)\frac{O(10^{-2})^2}{10^1}}\frac{O(10^{-2})^2}{10^1} \approx O(10^{-3}) \tag{B.6}$$

The one-dimensional model calculations, the influence of secondary flow on the discharge distribution shows to increase for increasing crest height. This is explained by an increase of the velocity head relatively to the water depth (decreasing y value in equation 3.2). One should be careful, though, when using studying the effects of secondary flow on the discharge over a side weir with the above stated method. Some very general assumptions have been made in which the transverse velocity magnitude induced by the secondary flow, is assumed to be equal to the velocity obtained by Rezovskii's equation (see equation 2.4. Secondly, the influence of the secondary flow in real river situations is much more complicated as the velocity magnitude decrease near the river banks (in this case the longitudinal training dam) and secondary flow patterns might change due to the interaction with the side channel. This research only provides a rough order of magnitude estimate for the influence and for more detailed analysis on the influence of secondary flow, reference is made to, for instance, Agaccioglu and Yksel [1998].

B.3.1 Lateral velocity

The lateral (or radial) velocity component can be obtained as shown in equation 2.4 as introduced by Rozovskii [1957].

$$v = \frac{ud}{r}\frac{1}{\kappa}[F_1(\eta) + \frac{\sqrt{g}}{\kappa^2 C}F_2(\eta)][1 - exp(-\frac{2\kappa C}{\sqrt{g}}\frac{x}{d})] \tag{B.7}$$

where d is the water depth, C is the Chezy coefficient, κ is the Von Karma constant ($\kappa\ = 0.4$) and F_1 and F_2 are coefficients influenced by the relative vertical position ($\eta = \frac{z}{d}$). The last part of the right-hand side in equation B.7 represents the growth of the lateral velocity with longitudinal distance. Both F_1 and F_2 can be estimated with the help of figure B.8 taken from Tanguy [2009]. It should be noted that Rozovskii's equation tends to "overestimate the lateral velocity" [Baek and Seo, 2009] but can be used to estimate an order of magnitude for the strength of the secondary flow velocity as shown in equation B.8.

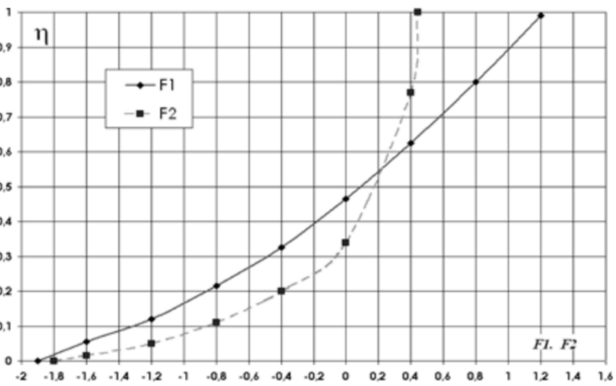

Figure B.8: Values of F1 and F2 in Rozovskii's formula [Tanguy, 2009]

$$\begin{aligned} O(v) &= \frac{O(d)O(u)}{O(r)}\frac{1}{\kappa}[O(F_1(\eta)) + \frac{\sqrt{g}}{\kappa^2 O(C)}O(F_2(\eta))] \\ &= \frac{O(10^1)O(10^0)}{O(10^3)}\frac{1}{0.4}[O(10^{-1}) + \frac{10^1}{10^{-1} * O(10^1)}O(10^{-1})] \\ &= O(10^{-2}) \end{aligned} \tag{B.8}$$

Porous flow

The inlet and openings in between the longitudinal training dams are constructed by rocks with a single mass-grading of 40 - 200 kg, as is shown in figure B.9. The porous rock layer results in flow through the openings between the main and side channel, even during water levels below the crest of the inlet or openings. As the crest of the openings is relatively high in relation the crest of the dam itself, the amount of water potentially flowing through the porous rocks layer is also taken into account.

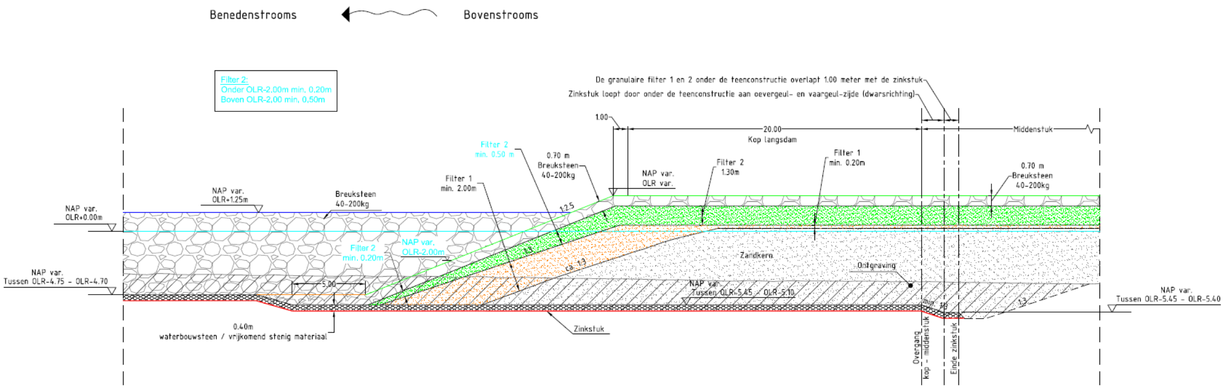

Figure B.9: Technical drawing showing the porous openings [Herik and Boskalis, 2014]

Flow through porous soils and rocks can be approximated with the general Darcy formula for flow through porous media, given by equation B.9.

$$v_{porous} = k * I \tag{B.9}$$

where v_{porous} is the fluid velocity through the porous medium, k is the permeability and I is the hydraulic pressure gradient. The hydraulic pressure gradient can easily be calculated by the water levels on opposite sites of the openings in the main and side channel and the width of the openings. The permeability can be approximated with the help of figure B.10 that relates the permeability to the size-grading of the rock layer. The size-grading corresponding to a rock grading of 40-200 kg can be calculated with the help of the Rosin-Rammler equation from the Rock Manual [CIRIA, 2007] and the grain sizes used in the inlet and openigs [Herik and Boskalis, 2014].

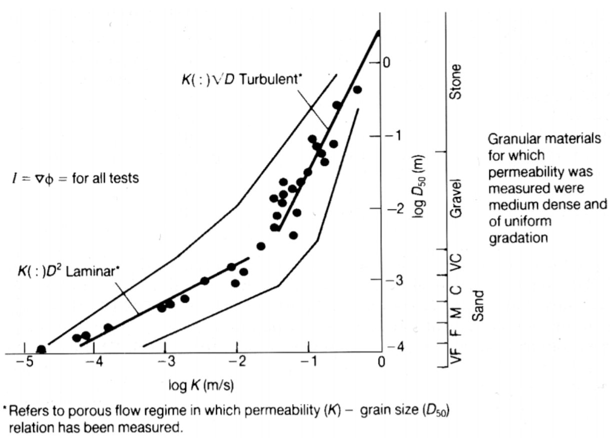

Figure B.10: Permeability of granular materials vs grain size D_{50} [CIRIA, 2007]

$$\begin{aligned} D_{15,min} &= 323 \text{ mm} \\ D_{50,ave} &= 450 \text{ mm} \\ D_{85,max} &= 536 \text{ mm} \end{aligned} \tag{B.10}$$

According to figure B.10, the permeability of grain-sizes ranging between 300 mm and 550 mm is approximately $k = 0.4$ m/s. The total discharge through the porous rock layer can then be calculated by multiplying the flow velocity by the height and effective width of the rock layer.

Mixing layer

The possibility of including the transport processes induced by a mixing layer at the inlet and openings in the one-dimensional model has shortly been looked at but not treated in enough detail to draw conclusions from. Below, a very short description is given of this attempt to show that schematization of mixing layer development in the one-dimensional model is very possibly and would be very interesting to investigate further.

Use is made of knowledge found in literature and described in appendix A.5. The mixing layer thickness at the inlet and openings can easily be determined using equation A.58 and the velocities in both channels. Figure B.11 shows the schematize mixing layer development as calculated by the one-dimensional model.

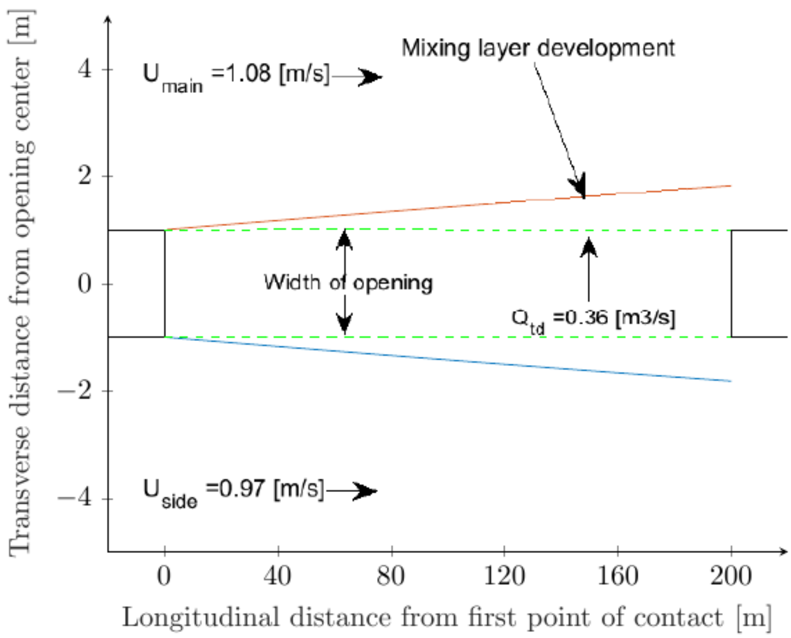

Figure B.11: Mixing layer development in the one-dimensional model

B.4 Model assumptions

Some of the important assumptions made in the model set-up are listed below.

1. **Channel geometry:**
   (a) The channels are assumed to be uniform. The channel width and Nikuradse roughness height are thus described by one value for an entire branch.

   (b) The channel shape is assumed to be rectangular. Effects of a trapezoidal channel are only implicitly included in the weir discharge coefficients.
   (c) The bend radius is parameterized by a single value for the entire river section. This model, thus, does not include variations in the longitudinal direction of a river bend.
   (d) The one-dimensional model does not include losses in the outflow region.

2. **Longitudinal training dams:**
   (a) Flow over the longitudinal training dams itself is not considered. Therefore, river discharge larger than 3000 m^3/s, which correspond to water levels exceeding the dam's crest, cannot be modelled correctly.

3. **Weir flow:**
   (a) In the one-dimensional model it is assumed that the discharge over the inlet and opening and the flow patterns around them can be schematized as weir structures. This is a assumption results in the neglection of many effect including porosity and friction caused by irregular stones as these are (usually) not taken into account in weir flow literature.
   (b) The weir discharge is calculated by (side) weir formula that only requires the upstream water level as direct input parameter. Other effects including the centripetal forces, viscous effects, increased turbulence, submergence, and non-uniform velocity distribution are captured in different coefficients. All these effects are thus only included implicitly through an added empirical coefficient found for reasonably similar experimental studies.
   (c) The discharge over the inlet or openings is calculated as a single value that thus does not provide any spatial variations (not in flow velocities nor flow direction).
   (d) The side-weir equation that is used assumes constant specific energy along the side weir.

B.5 Model performance

B.5.1 Model consistency

In order to determine if the model produces correct outputs, a combination of input parameters are tested for which the outputs are known or should lie within an expected domain. This is done for a number of conditions for which the first represents two channels with equal width, a long weir length (1000 m) and fully open inlet crest height. As there is no side-weir present and a long opening to allow the discharge to spread evenly with zero crest height, this configuration is expected to result in an (almost) equal distribution between the main and side channel. Small deviations from an equal distribution can occur as the water will still needs to be directed in lateral direction to enter the side channel. The second case represents fully closed crest height at the inlet and openings. This means that there will be no weir flow over present. In this case it is thus expected that (almost) all water will remain in the main channel. A small amount of water will still be able to flow towards the side channel due to the porous properties of the inlet and openings. Thirdly, a regular condition is tested with conditions representative to the Waal are tested, for which the water level difference will be evaluated. Table B.2 shows the discharge distributions calculated for the different conditions in the validation tests.

- **Equal width and fully open inlet height and openings:** As can be seen in table B.2, the discharge distribution deviates slightly from a discharge distribution of 50% towards the side channel. This can be explained by the fact that the model still uses a side-weir formulation to calculate the discharge at the inlet. The discharge coefficients calculated will still result in a resistance term that results in a deviation from an exact discharge distribution of 50% towards the side channel. When decreasing the opening length, the discharge distribution to the side channel will also decrease.

Table B.2: Overview of parameters in validation tests

	Width		**Specific discharge**		**Distribution**		**Water level**
	Main	Side	Main	Side	Main	Side	difference
Fully open (long+equal width)	230 m	230 m	4.7 m^2/s	4.0 m^2/s	54 %	46 %	0.04 m
Fully closed	230 m	90 m	8.7 m^2/s	0 m^2/s	100 %	0 %	0.33 m
Waal conditions	230 m	90 m	6.1 m^2/s	4.6 m^2/s	76 %	24 %	0.16 m

- **Fully closed inlet height and fully closed openings:** Table B.2 shows that all water remains in the main channel. The calculated water level in the side channel remains equal to the downstream water level as expected in a physical itisense.

- **Regular:** With the regular condition a water level difference between the two channels is calculated with a maximum value of 0.16 m at the inlet. The maximum expected gradient can be related to the bed elevation due to the adopted bed level gradient. With a gradient of 10^{-4} m/m over a length of 3 km, a maximum water level difference of 0.30 m is physically expected. The value found is well within this range.

The one-dimensional model performs well in the above stated validation tests, but does show a small deviation from full equilibrium for equal channel widths. One must thus be careful when trying to obtain exact numerical output values. The model does provide useful insights in the mechanisms and factors and the influence of control strategies.

B.5.2 Sensitivity analysis

A sensitivity analysis is a tool that can help to determine the important sources of uncertainties in the model. The errors generated by the input parameters is investigated by varying their value. Some of the parameters in the one-dimensional model present the regulatory design dimensions (inlet- and opening crest heights). Other parameters express the actual conditions at the pilot project and are subject to statistical or inherent uncertainties. These parameters include the permeability, bend radius, and friction coefficients. The domain and sensitivity of these parameters are discussed in more detail below.

- **Bend radius:** The bend radius in the Waal river differs per alternating bend. In the pilot project's river section in the Waal, the bend radius varies between values of 1000 m and 8000 m for both left and rights bends as seen in figure B.12. An average bend radius of 2000 m matches the bend radius at the pilot project. A sensitivity analysis is performed to determine the sensitivity of the bend radius. The result is shown in figure B.14. The discharge ratio is not so much effected by the bend radius of the river. When zooming in closer, it is seen that a larger bend radius results in an increasing discharge towards the side channel. This is expected, because of the combined effect of a smaller river length and larger lateral gradient with increasing bend radius. This results in a larger bed gradient in the side channel and a larger water difference between the two channels respectively.

- **Bed friction** The bed friction in a measure of the amount of friction generated by the bed roughness in river. The bed friction can be expressed expressed in a variety of parameters. One of these parameters is an equivalent sand roughness height expressed by a Nikuradse roughness height k_r. Another well known coefficient is the Chezy value, that actually is a smoothness coefficient with unit $\sqrt{m}/s$. The Chezy value can be related to the shear velocity and is also

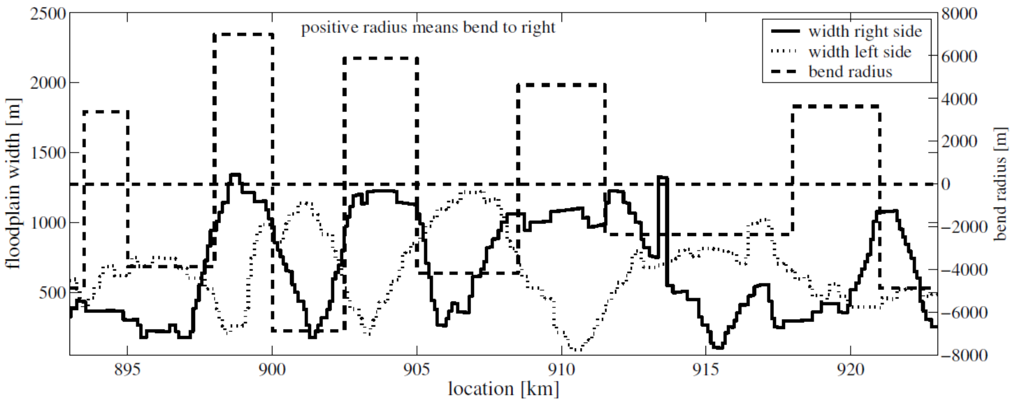

Figure B.12: Bend radius variation in the Waal [Vuren, 2005]

depended on the river discharge. The empirical relationship between the Nikuradse roughness height k_r and the Chezy values C is given by the following formula:

$$C = 18 * log10(12 * R/k_r) \tag{B.11}$$

where R is the hydraulic radius and k_r then Nikuradse roughness height. The bed friction is often used as calibration parameters to ensure accurate water levels or other relevant model results. For the Rhine river, Vuren [2005] found that Nikurakse roughness heights in the Waal roughly vary between 0.1 and 0.4 m, as shown in figure B.13. These roughness heights are iteratively converted to Chezy values that are used in the backwater curve equations. The results are shown in figure B.14. Increasing the roughness height in both channels equally results in a discharge distribution that changes in the order of 3% more towards the main channel. When increasing the roughness height in the side channel, with respect to the main channel, less water is directed towards the side channel. This can be explained by a larger resistance in the side channel that slows down water flowing through.

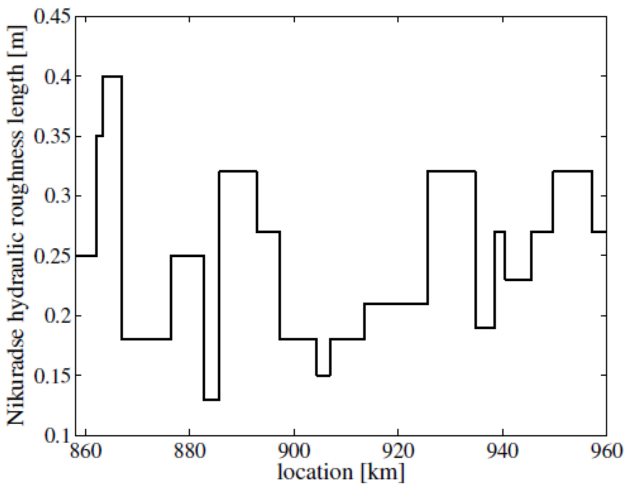

Figure B.13: Variation of Nikuradse roughness height in the Waal [Vuren, 2005]

- **Permeability opening:** The permeability of the inlet and openings is determined by the size and packing of the rock layer. A permeability can potentially vary between (almost) 0 for very fine and dense packed clay layers to 1 for very open rock layers. The results for the sensitivity analysis is shown in figure B.14. The permeability of the inlet and openings does not influence the discharge distribution. The is the result of the weir discharge over the inlet and openings being orders larger than the porous discharge.

When combining the extreme calibration parameters values, insight can be given in the model's error domain. The extremes values for the Chezy value in the main channel, the Chezy value in the side channel, the bend radius and the permeability of inlet and openings are used as input in the one-dimensional mode. Two model runs are performed for applying the combination of parameters resulting in minimal and maximal discharge distribution towards the side channel, as shown in table B.3. The resulting discharge distribution is presented in the same table and shows a deviation of 4% less and 3% more discharge towards the side channel.

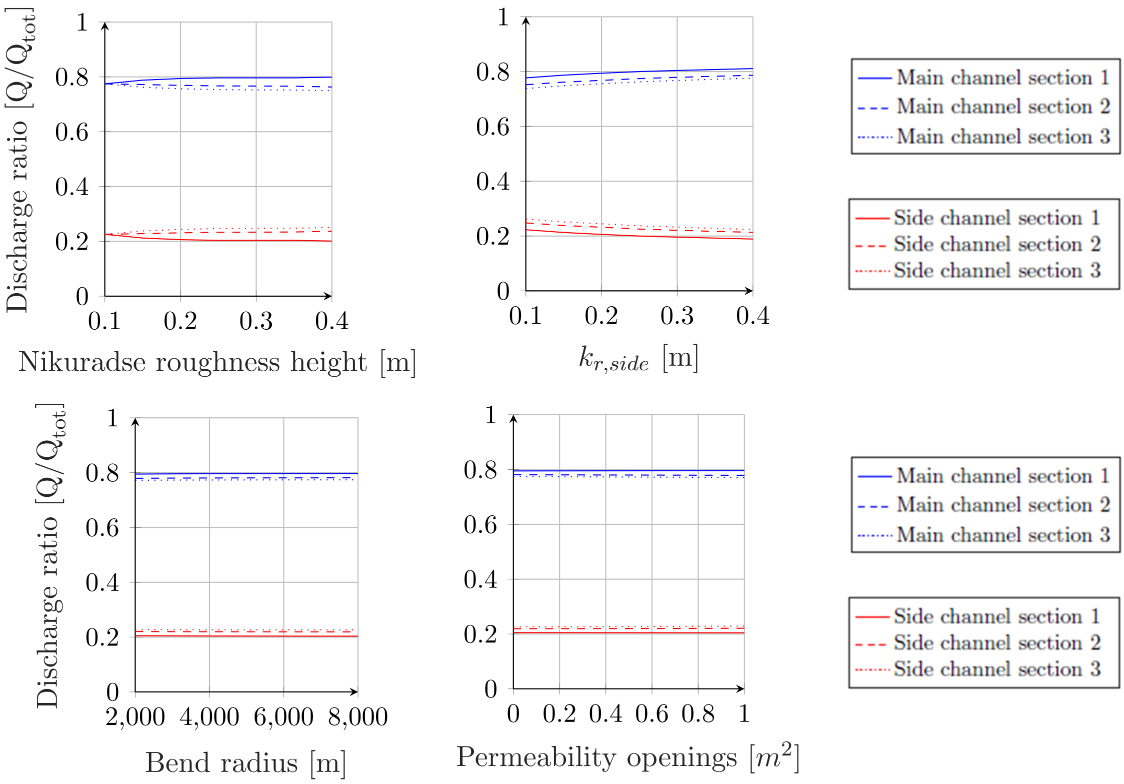

Figure B.14: Sensitivity analysis

Table B.3: Discharge distribution to main channel for extreme combinations of parameters

	Input parameters				**Calculated discharge distribution**		
	Nikuradse		Bend radius	Permeability	Main channel		
	(main) m	(side) m	m	-	section 1	section 2	section 3
normal	0.20	0.20	2600	0.4	80 %	77 %	76 %
max	0.40	0.60	1000	0	81 %	78 %	77 %
min	0.10	0.08	8000	1	77 %	77 %	77 %

B.6 Model limitations

The one-dimensional model shows to be stable in a large parameter range and can be adjusted easily for a great number of river parameters, design and control dimensions, numerical parameters or different discharge or submergence formulations. However, the model also has some limitation that should be considered and are described below.

B.6.1 Rough schematization

The schematization as used in the one-dimensional model is a very rough schematization of the system of longitudinal training dams and should be used with care when comparing to the actual situation in the Waal. The model assumes that both the side and main channel are uniform and rectangular over the entire river section. The assumption of a rectangular channel is made for simplification and does not resemble the real situation in river bend. The bend flow results in a lower bed topography in the outer bend that changes in stream-wise direction. This is not incorporated in the model. An uniform channel is, more or less, the case for the main channel were the trainings dams and groynes (on opposite side) result in a relatively equal channel width. In the side channel, however, parts of the old river groynes have not been removed completely and block the flow considerably. This could be included in the one-dimensional model by decreasing the side channel width to an effective width resembling the smallest width found in the river section. Also, in the side channel more blocking factors are found in form of cables crossing underneath the river. The effects of these cables on the flow and discharge distribution is not known nor modelled.

B.6.2 Weir discharge and submergence coefficients

Within the one-dimensional model, the weir formulations play a dominant role in the determination of discharges. The user can easily switch between different formulations for the discharge and submergence coefficient as found in literature. However, no formulations have been found for which experimental validations tests have been found that corresponding to the conditions resembling the longitudinal training dams in the Waal. The use of the discharge coefficient as proposed by Hager [1987] and the submergence coefficient by Ka-Leung Lee [2002] are expected to be most universally applicable to different side-weir configurations as found at the longitudinal training dams in the Waal. These formulations also show the best agreement with the two-dimensional model results but are not validated with laboratory or field data. The numerical results from the one-dimensional model should thus be used with care and probably do not exactly match the conditions of the longitudinal training dams. They are, however, expected to provide good insights in the order of magnitude of different parameters.

For the discharge coefficient, as described by Hager [1987], several assumptions have been made that should be kept in mind. These assumptions include:

1. The flow in the channel is considered one-dimensional and the water is considered homogeneous and incompressible.
2. The flow is considered stationary.
3. The pressure distribution is considered to be hydrostatic.
4. The flow is considered to be gradually varied over the weir-like structure.
5. The bed level gradient is considered constant and not exceeding 10%.
6. Surface tension and viscosity effects are considered insignificant.

Besides the above stated assumptions, the formulations by Hager are originally designed for non-submerged weirs and can be altered with help of a submergence factor [Hager, 1982]. The calculated discharges over the weir-like structure are expected to be modelled reasonably with by the introduction of this submergence coefficients. However, the lateral flow coefficient ω_ϕ is expected to not correctly reflect the lateral outflow angles anymore. The one-dimensional model is thus expected to provide reliable information on the discharge distributions at the longitudinal training dams, however, is not expected to provide insights in the flow patterns at the inlet or openings.

B.6.3 Convergence

The model is programmed such that the discharges at each river section is converged iteratively. The combination of an inlet and multiple openings thus results in multi iteration loops inside each other. The model show difficulties when the steps between each iteration is large and the difference in roughness height ($kr_{main}/kr_{side} > 5$) or channel width ($B_{main}/B_{side} > 4$) between the two channels is large. In these cases, the iteration steps should be decreased in order to ensure models convergence but simultaneously also increases the computation time greatly. One of the positive sides of this one-dimensional model is the fast computation time that thus diminished with large differences in roughness heights or channel width between the channels. Choosing the initial conditions smart will again limit the computational time but requires a try and error method to optimize. The optimization of the initial conditions or iteration steps are required to be performed by hand and could potentially be included in this model.

Appendix C: Two-dimensional model

The two-dimensional model is made with the help of the Delft3D-Flow modelling software. This is a numerical hydrodynamic modelling program that is able to calculate flow and transport forced by constant, time depended or relation based boundary conditions. A Delft3D-Flow model uses a rectangular or curvilinear, boundary fitted grid, that is multi-dimensional. The equations used to solve for the hydrodynamics are the Navier-Stokes equations, based on conservation properties of the fluid and its motion.

The created Delft3D-Flow model for the system of longitudinal training dams is discussed in this appendix. Further explanation of conservation equations is given in appendix A and descriptions of the modelling program Delft3D-Flow can be found in the associated user's and technical reference manuals [Deltares, 2008].

C.1 Model set-up

Two different Delft3D-Flow models are constructed, for which the model set-up of both models is discussed in this section. The first is a representation of only the first inlet opening. The second is a schematization of the a system of longitudinal training dams with one inlet and 2 openings.

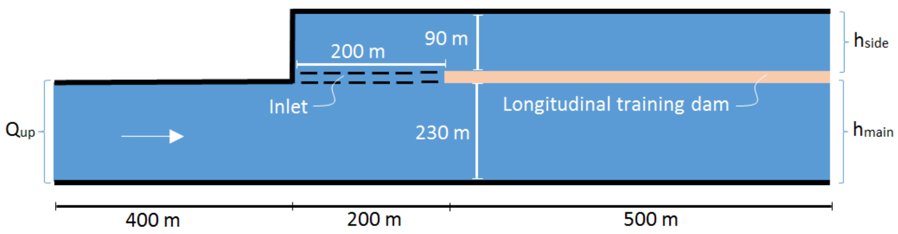

Figure C.1: Short two-dimensional Delft3D-Flow model schemetization (top view)

C.1.1 Grid

The Delft3D-Flow models schematize the longitudinal training dams with help of a two-dimensional depth-averaged M by N grid. In vertical direction, only a single layer has been defined (resulting in a 2DH model). In horizontal transverse direction, the models schematize the main channel with a width of 230 m and a side channel on the left bank with a width of 90 m. In longitudinal direction the model includes a 400 m length before the inlet to ensure a uniform flow from upstream direction, as shown in figure C.1. Upstream of the inlet, the side channel has not started yet and the associated empty grid cells are deleted.

Depending on the level of refinement, the short Delft3D-Flow model has a grid mesh that consists of a multiplication of 107 by 332 grid cells (see table C.1). The grid sizes used in the dM=3.33 m and dN=3.33 m. The total length thus includes 400 m upstream of the inlet, 200 m of inlet length and 500 in downstream direction. The second longer model is created by extending the first model in downstream longitudinal direction by an additional 2000 m (total length of 3500 m) to a grid size of 105 by 1052 grid cells. Two openings are included in downstream direction, that are similar to

Table C.1: Two-dimensional model runs for various grid sizes

Model run	Refinement	Number of grid cells		Grid size	
	[-]	M [#]	N [#]	dM [m]	dN [m]
E-1	1	35	110	10	10
E-2	2	70	220	5	5
E-3	3	105	330	3.3	3.3
E-4	4	140	440	2.5	2.5
E-5	5	175	550	2	2

the inlet. Thereby an entire section of longitudinal training dams is schematized that will be used to further investigate the system of longitudinal training dams.

C.1.2 Timestep

The time step has been chosen such that a CFL criterion conditions relating to a Courant number of 1 is satisfied. The CFL condition is given by equation C.1.

$$C = \frac{\Delta t u}{\Delta x} < 1 \tag{C.1}$$

where C is the Courant number, Δt is the time step, Δx the grid size and u the maximum velocity in the simulation. Considering the chosen grid sizes and maximum velocities around 2 m/s, a time step of 0.02 min is used. As will be discussed in the following chapters, for a flood scheme and large crest heights a smaller time step of 0.005 min is required. The total simulation time is influenced by the time it takes for the numerical errors created by the difference between the initial and boundary conditions to be dissipated. When the boundary conditions are time independed the calculated parameters converge to a time-independed solution, that is also called a steady-state solution. The time this takes is called the spin-up time. It was noticed that for all model runs, a steady-state solution is reached after a run time of 1.5 hours, see figure C.2.

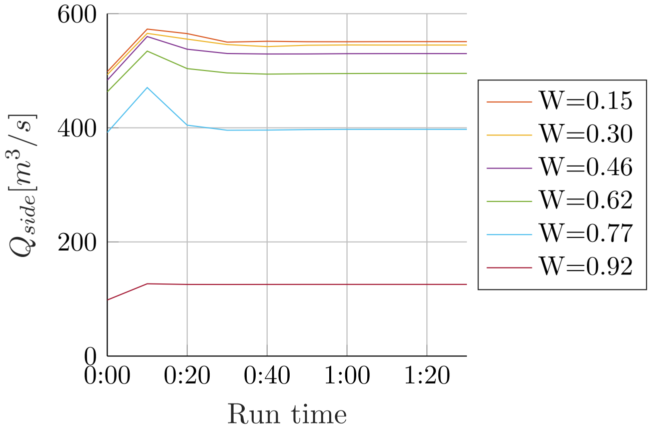

Figure C.2: Calculated discharge in side channel as function of model run time for various dimensionless crest heights ($W = w/H$)

C.1.3 Boundary conditions

As boundary conditions, a total discharge is assigned to the upstream boundary, a water level boundary at the downstream side of both the main and side channel. The combination of these downstream water level boundaries provides the ability to set the submergence factor in the 'small' model as explained in equation 2.4.2 and equal downstream water levels in the 'large' model. A uniform initial condition of 6.5 m has been applied that closely matches the boundary conditions to minimize the model's spin-up time. In later model runs, a restart file is used, as created by previous runs, to minimize the required spin-up time. Water level boundaries of $h_{side} = 6.39$ and $h_{side} = 6.47$ m +bed level are used. These values are obtained from the one-dimensional model at a distance of 500 m from the downstream end of the inlet for a crest height of 3 m + bed level. These boundary conditions are kept constant to compare the different model results. A constant upstream discharge boundary of $Q_{up} = 2000$ m^3/s is used.

On the water level boundaries, an additional reflection parameter has been defined to prevent numerical oscillations created to again minimize the model's spin-up time. A reflection parameters is chosen according to the relationship as given by equation C.2, where α_r is the reflection parameter, L is the river section length and g is the gravitational acceleration constant.

$$\alpha_r = \sqrt{L/g} \tag{C.2}$$

C.1.4 Bathymetry

A bathymetry is included as input file in the Delft3D-Flow model runs. For the system of longitudinal training dams a longitudinal bed slope of $i_b = 10^{-4}$ has been included in the bed topography. As mentioned before in chapter 2, there are two ways of including the inlet and openings in a two-dimensional model: either by schematization within the bed topography or as a subgrid weir. For the first, the inlet and openings are also included in the bathymetry as will be described below; for the latter they are not.

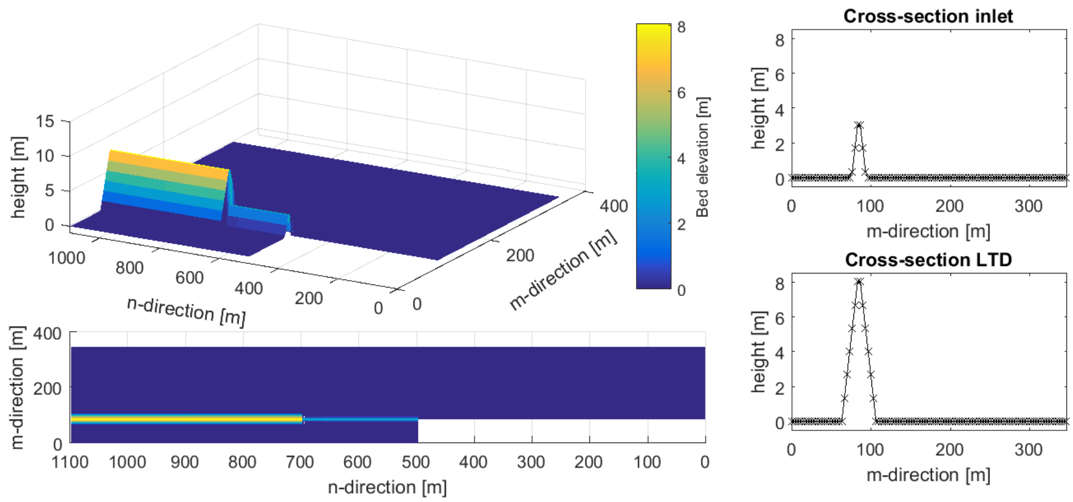

Figure C.3: Overview of two-dimensional model schematization in bed topography

The inlet and openings are by elevating grid cells within the initial bed topography. For this purpose, the bed has been elevated to the required crest height. Side slopes of 1 : 2.5 on both sides are also included, as shown in figure C.3. The crest is defined with a minimum of 2 data points to prevent strange numerical phenomena (such as unreasonable water levels and velocity magnitudes) at the crest. Figure C.4 shows a cross section of the inlet bed level point for various crest heights above bed level.

C.1.5 Subgrid weirs

Within the Delft3D-Flow and Waqua (also known as Simona) modelling software, the schematization of the system of longitudinal training dams using subgrid structures is also reviewed. Thereby, the parameterization of the inlet and openings for projection onto larger grid sizes is investigated. One

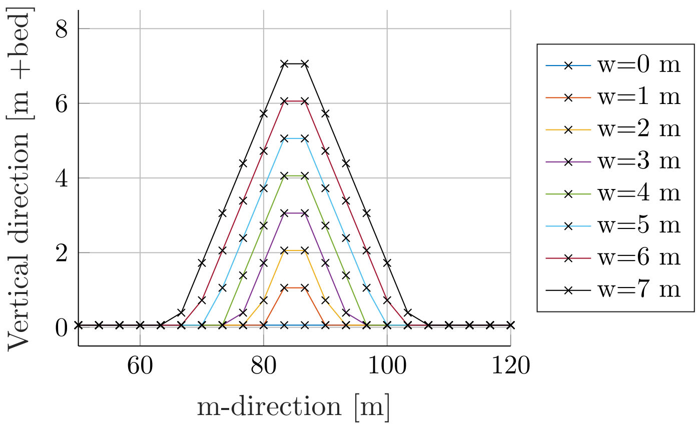

Figure C.4: Cross-section of inlet schematization in bed topography for various crest heights (w)

type of subgrid structure is the 2D subgrid weir that can be specified upon grid cells with the help of an addition weir file (.2*dw* file). Figure C.5 shows the weir as schematized in Delft3D-Flow where the pink line depicts the 2D weir. The weir coefficients are calculated according to the tables by Vermaas [1987] or the submergence relationship found by Villemonte [1947] as shown in equation C.3 and C.4. Fur further information, reference is made to the technical reference manual of Delft3D-flow.

$$C_d = 1 + \frac{\xi_1}{3}^{-3/2} c_1(w(1 - 0.25e^{-m_1/2}) + (1 - w)(0.8 + 13/20e^{-m_2/10})) \quad \text{where} w = e^{-E_1/W_{opening}} \tag{C.3}$$

$$C_s = \sqrt{1 - \frac{H_2}{H_1}^p} \tag{C.4}$$

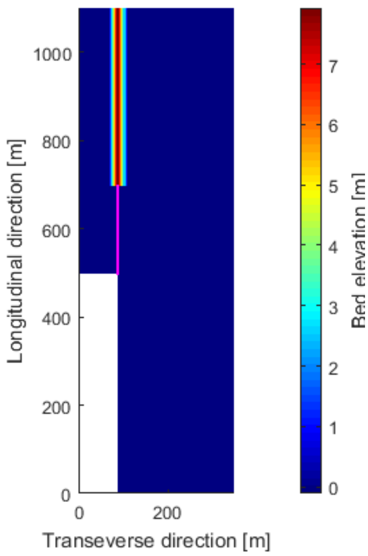

Figure C.5: Two-dimensional model schematization of inlet crest using weir structure

Only the flow component perpendicular to the crest (only the u or v velocity component depending on the user defined weir type) is taken into account in the calculation of flow over the weir. This means that no difference is made in calculations for plain, oblique or side weirs and thus no lateral outflow coefficient (ω_ϕ) is applied. This also results in no alteration of the flow angle over the weir crest. This is treated in more detail in chapters 4 and 5 and in appendix B.

Due to the inconsistent results found in the use of subgrid weirs in Delft3D-Flow, a second modelling program has been used to evaluate the use of subgrid weirs. The model schematization of Delft3D-Flow, as proposed above, has been converted to a Waqua model (also known as a Simona model). The conversion has been performed with the help of Matlab tools that automatically convert the model files. New weirs have been defined in the exact same location as in the Delft3D-Flow models. The resulting model input and inlet schematization are identical to that of the above-described Delft3D-Flow model (see figure C.5). Also, the calculation core of Waqua is identical to the Delft3D-Flow Waqua advection scheme.

C.1.6 Advection schemes

Delft3D uses by default the cyclic scheme. Both the normal advection $u\frac{\partial u}{\partial x}$ and cross advection $v\frac{\partial u}{\partial x}$ are discretized by the dissipative reduced phase error scheme. This scheme makes use of the two steps of the ADI-method to reduce the amplitude and the phase error. At the implicit step a BDF-method is used, which introduces a leading phase error and a small amplitude error. At the explicit stage central differences is used, with a lagging phase error and no amplitude error.

Another advection scheme Delft3D is able to use is the Waqua scheme. In the Waqua scheme the normal advection is discretized by central differences, the cross advection term is the same as for the cyclic scheme. Because of the absence of an amplitude error of the central differences method, the Waqua scheme has little dissipation. The scheme, however, is not diagonally dominant for large time steps and in that case may lead to incorrect convergent.

The third option is the flood scheme. This scheme is very suitable for rapidly varying depth-averaged flows. Such flow conditions require different conservation quantities in the flow contraction and flow expansion region, as shown in figure C.6. This can be the case for the inundation of dry land or flow transitions due to large gradients such as step formed bathymetry. The last conditions is also the case in the schematization of the inlet and opening crests in Delft3D-Flow, where the local increasing and decreasing bathymetry cause flow contraction and expansion patterns.

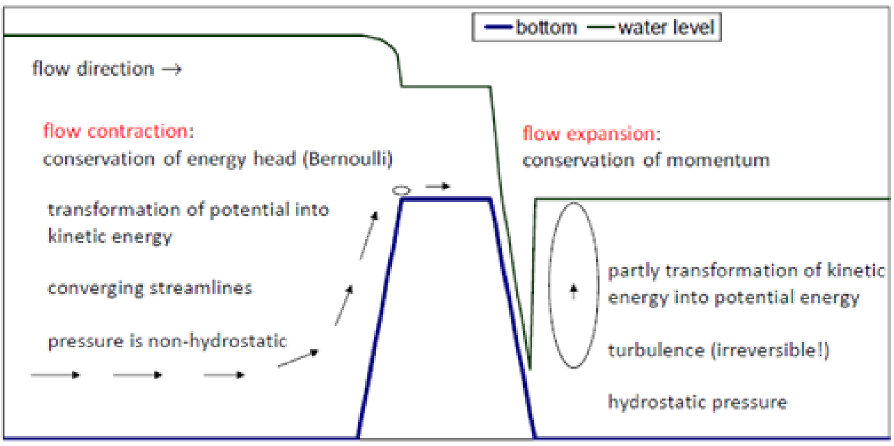

Figure C.6: Flow contraction and expansion at weir structures [Zijlema, 2014]

C.1.7 Additional model parameters:

The additions model parameters and input files are summarized below in table C.2.

Table C.2: Input used in two-dimensional Delft3D-Flow model

Component	**Input file**	**Description**
Simulation time	.mdf	1.5 hour
Time step	.mdf	0.02 min
Bathymetry	.dep	Values specified at Grid cell centres
Additional processes	.mdf	Secondary flow
Upstream boundary	.bct	Total discharge (2000 m^3/s)
Downstream boundary	.bct	Main channel: water level (6.51 m)
		Side channel: water level (6.51 m)
Reflection parameter	.bnd	300 s^2 (only at water level boundaries)
Roughness	.mdf	Chezy: 45 $\sqrt{m}/s$
Wall roughness	.mdf	Free slip condition
Horizontal eddy viscosity	.mdf	0.5 $\sqrt{m}/s$
Smoothing time	.mdf	15 min
Advection scheme	.mdf	Flood
Threshold depth	.mdf	10 m

C.2 Model assumptions

Some of the important assumptions made in the Delft3D-Flow model are listed below.

- **Constant boundary conditions:** The applied boundary conditions are constant over time. This means the no varying of river discharge nor a full hydrograph is modelled. by using (time-independent) constant boundary conditions, the model results converge to a stead-state solution.
- **Two-dimensional model:** The Delft3D-Flow model that has been used is a two-dimensional depth averaged model (2DH) in which three-dimensional are thus not included (or partly parameterized). This means that only a single vertical layer is used and the three-dimensional continuity and momentum equations are integrated over the vertical. This means that the vertical velocities are assumed insignificant, which is a blunt assumption in the case of weir flow.
- **Hydrostatic pressure:** When considering the vertical momentum equation, a scaling of terms can be executed. In hydraulic practices it usually holds that all horizontal scales are order(s) of magnitude larger than the vertical scales. Secondly, flow is sub-critical in most regions with Froude numbers smaller than 1 (except parts atop the inlet crest for larger crest heights). Using this assumptions in the scaling of terms, it can be concluded that the balance in the vertical is only from the pressure term and the gravitational term (see equation A.8). In hydrostatic modelling no vertical accelerations are thus included.
- **Constant density:** In hydraulic engineering the considered fluid is water and this fluid has a rather constant density and density differences are small ($\Delta\rho \ll \rho$). This means that the density doesnt influence the terms in the momentum equations that much. Therefore, a constant reference density is introduced (ρ_0). This is also known as the Boussinesq approximation.
- **Incompressibility:** As water is not easily compressible, it is safe to assume that its density does not depend on pressure. By assuming a constant density, can be taken out of the mass balance of the Reynolds averaged Navier Stokes equation.

- **Shallow water:** Shallow refers to the assumption that the vertical scales are subordinate to horizontal scales. Delft3D uses these equations to solve for the interested variables, being the local water level elevation and the desired local velocities depending on the dimensions of the model.

C.3 Model limitations

The short two-dimensional Delft3D-Flow model - that only schematizes the inlet - can be used to evaluate the correct model set-up and (numerical) parameters to ensure reliable modelling of side weirs in Delft3D-Flow. The flow equations, as used by the Delft3D-Flow modelling software, have been validated for many different plain weirs Deltares [2008], and are assumed to provide reliable model outputs. However, the correct model set-up, schematization and numerical parameters should still be applied, of which a few are discussed below.

Figure C.7 shows the schematization of an inlet crest height of 5 m and 6 m in the bed topography in Delft3D-Flow. It can be seen that the 6 m crest height results in the formation of wiggles behind the inlet. Figure C.7 shows wiggle in the discharge over the inlet, that are produced by Delft3D-Flow for such a large crest height. This could be related to discretization of advection terms that "may give rise to non-physical spurious oscillations, the so-called wiggles" [Deltares, 2008].

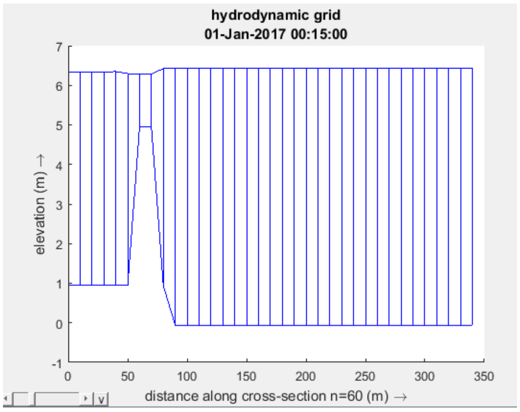

(a) Inlet crest height: 5 m

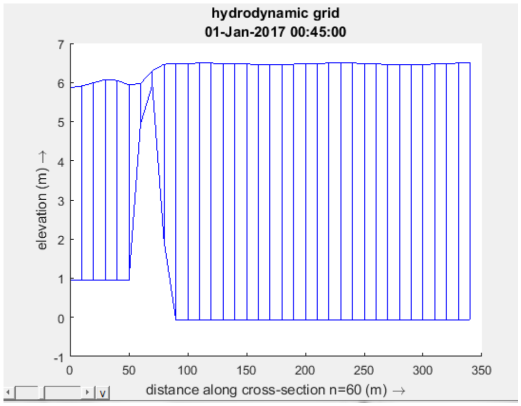

(b) Inlet crest height: 6 m

Figure C.7: Inlet crest height schematization in Delft3D